Evaluating the Impact of Microgravity on a Microphysiologic Model of Kidney Stone Disease

Kendan A. Jones-Isaac

A dissertation

submitted in partial fulfillment of the

requirements for the degree of

Doctor of Philosophy

University of Washington

2023

Reading Committee:

Edward J. Kelly, Chair

Catherine Yeung

Kenneth Thummel

Program Authorized to Offer Degree:

Department of Pharmaceutics

University of Washington

Abstract

Evaluating the Impact of Microgravity on a Microphysiologic Model of Kidney Stone Disease

Kendan A. Jones-Isaac

Chari of the Supervisory Committee:

Edward J. Kelly

Department of Pharmaceutics

The kidney is a key organ for filtering of waste products as well as elimination of drugs and their metabolites. The kidney also plays an important role in mediating calcium homeostasis and bone mineralization by through the bioactivation of calcitriol (25-hydroxyvitamin D3) to 1a,25-dihydroxyvitamin D3). Kidney dysfunction results in a range serious medical conditions including osteoporosis and nephrolithiasis (kidney stone disease, KSD). Understanding underlying pathophysiologic mechanisms of renal nephropathies and dysfunction can lead to improved modeling of disease states and novel avenues for pharmacotherapy. Microphysiological systems represent a novel, in vitro platform for studying organ-specific pathologies and drug-induced toxicities. We have developed a 3D microphysiological model of the human renal proximal tubule to study kidney function as well as biomarkers of developing pathologies. Our kidney

microphysiologic model of the proximal tubule (PT-MPS) has been previously established as capable of both evaluating extent of cytotoxicity caused by a nephrotoxic agent and investigating the underlying mechanisms responsible. We utilized the kidney MPS to assess the impact of three pro-oxidative and nephrotoxic agents representing three potential sources of oxidative stress induced renal tubule injury. The antibiotic drug polymyxin, the plant-derived environment toxin aristolochic acid 1, and crystals of calcium oxalate monohydrate representing early-stage constituents of forming kidney stones were each evaluated for their impact on 2D and 3D proximal epithelial cell cultures.

To model the early events underlying kidney stone disease progression, we evaluated the response of MPS cultured PTECs to conditions replicating the early stages of kidney stone formation, we challenged our kidney MPS with calcium oxalate monohydrate crystals. We aimed to identify biomarkers reflective of response to COM crystal exposure as identification of perturbed signaling/stress response pathways may serve to guide disease treatment possibilities. Due to characteristics of the crystals, they cannot perfuse through the MPS device. Therefore, we performed crystal exposure studies in the microgravity environment available abord the International Space Station National Laboratory. We hypothesized that in microgravity, the calcium oxalate crystals would evenly disperse within the treatment media allowing them access to the internal culture chamber within the MPS Devices. Our results confirm that microgravity does facilitate the access of COM crystals into the MPS devices allowing for direct exposure to MPS cultured PTECs. Renal dysfunction and progression of disease states is frequently accelerated and exacerbated in the microgravity. Our MPS model of kidney stone disease allowed us to investigate the effects of microgravity induced physiological alterations on kidney function

and disease progression, given the known increased incidence of nephrolithiasis in a very healthy patient population-Cosmonauts and Astronauts.

Acknowledgments

I would like to thank my advisor Dr. Edward J. Kelly, for his continued inspiration and friendship throughout my long educational trek. We share an influence of science fiction motivating our real-life scientific careers and it has been my great pleasure to work with such an outstanding scientific mind. I would also like to thank the members of my thesis committee: Catherine Yeung, Nina Isoherranen, Terrance Kavanagh, Shreeram Akilesh, and Kenneth Thummel for their exceptional guidance throughout this process. I want to give a special shout out to Karlotta Rosebaugh and Teri Ward from the Stipends for Training Aspiring Researchers (STAR) and Initiative for Maximizing Student Development (IMSD) programs for their amazing mentorship through my education and career at the University of Washington. And most importantly, I would like to thank my family, friends, classmates, and mentees who have supported and encouraged me throughout my journey. In particular, I want to express my deepest appreciation for my mother Morgan, my father Oliver, and my little sister Carmay. Finally, I want to acknowledge the overwhelming and everlasting inspiration to succeed that my wife Chalia and son Makai have provided to me through the years.

Dedication

To all those who boldly strive to expand our knowledge into new frontiers of science.

Contents

1. Introduction

1.1. Kidney Physiology

The kidney is a primary organ of filtration and excretion; responsible for efficient elimination of both endogenous and exogenous water-soluble waste compounds through the formation of urine. The nephron is the functional unit of the kidney and is comprised of the glomerulus and the tubule, which are further subdivided into the proximal; Loop of Henle (LoH); and distal segments. Renal tubule epithelial cells (RTECs) line the nephron's luminal walls and are critical for proper urine formation. Proximal region epithelial cells (PTECs) are primarily responsible for reabsorption of critical solutes such as calcium ion (Ca^{2+}) and phosphates, and actively secreting waste products. Cells originating from the distal segments in the thick ascending limb and the early distal convoluted tubule (DTECs) regulate potassium, sodium and calcium via water reabsorption; concentrating urine on its course to the collecting duct.

In addition to maintaining physiologic blood homeostasis, the kidney's endocrine functions include regulating serum Ca^{2+} plasma concentrations; and bioactivation of vitamin D from its inactive calcidiol form ($25(OH)D_3$) to the active calcitriol ($1,25(OH_2)D_3$) species. Calcium enters the systemic circulation through the gastrointestinal (GI) tract and reabsorption by the kidneys. The process of bone formation fixes calcium into mineral form and bone reabsorption releases it back into systemic circulation. The calcium sensing receptor (CASR) monitors serum calcium levels and signals the thyroid to release parathyroid hypocalcemia hormone (PTH) to increase bone reabsorption and calcium uptake in the GI tract when serum calcium is low. Disruptions to this tight regulation of system calcium homeostasis can result in hypercalciuria, a condition associated with the development of calcium kidney stone disease KSD).

1.2. Kidney Stone Disease

An estimated 15% of the US adult population has developed some degree of chronic kidney disease (CKD) [1]. Kidney dysfunction can precipitate serious medical conditions including proteinuria, osteoporosis, and KSD. Nearly 12% of the global population will develop KSD in their lifetime with the experience being reported as exceedingly painful and debilitating for the patient. Furthermore, estimated recurrence rates for KSD have been reported as high as 66.9%—further compounding the considerable disease burden on the individual patient and economic strain on healthcare systems globally [2].

Around 80% of kidney stones that are smaller than 4 millimeters (mm) will pass on their own in about 31 days. Approximately 60% of kidney stones that are 4–6 mm will pass on their own in about 45 days. Around 20% of kidney stones that are larger than 6 mm will pass on their own in about 12 months.

The rate at which a renal stone grows depends on the patient. It can take several months for even a small stone to form while in patients at risk for KSD it can happen in weeks [3]. Since smaller stones are typically passed, treatment is primarily focused on palliative care, while larger stones often require more invasive intervention.

Physiologically, the events leading to the formation of kidney stones occur primarily in the basement membrane of the LoH and distal convoluted regions of the nephron [4]. The progression to KSD results from crystalline deposits within the tubule lumen that aggregate into larger stones as they pass through the urinary system—causing tissue damage and blocking urinary filtrate flow. Roughly 80% of kidney stones contain calcium in the form of crystalized calcium phosphate

(CaP) or calcium oxalate (CaOx) either individually or in combination. Calcium oxalate ($CaC_4O_2 \cdot nH_2O$) monohydrate (COM) and dihydrate (COD) crystals are commonly observed constituents in the urinary filtrate. A relative abundance of COM crystals in the urine in relation to COD crystals is associated with kidney stone formation. Conversely, healthy urine is characterized by a predominance of COD crystals over COM [5].

Elevated calcium levels in the urinary filtrate resulting from increased bone resorption in microgravity is a risk factor for developing KSD and several epidemiological studies have reported a history of KSD as a potential risk factor in the development and progression of CKD [6]. Several theories describing the pathophysiology of stone formation in the nephron have been proposed, but an overarching similarity involves particle retention and an initial nidus for stone formation, such as a crystal or an interstitial plaque. A high CA^{2+} concentration in the urinary filtrate can hinder collagen self-assembly leading to disruption and dysregulation of the epithelial extracellular membrane [7]. Pathogenic calcium-dependent mineralization of extracellular collagen fibrils is a key component of developing adhesion points for forming CaP and CaOx creating what are referred to as Randall's plaques. Stationary nidi have been found in renal papillae below the LoH and near the distal collecting duct [8]. Over time, ions use such nidi to form crystalline structures and eventually, kidney stones.

The driving thermodynamic force behind calcium kidney stone formation is the supersaturation of these constituent ions in the urinary filtrate. Therefore, any factor influencing urine output volume, such as dehydration, or the abundance of these ions in the filtrate will have a direct impact on the probability of a cascade of events that will result in the formation of a full kidney stone. Urinary CaOx crystals can be found in either a COM or COD hydration state and

range in size from the nano scale to >30 μm, nearly half the 70 μm diameter of a typical nephron. This difference in pathogenicity can be attributed to the nature of direct interactions between CaOx crystal surfaces and cellular outer membranes. Polyanionic urinary solutes such as citrate inhibit CaOx kidney stone formation and dietary supplementation with potassium citrate can be an effective prophylactic treatment for the prevention of KSD. Citrate inhibits calcium kidney stone formation by preferentially complexing with excess free Ca^{2+}, forming calcium citrate (CaCit) and preventing crystal nucleation and aggregation by dissolving harmful crystal edges [9]. It has been previously reported that 250 μM citrate reduced adhesion of COM crystals to renal epithelial cell membranes [10].

Alterations in urine chemistry can result strongly to a pro-crystallization environment in the luminal filtrate leading to crystal formation, adhesion, and growth into a mature kidney stone. Physiological factors such as dehydration or a diet high in protein, calcium or oxalate elevate the risk of developing a kidney stone [11]. Several theories describing the pathophysiology of stone formation in the nephron have been proposed, but an overarching similarity involves particle retention and an initial nidus for stone formation, such as a crystal or an interstitial plaque. Evidence indicates that the nidus of crystal formation can initiate in the proximal region of the nephron, but more frequently occurs in the thick ascending limb and early distal convoluted. Oxalate, a primary component in ~64% of all kidney stones, has been shown to induce oxidative stress, mitochondrial damage, and immune response signaling [12]. At a concentration of 1.0 mM sodium oxalate, et al., demonstrated formation of 300-400 x 105 crystals in the presence of calcium and induced necrotic cell death without signs of programmed cell death [13].

CaOx crystals cause different cytotoxic effects depending on their shape and size, with COM crystals exhibiting more sharp edges [14]. These characteristic sharp edges interact extensively with the tubule epithelium, resulting in extracellular matrix disruption; phospholipid degradation; outer membrane rupture caused by physical contact with CaOx crystals; and greater exposed surface area on COM crystals further promoting deposition and adhesion [15]. In these cases, cell death is most frequently necrotic in nature. Conversely, nano-sized (~50-100 nm) crystals readily transit the apical and lysosomal membranes, precipitating lysosome dissolution, release of free Ca^{2+} and Ox^{2+}, and disruption of mitochondrial membrane potential; resulting in increased Reactive oxygen species (ROS) generation and oxidative stress responses [5] [12]. In this scenario, resulting cell death will be apoptotic in nature (Fig. 1) [5] [16].

ROS induced oxidative stress is a feature of many pathologies, both as a cause and an outcome. Cardiovascular disease, arthritis, diabetes, Alzheimer's disease and various metabolic syndromes have all been linked to elevated levels of oxidative stress [17].

Oxalate, a primary component in ~64% of all kidney stones, has been shown to induce oxidative stress, mitochondrial damage, and immune response signaling [12]. Oxalate exposure to the proximal tubule epithelial cell line HK-2 has been shown to lead to increased IL-6 secretion [18]. These crystals are present in sizes ranging from <50nm to >10μm, with larger sizes being more associated with developing KSD [5]. Citrate supplementation in the form of potassium citrate (KCit) is an established pharmacologic countermeasure which has been demonstrated to decrease the risk of kidney stone formation in spaceflight crewmembers by reducing hypercalciuria [11]. We studied the renal protective effects of citrate against COM crystal induced PTEC toxicity in our microphysiological systems (MPS) model of nephrolithiasis.

The microgravity environment induces many pathophysiological changes that resemble accelerated aging, including wasting of skeletal muscle; bone demineralization; and metabolic and cardiovascular dysregulation[19] [20] [21] [22, 23]. To maintain bone mineral homeostasis, kidneys control the excretion and retention of calcium, phosphate, and other essential ions [24]. They are also responsible for generation of the active form of vitamin D, 1α,25-$(OH)_2$ vitamin D_3, which plays a critical role in a multitude of biological functions including bone health [25].

1.3. Reactive Oxygen Species & Cellular Oxidative Stress Response

Cellular oxidative stress response to ROS is a key feature in the pathogenesis and progression of KSD. Once generated, ROS readily react and modify several classes of endogenous biomolecules creating covalent adducts or lesions which disrupt normal cellular functions. Oxidative modification of polyunsaturated lipids can disrupt membrane function, adducted amino acids can lead to malformed proteins and oxidation of specific co-factors leads to inactivated enzymes. Oxidation of the nucleic acid base components of DNA and RNA are readily oxidized by superoxide ($O_2^{\bullet-}$) radicals resulting in mutagenic lesions in the dsDNA template and the production of abnormal proteins from modified mRNAs [26, 27]. Guanine has the lowest oxidation potential of the nucleic acid bases resulting in a high susceptibility to oxidation by ROS forming the oxidized DNA product 8-oxo-7,8-dihydro-2'-deoxyguanosine (8-oxo-dGsn) and oxidized RNA product 8-oxo-7,8-dihydroguanosine (8-oxo-Gsn). Both of these oxidatively generated nucleic acid damage products have been studied as urinary biomarkers for CKD and their levels are elevated in the urine of patients with KSD [28-30]. 8-oxo-dGsn is by far the most studied and abundant modified product and progressive accumulation of 8-oxo-dGsn DNA lesions have long been considered as a marker of progressing physiologic age [26]. However, the

correlated RNA product, 8-oxo-Gsn, has been less studied. Relative to DNA, mRNA is more abundant, differentially localized, less stable and lacks repair machinery. Due to these differences, 8-oxo-Gsn potentially represents a biomarker more responsive to in-vitro experimentation and provides a more representative snapshot of cellular response to oxidative stress conditions.

1.4. Impact of Spaceflight on Human Physiology

Direct evaluation of the impact of microgravity on kidney function at the molecular and cellular level is not feasible in crewmembers due to the invasiveness and inherent risks of performing renal biopsies; while it is possible to conduct studies in rodents, the results may not truly reflect changes that occur in humans [31]. To address concerns about the effects of microgravity on human physiology, the National Center for Advancing Translational Sciences (NCATS) at the National Institutes of Health created the "Tissue Chips in Space" program (Tissue Chips in Space | National Center for Advancing Translational Sciences (nih.gov)) that leveraged novel tissue engineering platforms to recapitulate human physiology in the environment of space. Selected research teams each sent two projects to the International Space Station National Lab (ISSNL) during the four-year funding period.

Exposure to microgravity increases the risk of kidney stone disease in humans [32]. Elevated calcium levels in the urinary filtrate resulting from increased bone resorption in microgravity is a risk factor for developing KSD and several epidemiological studies have reported a history of KSD as a potential risk factor in the development and progression of CKD [6]. The conditions experienced by in crewmembers stationed on the International Space Station result in a dehydration-like state caused by altered body fluid distribution, accelerated bone and muscle

atrophy, and oxidative stress responses to elevated ROS generation during spaceflight [32]. Renal dysfunction and progression of disease states is frequently accelerated and exacerbated in microgravity. Extended exposure to the environment present during spaceflight increases inflammation and oxidative stress response [33]. Altered physiology and urine chemistry resulting from exposure to microgravity increases the risk for astronauts of developing kidney stones [34]. In addition to the physiological impacts, dietary factors such as increased dietary protein and sodium can of promote kidney stone formation elevating the risk to crewmember health and mission success [11, 32]. A recent study characterized the incidence rates for CaOx kidney stones in crewmembers to quantify the impact of microgravity on the relative risk of developing KSD. The authors reported that a 28% increase of prescribed fluid intake during spaceflight would be required to reduce the relative risk to a pre-flight level and noted that countermeasures against microgravity induced bone reabsorption could reduce this recommendation. This situation in which spaceflight induces alterations in KSD risk relative to terrestrial 1G highlights the ever-growing confluence of traditional terrestrial biomedical research and space-based endeavors is continuously revealing new paths of investigation.

1.5. Microphysiologic Systems

Microphysiological systems (MPS) represent a novel, in vitro platform for studying organ-specific pathologies and drug-induced toxicities. Nortis, Inc. has developed and commercialized a microfluidic technology for the in vitro generation of living 3D perfused microenvironments [35]. The interior of each chip contains a 25-µl culture chamber in which a lumenally perfused microtubule can be formed by casting collagen I around a thin glass fiber. After this matrix polymerizes the fiber is removed, creating a lumenal channel 120 microns in diameter. These

chips enable real-time microscopy, collection of effluent from lumenal and ablumenal compartments, and cell isolation for further analysis. Effluents from these devices can be analyzed to determine mRNA expression, protein quantitation and localization, metabolic capacity, and tubular damage.

To seed the devices, PTECs must first be propagated in 2D culture. MPS channels will be coated with collagen IV and cells injected into the MPS and cultured without flow for 6 hours. Once the cells have adhered to the lumenal surface, media flow will be initiated, and they will be cultured 3-5 days in order to develop intact tubules. Cell coverage and integrity of the tubule structure will be assessed daily under light microscopy to ascertain proper lumen formation. The devices will be analyzed to determine mRNA expression, protein quantitation and localization, metabolic capacity, and tubular damage. Successful tubule recapitulation (PTEC and DTEC) will be considered achieved when tubule cells maintain viability for 14 days in the MPS under continuous flow and exhibit appropriate markers characteristic of functional PTEC (e.g. aquaporin-1, Na+-K+-2Cl− cotransporter, uromodulin) and DTEC identity (e.g., aquaporin-2, uromodulin or prominin-2 MUC1, E-cadherin) while being negative for specific markers of PTEC identity (e.g., sodium glucose cotransporter-2, N-cadherin, Lotus lectin) [36] [37].

To adapt the system to the infrastructure aboard the ISSNL, we developed and tested the Kidney Chip Perfusion Platform (KCPP) novel hardware support system with BioServe Space Technologies, our Implementation Partner and Payload Developer. BioServe Space Technologies is a research center within the University of Colorado, Boulder and has a proven track record designing life sciences hardware for microgravity experiments with their hardware having flown on over 85 space flight missions. Herein, we report the development of the KCPP in support of

two missions to the ISSNL. The KCPP is a precision, syringe pump-based platform designed to perfuse up to six Nortis™ Triplex (each unit has three independently perfused tubules) PT-MPS built to support NIH/NCATS Kidney Cell 1 and 2 experiments.

Our MPS of the proximal tubule (PT-MPS) was used to assess the impact of nephrotoxic impact of a selection of pro-oxidative agents, including COM crystals prepared in the lab representing the principal early constituents of CaOx kidney stones. We describe here a test of the impact of spaceflight at the ISSN) on our PT-MPS model of KSD and compare these results to a replicate ground study conducted concurrently at Kennedy Space Center (KSC). To evaluate the response of the PTECs to conditions replicating the early stages of KSD, we challenged the PT-MPS with calcium oxalate crystals with the aim of identifying biomarkers reflective of renal tubule response to crystal exposure on earth and in orbit.

Microfluidic-based MPS represent an advancement in cell culture techniques aimed at better replicating the tissue-specific *in vivo* environment. We have previously reported our development of a PT-MPS model utilizing a commercially available platform developed by Nortis Inc [38]. The Nortis™ system is designed for use with a tubing-free pneumatic-driven pump system but requires a substantial footprint, presents logistical challenges within the lab and is not suitable in all research contexts. Therefore, the KCPP, a piston-based device, was developed by BioServe Space Technologies to support a PT-MPS model.

We have developed a novel 3D, microphysiological system (MPS) modeling the human renal proximal tubule based on the ParVivo^{TM} Triplex platform from Nortis, Inc. We have utilized this model to study kidney function as well as response to nephrotoxic compounds [39-42].

Nortis, Inc. is a biotechnology company originally founded at the University of Washington. Nortis has developed and commercialized a microfluidic technology for the in vitro generation of living 3D perfused microenvironments [35]. The system is composed of disposable microfluidic chips, perfusion platforms, and an incubator gas pump, which pressurizes air from inside the incubator to pneumatically drive fluid through the chips. The interior of each chip contains a 25-µl culture chamber in which a lumenally perfused microtubule can be formed by casting collagen I around a thin glass fiber. After this matrix polymerizes the fiber is removed, creating a lumenal channel 120 microns in diameter. Culture media can then be perfused directly through the lumen of this microtubule at a variable rate using a syringe pump or pneumatically driven pump. The chips enable real-time microscopy, collection of effluent from lumenal and ablumenal compartments, and cell isolation for further analysis. (Figure 1)

Successful tubule recapitulation (LoHC and DTEC) will be considered achieved when tubule cells maintain viability for 14 days in the MPS under continuous flow and exhibit appropriate markers characteristic of functional LoHC (eg. aquaporin-1, Na^+-K^+-$2Cl^-$ cotransporter, uromodulin) and DTEC identity (eg., aquaporin-2, uromodulin or prominin-2 MUC1, E-cadherin) while being negative for specific markers of PTEC identity (eg., sodium glucose cotransporter-2, N-cadherin, Lotus lectin) [36, 37].

The PT-MPS has been used to study a variety of disease states (e.g., aristolochic acid nephropathy and proteinuria [43, 44]) and the responses to drug/xenobiotic-induced kidney injury [39, 45, 46]. In addition, the robustness of this system was independently tested in collaboration with the NCATS-funded Tissue Chips Testing Centers [47, 48]. To test the premise

that microgravity is an accelerated environment for aging/disease progression, we evaluated proteinuria, kidney vitamin D metabolism, and nephrolithiasis/KSD [49].

The characteristics of the crystals and the MPS devices themselves inhibit the introduction of COM crystals through the inlet to the flow port as they would quickly settle to the bottom of the input reservoir and would not transit through the flow path. Instead, COM crystals with or without KCit were introduced into the lumen by direct injection via the abluminal injection port. The within the microgravity environment aboard the ISSNL, there will not be an issue with the crystals settling. Instead, the crystals will disperse in solution and maintain a largely homogeneous suspension within the solution. Therefore, culture media containing the COM crystals will be introduced through the inlet and flow towards the lumen facilitating continuous dynamic interactions between the crystals and PTEC outer membranes.

1.5. Summary & Research Aims

Successful completion of these aims may yield novel therapeutic targets for the treatment prevention of kidney stone formation and provide insight into other nephropathies. This study would allow us to investigate the effects of microgravity induced physiological alterations on kidney function and disease progression, given the known increased incidence of kidney stones in an exceptionally healthy patient population—cosmonauts and astronauts (crewmembers). Existing treatments, aside from palliative care, involve either invasive surgery or extracorporeal shock wave lithotripsy (ESWL). Each procedure presents risks to the patient as well as significant discomfort [50]. Prophylactic treatment, particularly in individuals with a history of kidney stones and thus at higher risk, would represent a significant advancement. In addition, this kidney tubule model can be linked with MPS containing cell types from key sites of drug elimination or

distribution to further study inter-organ interactions [40]. Such integrated systems hold the potential to reveal new avenues of pharmacotherapeutics and better prediction of drug induced toxicities.

1.6. Hypothesis & Specific Aims

1.6.1 Hypothesis 1**:** COM crystals induce acute kidney injury via direct interactions with the outer membrane of the epithelial surface and increased oxidative stress.

Aim 1.1: Generate and characterize COM crystals using microscopy and spectrographic techniques.

Aim 1.2: Assess acute-phase responses to COM crystal exposure in 2D PTEC culture.

Aim 1.3: Assess acute-phase responses to COM crystal exposure in 3D kidney MPS during engineering validation testing (EVT).

1.6.2 Hypothesis 2**:** The microgravity environment aboard the International Space Station is a superior environment in which to test our PT-MPS model of KSD.

Aim 2.1: Evaluate the utility of the microgravity environment of the ISS-NL on to enhance the recapitulation of the early events of kidney stone formation.

Aim 2.2: Identify protective mechanisms of KCit terrestrially and during spaceflight.

2. Utilizing the Kidney Microphysiologic System to Investigate the Involvement of Oxidative Stress in Renal Pathologies.

2.1. Abstract

The proximal tubule is a site of extensive bi-directional active transport across the tubular epithelium necessitating one of the highest mitochondria contents of any cell type. This leaves proximal tubular cells highly susceptible to substantial intracellular concentration of nephrotoxic and pro-oxidative agents. Our kidney microphysiologic model of the proximal tubule has been previously established as capable of both evaluating extent of cytotoxicity caused by a nephrotoxic agent and investigating the underlying mechanisms responsible. We utilized the kidney MPS to assess the impact of three pro-oxidative and nephrotoxic agents representing three potential sources of oxidative stress induced renal tubule injury. The antibiotic drug polymyxin, the plant-derived environment toxin aristolochic acid 1, and crystals of calcium oxalate monohydrate were each evaluated for their impact on 2D and 3D renal epithelial cell cultures. With the aim of developing a kidney MPS model of the distal tubule, immunomagnetic selection was performed on whole kidney cell isolates to enrich separate distal and proximal fractions. The PTEC MPS successfully replicated and extended studies performed previously by our group and these experiments served as the basis for the development of a microphysiologic model of kidney stone disease.

2.2. Introduction

The kidney is a primary organ of filtration and excretion, responsible for efficient elimination of both endogenous and exogenous water-soluble waste compounds through the formation of urine. The nephron, the functional unit of the kidney, is comprised of the glomerulus and the tubule, which is further subdivided into the proximal, Loop of Henle (LoH), and distal segments. Renal tubule epithelial cells (RTECs) line the luminal walls of the nephron and are critical for proper urine formation. The epithelial cells residing in the proximal region of the nephron (PTECs) are primarily responsible for reabsorption of critical solutes such as Ca2+ and

phosphates and the active secretion of waste products. Cells originating from the distal segments in the thick ascending limb and the early distal convoluted tubule (DTECs) regulate potassium, sodium and calcium via reabsorption of water, concentrating urine on its course to the collecting duct.

Kidney Stone Disease (KSD) is a painful and debilitating ailment resulting from nano and micron-sized crystalline aggregations within the tubule lumen. These deposits subsequently aggregate, forming larger stones, as they pass through the urinary system. Alterations in urine chemistry can result strongly a pro-crystallization environment in the luminal filtrate leading to crystal formation, adhesion, and growth into a mature kidney stone. Physiological factors such as dehydration or a diet high in protein, calcium or oxalate elevate the risk of developing a kidney stone [11]. While the mechanisms that lead to the formation of kidney stones are not yet fully understood, evidence indicates that the nidus of stone formation occurs in the basement membrane of the LoH [4]. Several theories describing the pathophysiology of stone formation in the nephron have been proposed, but an overarching similarity involves particle retention and an initial nidus for stone formation, such as a crystal or an interstitial plaque. Stationary nidi have been found in renal papillae below Loops of Henle and near the distal collecting duct [8]. Over time, ions use such nidi to form microscopic crystalline structures and eventually, calculi. Evidence indicates that the nidus of crystal formation can initiate in the proximal region of the nephron, but more frequently occurs in the thick ascending limb and early distal convoluted. Oxalate, a primary component in ~64% of all kidney stones, and has been shown to induce oxidative stress, mitochondrial damage, and immune response signaling [12].

Calcium oxalate ($CaC_4O_2 \cdot nH_2O$) monohydrate (COM) and dihydrate (COD) crystals are commonly observed constituents in the urinary filtrate with COD crystals being more abundant in

normal urine and COM more abundant in stone formers [5]. CaOx crystals cause different cytotoxic effects depending on their shape and size with COM crystals exhibiting more sharp edges [14]. These characteristic sharp edges interact extensively with the tubule epithelium resulting in outer membrane rupture and greater exposed surface area on COM crystals further promotes deposition and adhesion [15]. In these cases, cell death is most frequently necrotic in nature. Conversely, nano-sized crystals readily transit the apical and lysosomal membranes precipitating lysosome dissolution, release of free Ca^{2+} and Ox^{2-} and disruption of mitochondrial membrane potential resulting in increased ROS generation and oxidative stress responses. In this scenario, resulting cell death will be apoptotic in nature [5] [16]. Citrate supplementation in the form of potassium citrate (KCit) is an established pharmacologic countermeasure which has been demonstrated to decrease the risk of kidney stone formation in spaceflight crew members by reducing hypercalciuria. Citrate inhibits stone formation by preferentially complexing with Ca2+, preventing crystal nucleation and aggregation [9]. We evaluated the effects of citrate in our MPS model of nephrolithiasis.

2.3. Materials & Methods

Cell Sourcing and Isolation

Whole human kidneys that were not suited for human transplantation were obtained from Novabiosis, Inc. (Research Triangle Park, NC) with all patient identifiers removed in accordance with a University of Washington-approved IRB protocol. Primary human proximal tubule epithelial cells (PTECs) were isolated by mechanical and enzymatic dissociation and cultured as previously reported [51]**.** PTEC cultures were maintained serum-free in DMEM/F12 (Gibco, Grand Island, NY, Cat. # 11330-032) supplemented with 1x insulin-transferrin-selenium-sodium pyruvate (ITS-A, Gibco, Cat. # 51300044), 50 nM hydrocortisone (Sigma, St. Louis, MO, Cat. #

H6909), and 1x Antibiotic-Antimycotic (Gibco, Cat. # 15240062). Upon reaching 75-80% confluence, PTECs were passaged by enzymatic digestion with 0.05% trypsin EDTA (Gibco, Cat. # 25200056) and manual cell scraping to obtain a single-cell suspension which was subsequently neutralized with defined trypsin inhibitor/DTI (Gibco, Cat. # R007100) at a volume:volume ratio of 2:1 DTI:trypsin, then the cells were pelleted by centrifugation at 200 x g for 7 minutes, resuspended in maintenance media, and plated in cell culture treated flasks at >25% confluency (referred to as passage 1 or P1).

Calcium Oxalate Microcrystal Generation

Calcium chloride and sodium oxalate (Fisher Scientific, NH, USA) were used to create stock solutions at a concentration of 10 mM. The calcium chloride solution was diluted from the 10 mM stock solution to 2 mM. The sodium oxalate was also diluted from the 10 mM stock solution to 2 mM. In a 2000 mL Erlenmeyer flask, 500 mL of the 2 mM calcium chloride and 500 mL of the 2 mM sodium oxalate solution was combined. The Erlenmeyer flask was heated at 37° C for 1 hour and then cooled overnight at 4° C.

Calcium Oxalate Microcrystal Harvesting

The crystals were transferred to 50 mL conical tubes. The conical tubes were centrifuged at 3000 rpm for 5 minutes. The solution was then aspirated to the pellets, and all of the pellets were combined into one 15 mL conical tube. The 15 mL conical with the crystals was then centrifuged at 3000 rpm for 5 minutes. The solution was then aspirated from the COM crystals.

Calcium Oxalate Microcrystal Sterilization

The crystals were sterilized by adding 1 mL of MeOH or EtOH to the crystals and agitating. The crystals were spun in a microcentrifuge and left to dry overnight at 37° C and then collected into a sterile Eppendorf tube.

Fourier-Transform Infrared Spectroscopy

Fourier-Transform Infrared Spectroscopy (FTIR) was used to characterize the COM crystals. To create the disc for FTIR analysis, 2 mg of COM crystals and 200 mg of KBr were ground with an agate mortar and pestle until smooth. The powdered mix was then poured into a die and compressed with a pneumatic press for 5 minutes at a pressure of 15000-16000 psi with a vacuum hose attached to remove any excess water. The disc containing the COM crystals was then put in the Perkins-Elmer FTIR and read at 16 scans, 0.5 /cm resolution and the range of 500-4000 /cm.

Scanning Electron Microscopy and Energy-Dispersive Spectroscopy

Samples of prepared COM crystals were submitted for SEM and EDS analysis to the Molecular Analysis Facility at the University of Washington's Department of Molecular Engineering.

Kidney MPS Preparation, 2D and 3D MPS PTEC Culture and Fluorescent Imaging

Whole human donor kidneys were acquired as described above. MPS device preparation, cell culture, LIVE/DEAD assays in 2D and 3D MPS devices were performed as previously described; **[**48**]** Immunological staining for AL-1 adducts in AA-1 treated MPS devices was performed as previously described by Chang et al **[**40**].**

Immunocytochemistry to assess renal tubule marker expression was performed on P1 RTECs cultured in 8-well chamber slides to either >80% (PNA-) or > 50% (PNA+) confluency with this discrepancy due to a difference in the amount of cells available for each population. The cultures were fixed with 4% paraformaldehyde and the slides washed three times with PBS and

then incubated at room temperature for 1 hour in blocking buffer (PBS containing 0.5% normal goat serum and 0.025% TWEEN 20). Cells were washed once with PBS, permeabilized with 0.25% Triton X-100 for 2 minutes, washed twice with PBS, and incubated overnight with primary antibodies at 4^{o} C overnight. The following primary antibodies were tested: E-Cadherin at 1:200 (BD Biosciences, San Jose, CA), KI-67 at 1:10 (Abcam, Cambridge, MA), Megalin at 1:100 (Abcam, Cambridge, MA), TRPV5 at 1:100 (Abcam, Cambridge, MA), AQP-1-1 at 1:50 (R and D Systems, Minneapolis, MN), AQP-2 2 at 1:200 (Abcam, Cambridge, MA). Rabbit and mouse IgG's were used as isotype controls. All antibody dilutions were done in a blocking buffer. Following blocking buffer antibody incubation, cells were washed three times with PBST (PBS/0.05% TWEEN 20) for 15 minutes each at room temperature. Cells were incubated with secondary antibodies diluted in blocking buffer for 1 hour at room temperature (in light-protected container). The following secondary antibodies were used: AlexaFluor 488 goat anti-rabbit IgG (Invitrogen, Grand Island, NY), AlexaFluor 488 goat anti-mouse IgG (Invitrogen, Grand Island, NY), AlexaFluor 488 donkey anti-goat IgG (Invitrogen, Grand Island, NY), Rhodamine Red-X goat anti-mouse IgG (Invitrogen, Grand Island, NY), FITC-labeled lotus lectin (US Biological, Salem, MA). Following secondary antibody incubation, cells were washed three times with PBS. Cells are counter-stained with DAPI, and cover slipped using SlowFade Gold antifade reagent with DAPI (Invitrogen, Grand Island, NY). Fluorescein-labeled Lotus Tetragonolobus Lectin (LTL) Rhodamine-labeled Peanut Agglutinin (PNA) (Vector Laboratories, Newark, CA) were diluted 1:500 in blocking buffer and incubated overnight at 4^{o} C and were prepped for imaging as described above. Fluorescence imaging was performed on a Nikon Eclipse Ti-S microscope equipped with a Nikon DS-Fi3 camera and fluorescence intensity was quantified using ImageJ software.

Positive selection for DTECs using Immunomagnetic Cell Separation

All IMS equipment and reagents were obtained from Miltenyi Biotec (Radolfzell, Germany) An isolation buffer made of PBS-/- (no Ca2+ or Mg2+, Sigma-Aldrich D8537), 0.5% BSA: 200 mg (Sigma-Aldrich A7906-100G) and 2 mM EDTA: 29.8 mg (Sigma-Aldrich E4884-100G) was prepared. Immunomagnetic enrichment by anti-PNA microbeads was performed using the Germinal Center B Cell (PNA) MicroBead Kit (Miltenyi Biotec, 130-110-479). PTECs were harvested using trypsin incubation as described previously with the exception the use of DTI at 4° C to inhibit the trypsin digestion. All buffer and reagent volumes are per 10^7 total cells. The cell suspension was centrifuged at room temperature for 10 min at 300xg. The resulting pellet was resuspended in 40 µL of buffer. A volume of 20 µL PNA-Biotin microbeads was added to the cell suspension and mixed well with pipette aspiration before incubating for 5 minutes in a 4° C refrigerator. An additional 30 µL of buffer and 30 µL Anti-Biotin microbead reagent was added and mixed well using a pipette before incubating for 10 minutes in a 4° C refrigerator. The suspension was then washed with 2 mL buffer and centrifuged for 10 minutes at 300xg, the supernatant aspirated completely, and the cells resuspended up to 10^8 cells per 500 µL buffer. This cell suspension was then applied to a MACS MS/LS column (Miltenyi Biotec 130-042-201/130-042-401) within a QuadroMACS™ (Miltenyi Biotec 130-091-051) cell separator. The separation procedure was performed as instructed by the manufacturer. The effluent was collected containing unlabeled cells was designated PNA-depleted and the subsequent effluent collected after the column's removal from the cell separator was designated PNA-enriched. Both were cryopreserved and stored in liquid nitrogen for future use.

Positive selection for DTECs using AQP2-linked Immunomagnetic Cell Separation

Immunomagnetic enrichment by indirect magnetic labeling of AQP-2+ RTECs was performed as described above with the inclusion of 45-minute incubation with the rabbit anti-

AQP-2 primary antibody (Aviva Systems Biology, OABF01462) diluted 1:50 in incubation buffer at 4° C prior to the addition of the anti-rabbit magnetic beads (Miltenyi Biotec 130-048-602).

IL-6 and KIM-1 Quantification in PTEC Culture Supernatants and 3D MPS Effluents

Measuring IL-6 and KIM-1 in culture supernatants and effluents was performed using ELISA assays according to the manufacturer's protocol (R&D Systems, Minneapolis, MN). In brief, 100 µL of media supernatant was analyzed in duplicate and concentrations determined from standard curves generated using the kit's internal standards.

PTEC exposure to COM crystals and pro-oxidative agents in 2D culture

Primary human PTECs were first cultured to ~>50%-confluence in. Prepared crystals will be suspended in PTEC media (DMEM/F12 supplemented with Anti-Anti, ITS-A, and hydrocortisone) at a concentration of 200 µg/ml and blown across the cultured monolayer with a micropipette tip. The PTECs were then incubated for 24 hours at 37° C and 5% CO2. After this incubation period, the culture supernatants were collected and stored at -20° C.

Quantifying levels of kidney-specific injury marker KIM-1 in 2D culture supernatants and device effluents.

Quantification of KIM-1 levels in 2D PTEC cultures and device effluents was performed using the KIM-1 DuoSet® ELISA Kit (R&D Systems, Minneapolis, MN) following the manufacturer's suggested protocol. All samples were diluted 1:3 in reagent diluent and assayed in duplicate and concentrations determined from standard curves generated using the kit's internal standards.

PTEC exposure to COM crystals and pro-oxidative agents in MPS culture.

MPS devices were allowed to remain under flow for 3-5 days after initial seeding. Pro-oxidative agents containing treatment media were prepared by diluting AA-1, antimycin A, colistimethate, menadione, PMB and TBHQ in DMSO and serially diluting in PTEC media to the determined treatment concentration. COM treatment media was prepared by suspending pre-

massed COM crystals in PTEC culture media or by suspending 1000 µg crystals into PTEC culture media supplemented with 250 µM potassium citrate (KCit). In the case of MPS devices treated with COM crystal containing media, crystals were also injected directly into the abluminal injection port using a Hamilton syringe. This was done in pre-EVT and EVT phases to ensure PTEC exposure to crystals. The MPS devices were then allowed to incubate without flow for 48 hours before flow was initiated and effluents collected at 6, 12, 24, and 48 hours then stored at -20° C. After 48 hours, KIM-1 levels in MPS effluents were measured and PTEC cytotoxicity was assessed using a LIVE/DEAD cell viability assay before being formalin fixed for subsequent ICC.

Evaluating pro-oxidative agents in 2D HK-2 cultures CellROX™ and MitoSOX™ assays.

Assessment of intracellular ROS and mitochondrial superoxide release was performed using the CellROX™ and MitoSOX™ assays according to the manufacturers protocol (Invitrogen, Waltham, MA). All imaging was performed on a Nikon Eclipse Ti-S microscope equipped with a Nikon DS-Fi3 camera within 20 minutes of incubation. Both green and red fluorescence intensity was quantified using ImageJ software and normalized to control values.

2.4. Results

Colistimethate treatment results in dose dependent nephrotoxicity in PTEC MPS

The proximal tubule is rich with mitochondria due to active transport processes making PTECs particularly susceptible to drug induced kidney injury. Experimental evaluation of colistimethate nephrotoxic effects in the PTEC MPS was consistent with previous study in which we successfully evaluated cells and effluent from the PTEC MPS cultures after exposure to 50 µM polymyxin B (PMB), a known nephrotoxin [52]. Colistimethate (polymyxin E) is a related antibiotic and nephrotoxin and oxidative stress inducing agent [53]. We studied nephrotoxicity of colistimethate in the PTEC MPS over a 0-2000 µM concentration range **(Figure 1)**. PTEC lumens

demonstrated dose dependent toxicity after 48 hours of treatment with colistimethate, the injectable formulation of colistimethate. The ability of the PTEC MPS model to accurately replicate the dose dependency observed in vivo supports its utility as a tool for assessing the nephrotoxic potential of a wide range of compounds.

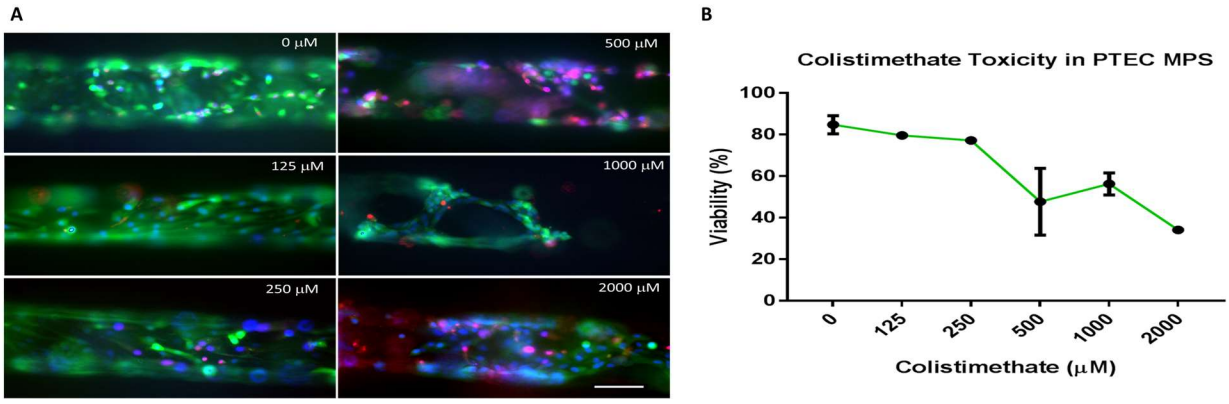

Figure 1. Exposure to colistimethate over 48 hours causes dose-dependent nephrotoxicity in PTEC MPS: (A) LIVE/DEAD staining showing PTEC lumens in MPS after treatment with increasing colistimethate concentration. (B) Percent cell viability in PTEC MPS cultures after colistimethate treatment. (N=1-2) Green = live stain. Red = dead stain. Blue = nuclear stain. Bar = 100 µm.

PTEC MPS maintains multi-day exposure to AA-1 by multiple perfusion conditions.

Aristolochic acid I (AA-1) is an agricultural contaminant associated with nephropathies and a causal agent of urothelial carcinomas [54]. Evidence also indicates that it acts as an OS inducing agent and has demonstrated to cause mitochondrial apoptosis through inducing OS states in the liver [54] [55] [56]. AA-1 is bioactivated in the liver by NQO1 into the carcinogenic metabolite, aristolactam I (AL-1) which is directly nephrotoxic and was demonstrated to exhibit hepatically enhanced nephrotoxicity in a linked hepatocyte-to-PTEC MPS model [40]. The rate of media perfused through the MPS is an important to the maintaining PTEC character in MPS cultures by controlling nutrient flow and by providing shear stress important for recapitulating PTEC

polarization and maintaining a proximal epithelial phenotype [41] [39] [57]. While the flow rate for initial PTEC culture is 0.5 µL/min of 100% PTEC maintenance media, this study was conducted with a 50:50 combination of hepatocyte maintenance media and PTEC media perfused into the devices at a flow rate of 1.5 µL/min over 24 hours. Hepatocyte linked PTEC MPS cultures treated with 10 and 25 µM AA-1 for 24 hours showed significant increases in cytotoxicity over control as determined by LIVE/DEAD fluorescence. No significant difference was observed in those PTEC MPS cultures that were not hepatocyte linked, but those devices treated with 25 µM AA-1 did trend towards significantly increased cell death. To test the impact of perfusion rate on PTEC MPS response to a 48-hour treatment with 25 µM AA-1, we replicated the PTEC MPS only arm from a previous study over 48 hours at two different perfusion rates, 0.5 and 1.5 µL/min, via syringe pump and at the standard PTEC perfusion rate of 0.5 µL/min **(Figure 2)**. We observed no significant increase in cytotoxicity between AA-1 treatment and control regardless of perfusion rate or platform. These results match those from the previous study which concluded that, absent preceding bioactivation AA-1 was not directly nephrotoxic. We performed immunocytochemistry to assess the formation of intracellular AL-1 in devices treated for 24 hours with 0, 1, and 10 µM AA-1 **(Figure 3)**. Again, similar to the previous study, we observed no significant increase in AL-1 staining in the treatment groups over control [40].

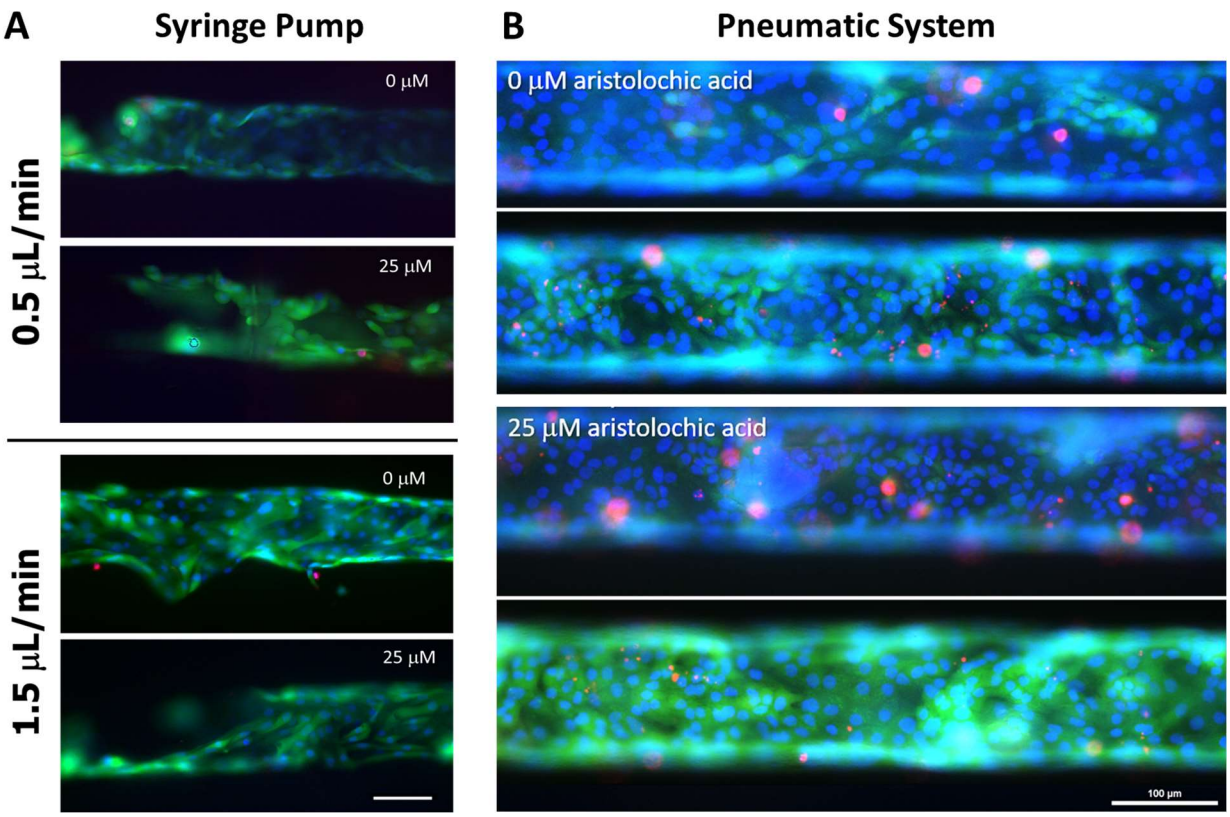

Figure 2. Impact of perfusion rate and high dose 48-hour AA-1 exposure on cell viability in PTEC MPS: (a & b) LIVE/DEAD cytotoxicity imaging of PTEC MPS lumens perfused by (a) syringe pump at a rate of 0.5 µL/min and 1.5 µL/min and (b) pneumatic system at a rate of 0.5 µL/min.

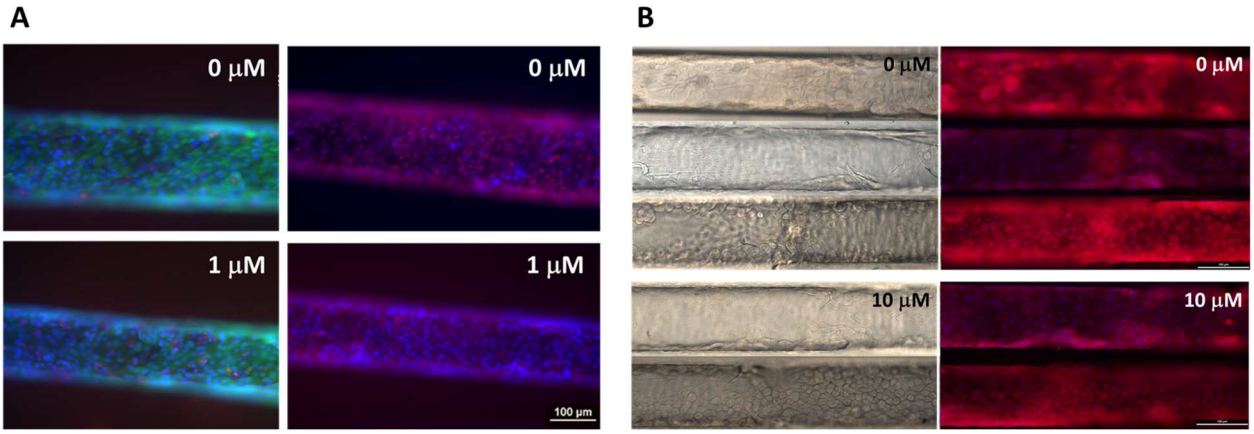

Figure 3. Effect of 24-hour AA-1 exposure on aristolactam adduct formation in PTEC MPS: (a) LIVE/DEAD viability (L) and aristolactam immunocytochemistry (R) imaging of PTEC lumens treated with 0 µM or 1 µM AA-1, (b) phase contrast (L) and aristolactam immunocytochemistry (R) imaging of PTEC lumens treated with 0 µM or 10 µM AA-1.

We studied the impact of time on KIM-1 release in PTEC MPS exposed to 0, 1, or 10 µM AA-1 over multiple days. When perfused via syringe pump, KIM-1 levels remained consistent with those observed in previous PTEC MPS studies and no significant change in KIM-1 levels were observed by time or by concentration [40]. While MPS devices perfused with the pneumatic system trended towards higher KIM-1 levels than those perfused with syringe pumps, no significant change was observed across concentrations or timepoints **(Figure 4)**. To determine how long a toxic exposure study can be carried out with the PTEC MPS, we carried out 7- and 23-day AA-1 exposure studies **(Figure 5)**. The study was terminated at 23 days to avoid MPS loss due to factors such as contamination or delamination of the collagen matrix due to dehydration. Dose- and time-dependent toxicity was observed in PTEC MPS dosed with 0, 1, or 10 µM AA-1. No significant difference was observed between treatments at day 7. However, we observed a dose-dependent increase in cytotoxicity at 23 days by LIVE/DEAD fluorescence stain in the AA-1 treated devices over both the day 7 treated lumens, and over the 23-day control. This finding indicates that extended exposure to or significant intracellular accumulation of AA-1 may

contribute to increased AA-1 nephrotoxicity over the long-term absent hepatic bioactivation to the toxic AL-1.

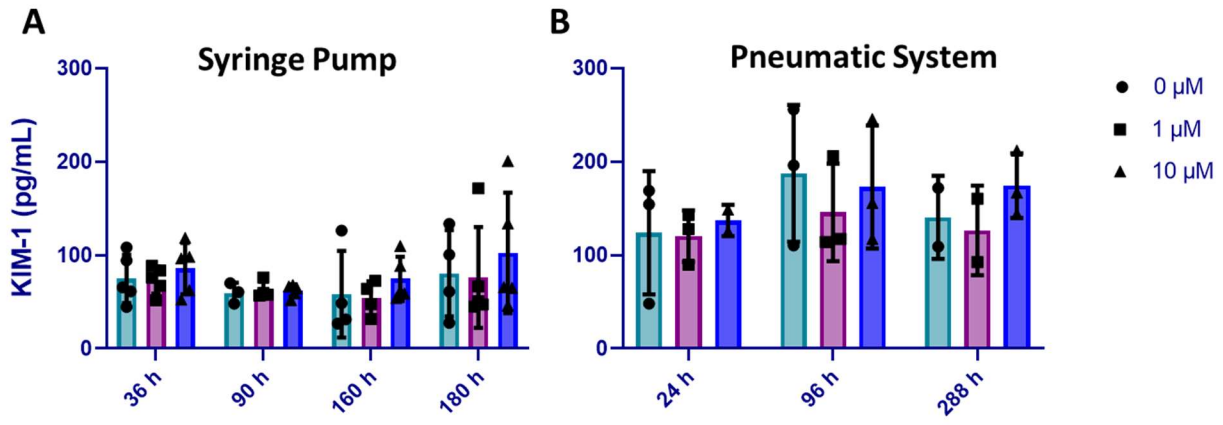

Figure 4. Effect of AA-1 treatment duration and perfusion method on KIM-1 secretion in PTEC MPS: KIM-1 release from PTEC MPS effluents generated over (a) 180 hours (7.5 days) syringe pump perfusion and (b) 288 hours (12 days) perfusion using a pneumatic system.

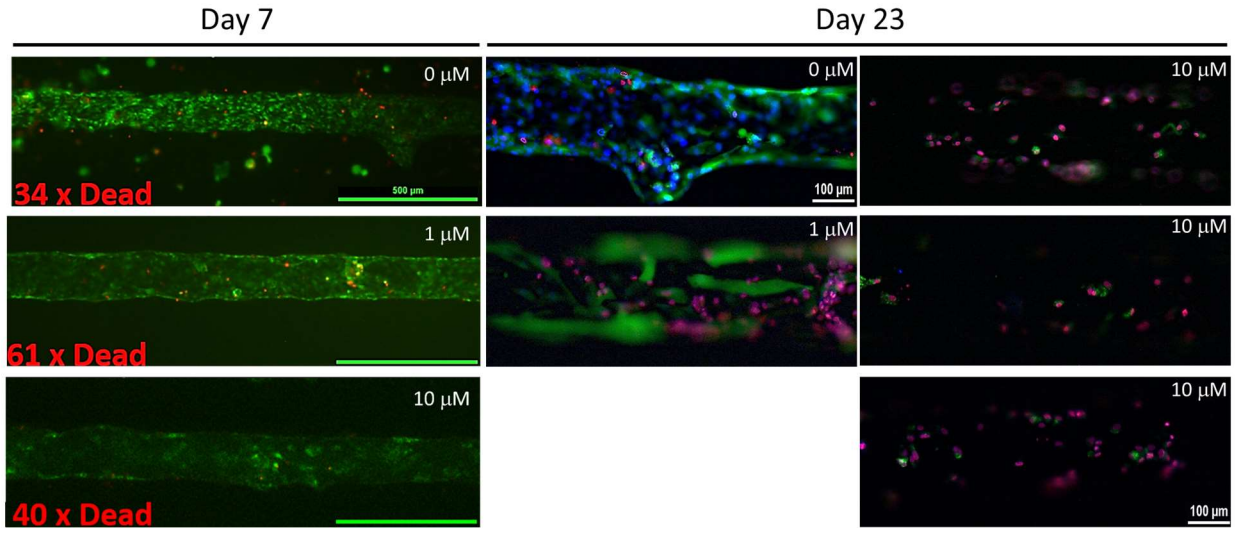

Figure 5. Impact of duration of AA-1 treatment on PTEC viability in MPS culture: AA-1 induced cytotoxicity as evaluated by LIVE/DEAD immunostaining after (a) 7 and (b) 23 days.

Immunomagnetic Separation to Isolate and Culture Distal Derived RTECs

During whole kidney cell isolation, cells and protein mass of proximal origin comprises roughly 44% and 65% of the total yield respectively **(Figure 6A)** [58]. The magnetic-activated cell sorting (MACS) system (Miltenyi Biotech-list City and State) is an immunomagnetic separation (IMS) technique in which cells are fractionated based on the presence or absence of labeling by an antibody-conjugated magnetic bead. When the cell isolate is applied to a separation column inside a strong magnetic field, the labeled cells are retained within the column while unlabeled cells pass through. This technique has been used to separate and characterize renal cells from different regions in both rodent and human kidney cells [59-65].

Isolation and culturing of renal tubule epithelial cells (RTECs) was performed consistent with our protocol previously described in Weber et al, KI, 2016 which uses cortical tissue and enriches for tubule cells versus glomeruli. Further supersaturation of RTECs into proximal (PTEC) or distal (DTEC) derived subpopulations was performed by IMS to enrich for RTECs of We first performed IMS on whole kidney cell isolates at the time of initial culture (passage #0 or P0) based on the distal and connecting tubule marker aquaporin-2 (AQP-2). Immunomagnetic separation was performed on a whole kidney cell isolate suspension immediately prior to initial RTEC culturing. We did not observe any significant visual differences between the resulting AQP-2 depleted and enriched cultures, but due to low cell counts in the AQP-2 enriched fraction we did not continue to investigate this option **(Figure 6B)**.

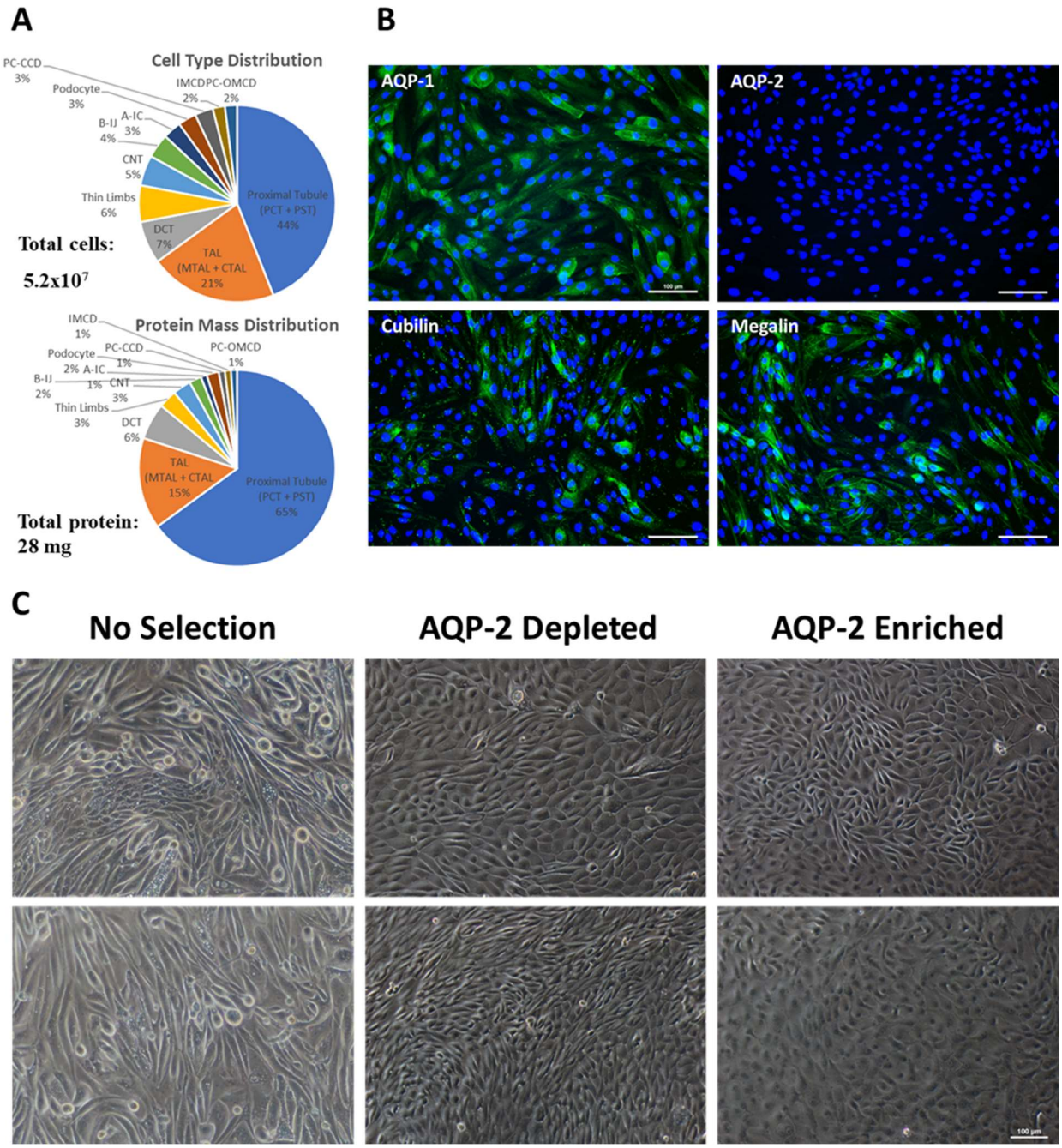

Figure 6. AQP-2-based immunomagnetic enrichment for distal derived RTECs: (a) graphic representation of the proportion of cell type (L) and protein mass (R) in a human kidney [58], (b) fluorescence imaging of proximal and distal markers AQP-1, AQP-2, Megalin and Cubilin in a typical P1 RTEC culture (Donor PT7M), (c) phase contrast imaging of a PTEC culture (Donor

PT7M) that has not undergone IMS (No Selection) and AQP-2 depleted (AQP-2 Depleted) or enriched (AQP-2 Enriched) cultures (Donor BIO78) resulting from IMS.

An alternative method for labeling cells for IMS is to utilize biotin conjugated peanut agglutinin (PNA) in combination with an anti-biotin antibody conjugated to a magnetic bead. Selecting this method for IMS of whole kidney isolates provides the benefits of reducing the handling of cells during the isolation process and reducing the time from isolation to initial culture. Positive staining by PNA has been established as a marker specific to both cortical and medullary distal regions of the nephron while positive staining for lotus tetragonolobus lectin (LTL) is used as a proximal tubule marker (**Figure 7A)** [66] [67]. In order to generate distinctly separate cultures of proximal and distal derived RTECs, we performed PNA-based IMS on P0 RTEC cultures from whole human kidneys at ~80-90% confluence during the first passaging procedure resulting in separate PNA-depleted (PNA-) and PNA-enriched (PNA+) RTEC populations **(Figure 7B).**

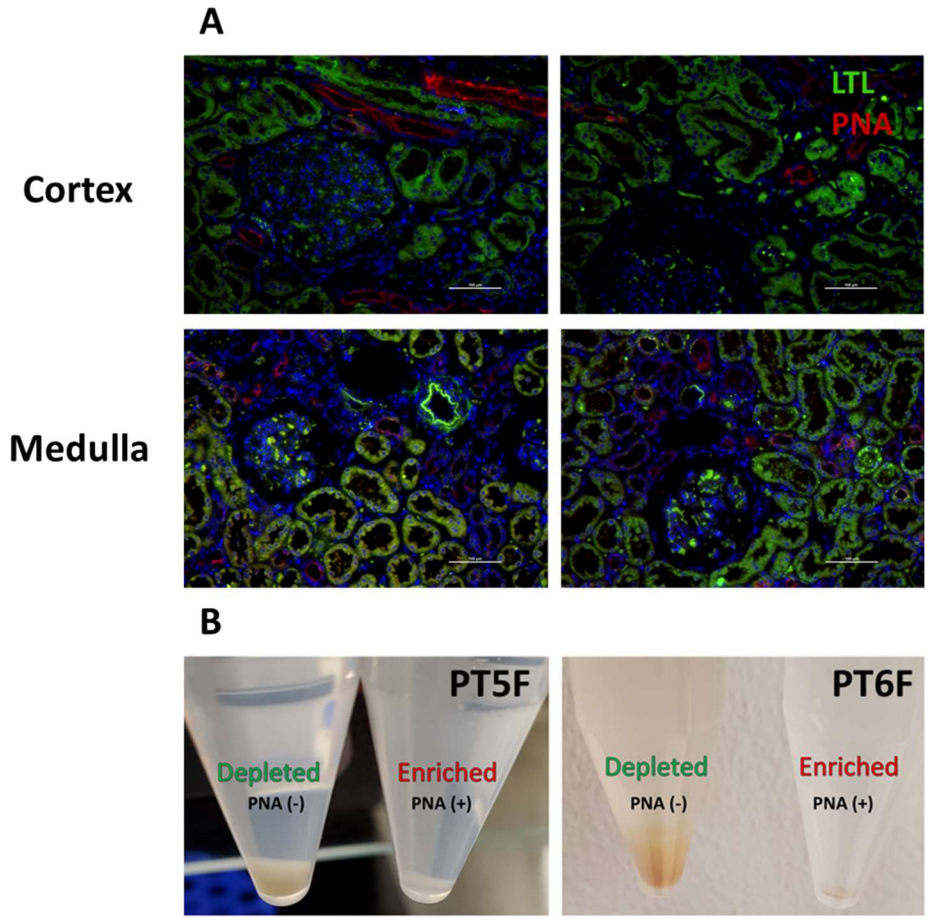

Figure 7. Immunomagnetic enrichment for PNA+ renal epithelial cell culture: (a) Human cortex (Top) and medulla (Bottom) FFPE sections. Direct staining of lectins to assess specificity of PNA (peanut agglutinin) as a marker of distal tubules versus LTL (lotus lectin), a marker of proximal tubules. (Scale bar, 100 um), (b) PNA depleted and enriched cell pellets resulting from immunomagnetic cell sorting of PT5F (L) and PT6F (R).

To determine the efficacy of the IMS method and the impact of cryopreservation on the resulting PNA- and PNA+ RTEC populations, we performed an LTL and PNA fluorescent stain on both RTEC populations, both before three months of LN_2 cryopreservation (pre-freeze) and a PNA fluorescent stain after re-culture (post-thaw) **(Figure 8)**. PNA- and PNA+ populations were cultured in 8-well chamber slides to ~80-90% confluence and stained for either LTL and PNA (pre-freeze) or PNA alone (post-thaw). We observed minimal fluorescence for both LTL and PNA

in those PNA-depleted RTECs cultured immediately prior to cryopreservation. In contrast, the PNA-enriched cultures displayed greater levels of LTL staining and a considerably greater level of PNA staining than the depleted cultures. PNA staining of the post-thaw cultures was again greater in the PNA+ cultures, however, isolated regions of intense PNA signal were observed. This is most likely the result of less than 100% efficacy in target cell labeling or some percentage of the target cells having been insufficiently retained in the column during the separation phase leading to residual PNA+ cell "contamination" in the PNA- cell fraction. Due to a lack of fresh LTL staining reagent, LTL staining was not repeated on the post-thaw cultures.

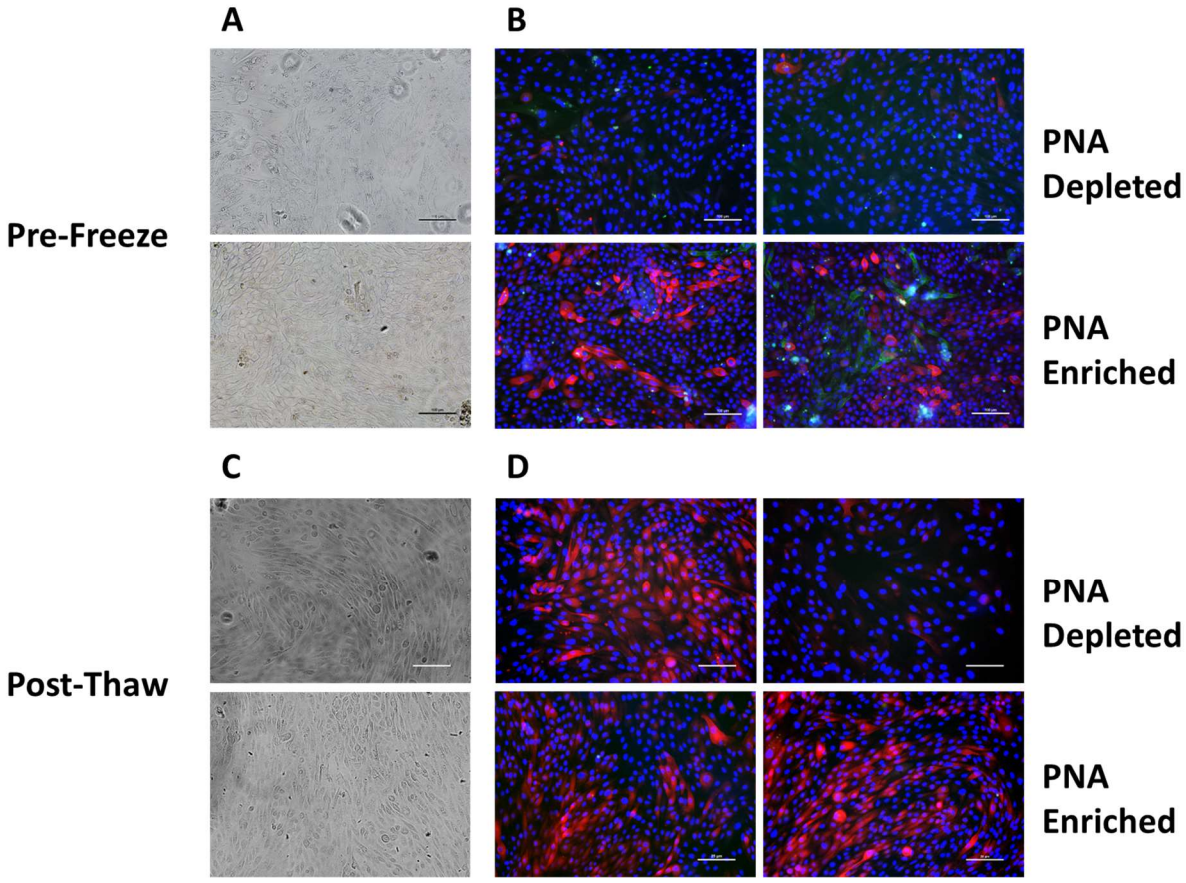

Figure 8. Impact of cryopreservation and re-culture on PNA depleted and enriched RTEC cultures: Brightfield (a & c) and fluorescence (b & d) microscopy of PTF8 P1 RTEC cultures after PNA-based immunomagnetic selection at P0, without cryopreservation (Top) or with after thawing and re-culture (bottom).

We used PNA-based IMS to enrich for RTECs of distal origin from whole kidney isolates. The predominantly distal origin of the resulting PNA+ cultures was confirmed by greater PNA staining than the matched PNA- cultures. The MACS© MS columns we used for the separation procedure have a total cell capacity of 1×10^7 labeled cells and 1×10^8 total cells [68]. The total cell count per kidney is estimated at 5.2×10^7, less than half of which are distal in origin and the PNA bead concentration used in each IMS incubation is sufficient to label 2×10^9 total cells for separation [58] [69]. Despite possessing sufficient capacity to label and selectively retain the entire target cell population, PNA+ cell fractions consistently contained fewer viable cells resulting in fewer initial colonies and less cells generated overall.

The residual PNA staining present in both the pre-freeze and post-thaw cultures indicates that some modifications to the protocol, or additional selection and separation methods, are necessary to achieve more complete separation resulting in pure PNA+ and PNA- RTEC cultures. Furthermore, consideration will have to be taken as to how to maintain features characteristic of distal origin. As described by Hauwaert et al, PTECs are characterized by CD10/13 double positive while single positive cells are heterogenous. Double negative CD10/13 cells have been shown to express more tight junction proteins as well as a higher TEER as previously reported by Denker et al., which is more characteristic of a DTEC phenotype. When cultured in vitro, DTECs frequently dedifferentiate or transdifferentiate and take on a more PTEC-like phenotype, including a downregulation of Tamm-Horsfall protein expression and increased expression of CD13 [36, 61, 70].

We performed ICC on pre-freeze P1 PNA+ and PNA- RTECs cultured in 8-well chamber slides to determine if they expressed markers characteristic of distal and proximal origins respectively **(Figure 9)**. The cultures were stained with the tight junction marker e-cadherin and co-stained with either, KI-67, a cell proliferation maker, megalin, a proximal tubule marker, or TRPV5, a distal tubule marker. In both PNA+ and PNA- cultures, e-cadherin was properly expressed and localized around the cellular periphery. We did not observe a difference in KI-67 signal between either population. However, the PNA+ cultures showed more extensive staining for TRPV5 than the PNA- cultures and conversely, megalin staining of the PNA- cultures was far more abundant than in the PNA+ cultures. Together, these results demonstrate that IMS is a valuable tool for generating RTEC populations enriched for cells from specific nephronal regions. If we can determine conditions required to maintain cells enriched from along the nephron has significant implications for future development of the kidney MPS model by allowing us to study regiospecific tubular nephropathies. Such an advancement benefit further development of this MPS model of KSD considering that the COM crystals most associated with disease progression impacts cells differently throughout the renal tubular epithelium with biomineralization events occurring in the proximal regions impacting those downstream [71].

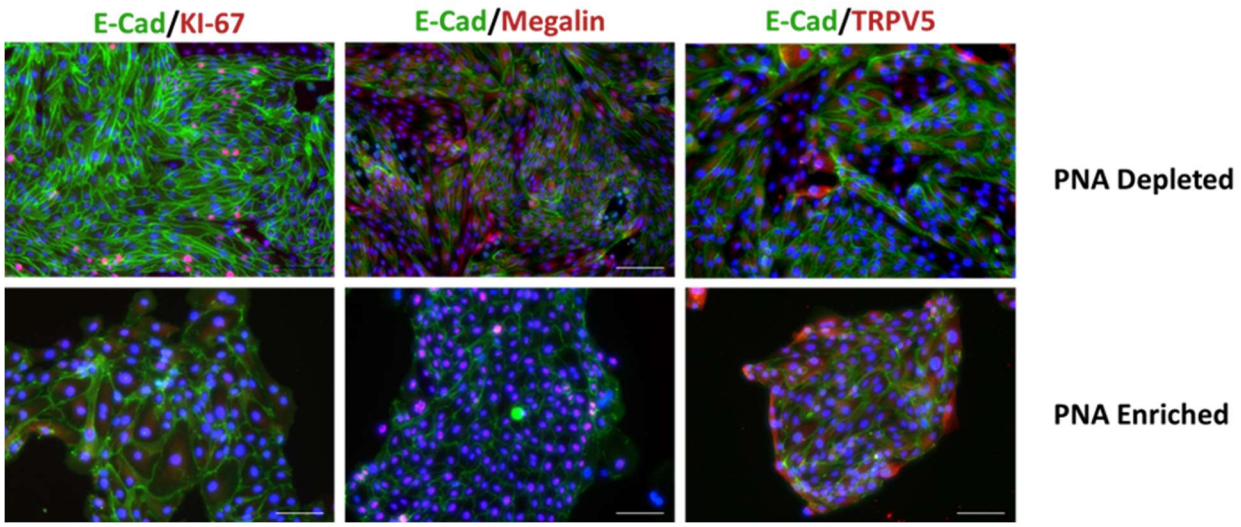

Figure 9. PNA-based immunomagnetic separation on segregates RTEC marker expression: Fluorescent imaging of PNA depleted (Top) and PNA enriched (Bottom) stained for regiospecific markers of RTEC phenotypes (red) and counterstained with the tight junction marker E-cadherin (green) present in all RTEC cell types. (R) KI-67, a marker of cell proliferation, (M) megalin, a proximal tubule epithelial marker, and (L) TRPV5, a distal tubule epithelial marker.

Generation and Physiochemical Characterization of COM crystals.

We developed a protocol for consistently generating preparations of COM crystals as confirmed by crystal morphologies and physiochemical characterization techniques. We initially replicated a previously published protocol to generate a population of COM crystals of differing sizes, shapes and hydration states **(Figures 10 & 11)** [72]. Further analysis confirmed that across all conditions, the crystal populations we generated consisted of almost entirely COM related morphologies composed of shapes consistent with a predominantly COM hydration state **(Figures 12 & 13).** Crystal formation occurred immediately after combining the $CaCl_2$ and $Na_zC_2O_4$ at T_0 and a greater quantity after one hour **(Figure 10a)**. Crystal size and quantity was observed at different temperatures and in two different incubation media, D.I. water and PTEC maintenance media with the aim of assessing potential variation in COM crystal populations in standard short-

term storage (4° C), benchtop (25° C) and treatment (37° C) conditions. The size of the crystals formed varied across the conditions and no trend was seen in the differences between the incubation media at either of the three incubation temperatures. At 37° C, greater crystal formation occurred in D.I. water than in PTEC media. The crystals formed in D.I. water at 37° C overall, were smaller than those formed in PTEC media. The reverse was the case at 25° C with smaller crystals forming in PTEC media than in D.I. water. At 4° C, the COM crystals formed were similar in both size and quantity between both incubation media**. (Figure 10b).** These findings may explain any discrepancy that may arise in future experiments between the calculated concentration of crystals and the effective concentration available for direct interactions with PTEC in both 2D and MPS culture. A combination of reaction conditions were evaluated in order to refine the COM crystal population**.** We combined calcium chloride ($CaCl_2$) and sodium oxalate ($Na_zC_2O_4$) in molar ratios of [0.5 mM : 1 mM], [0.5 mM : 5 mM], [1 mM : 0.5 mM], [1 mM : 10 mM], [5 mM : 0.5 mM], [5 mM : 5 mM], [10 mM : 1 mM] and [10 mM : 10 mM]. In general, higher Ca^{2+} concentrations drove increased the visible yield of COM crystals to a greater degree than did increasing the concentration of Ox^{2-} **(Figure 10c).**

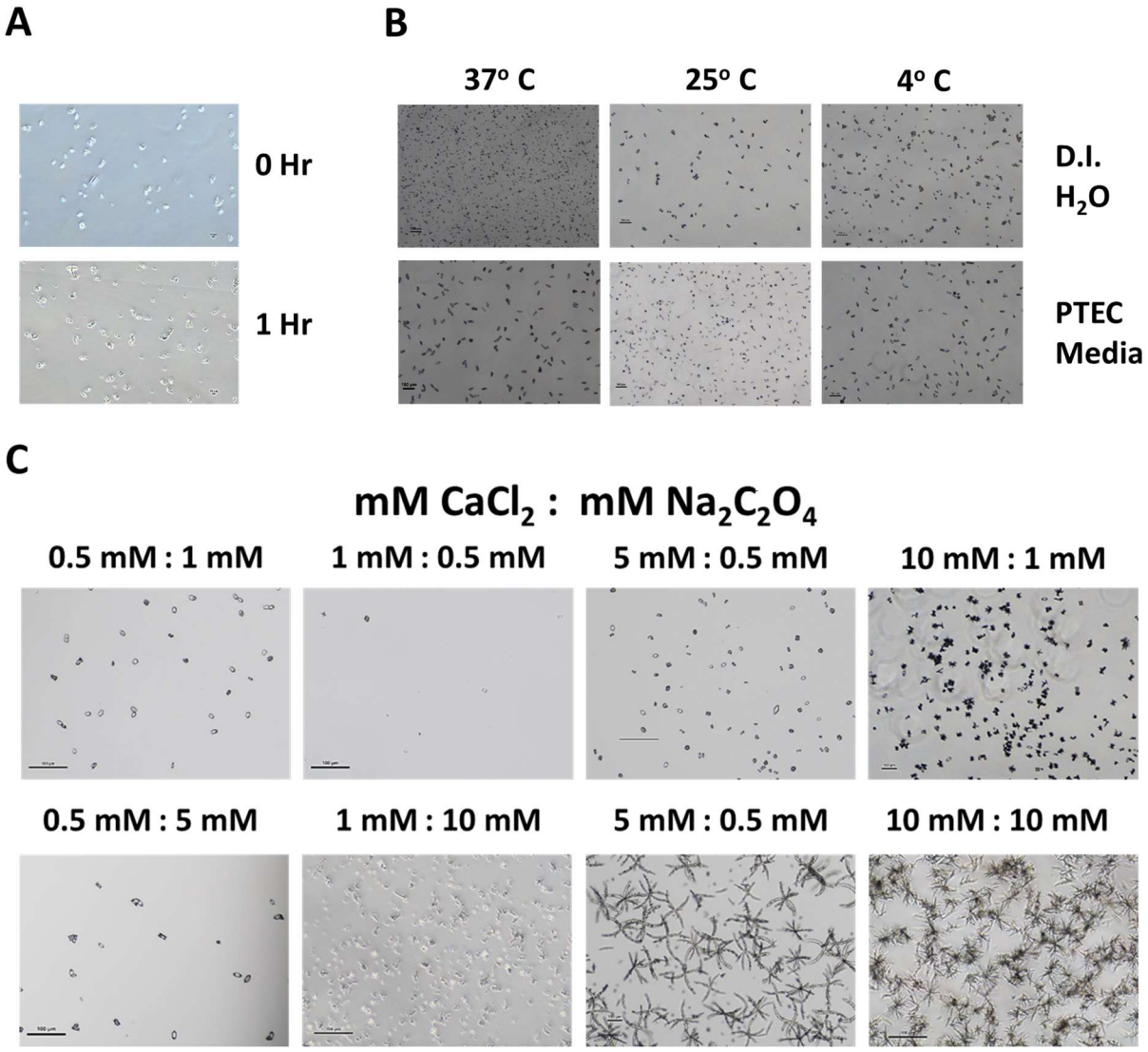

Figure 10. Generating COM micro scale crystals in the lab: Brightfield imaging of; (a) visible crystal formation at 0 and 1 hr, (b) COM crystals resulting from varying $CaCl_2$ and Na2C2O4 (in white) concentrations, (c) testing the impact of temperature and reaction medium (D.I. water vs PTEC media) on resulting batches of CaOx crystals.

Crystal shapes characteristic of COM represented by far the greatest abundance of crystals observed across all preparations (**Figure 11).** COM shapes observed included: hexagonal lozenge (COM-HL), twin hexagonal lozenge (COM-THL), double-twinned COM (DT-COM), multi-

twinned (MT-COM), super-twinned (ST-COM), and hyper-twinned (HT-COM). In contrast COD crystal shapes, primarily tetragonal bipyramidal (COD-TBP) and weddellite (COD-WDD), were rarely observed. Atypical COM (AT-COM) crystals were also frequently observed in crystal preparations **(Figure 12).** SEM imaging of COM preparations were consistent with those found in literature showing primarily sharp edges and greater relative surface area than comparable COD crystals [73]. Importantly, confirmation of crystal shapes consistent with COM means that cell membrane crystal interactions will primarily involve contact with sharp edges and extensive surface area.

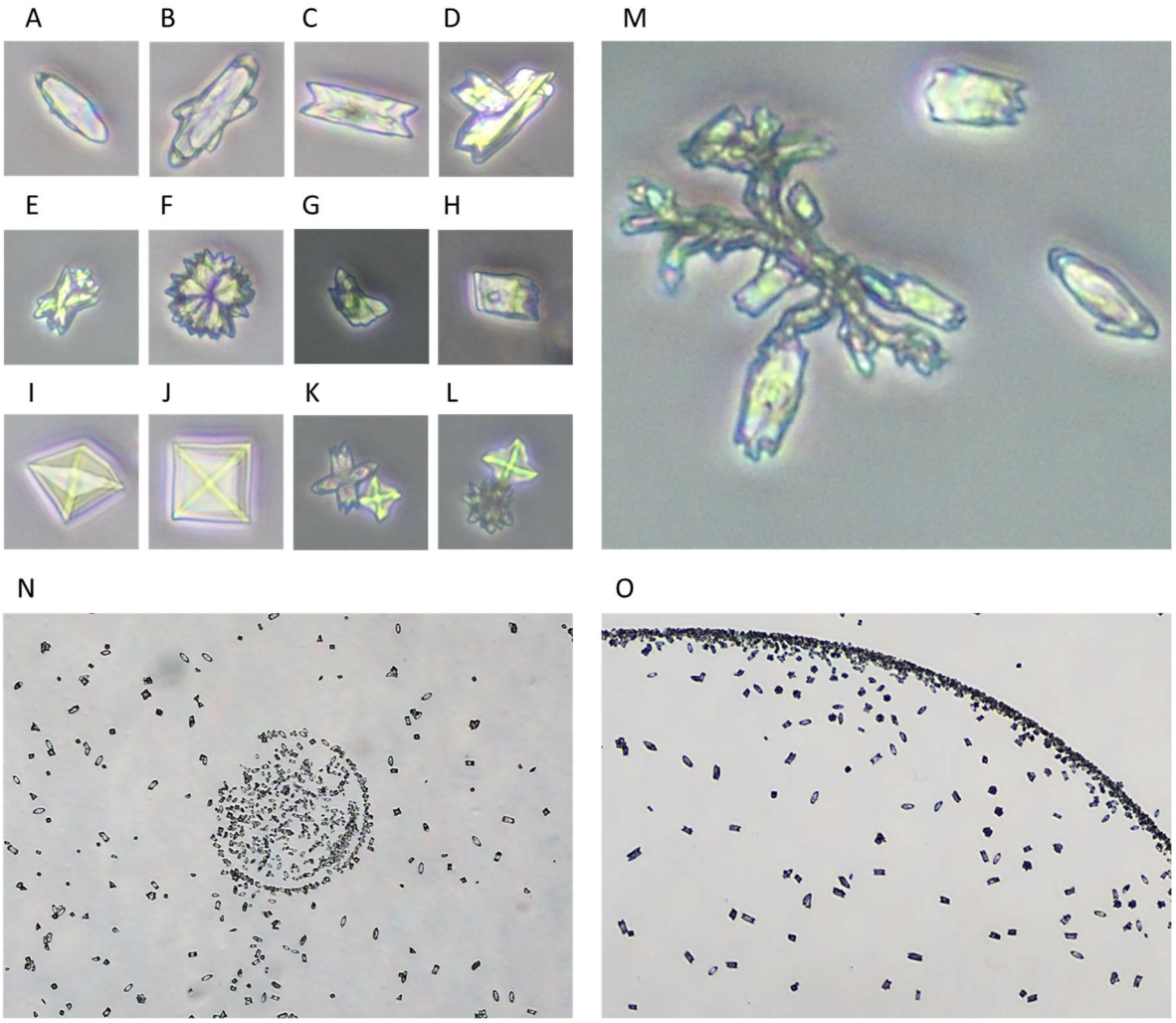

Figure 11. Visual assessment of prepared COM crystals: Phase contrast images depicting various hydration state-dependent crystal shapes including; COM types (a) hexagonal lozenge (COM-HL), (b) twin hexagonal lozenge (COM-THL), (c) double-twinned COM (DT-COM) (d) multi-twinned (MT-COM), (e) super-twinned (ST-COM), (f) hyper-twinned (HT-COM), (g & h) atypical CaOx (AT-CaOx); and COD types (I & j) tetragonal bipyramidal (COD-TBP) or (k & l) weddellite (COD-WDD); (m) a COM dendrite formation during the early growth phase. Phase contrast images at 4X (n) and 10X (o) representative of a typical crystal shape distribution.

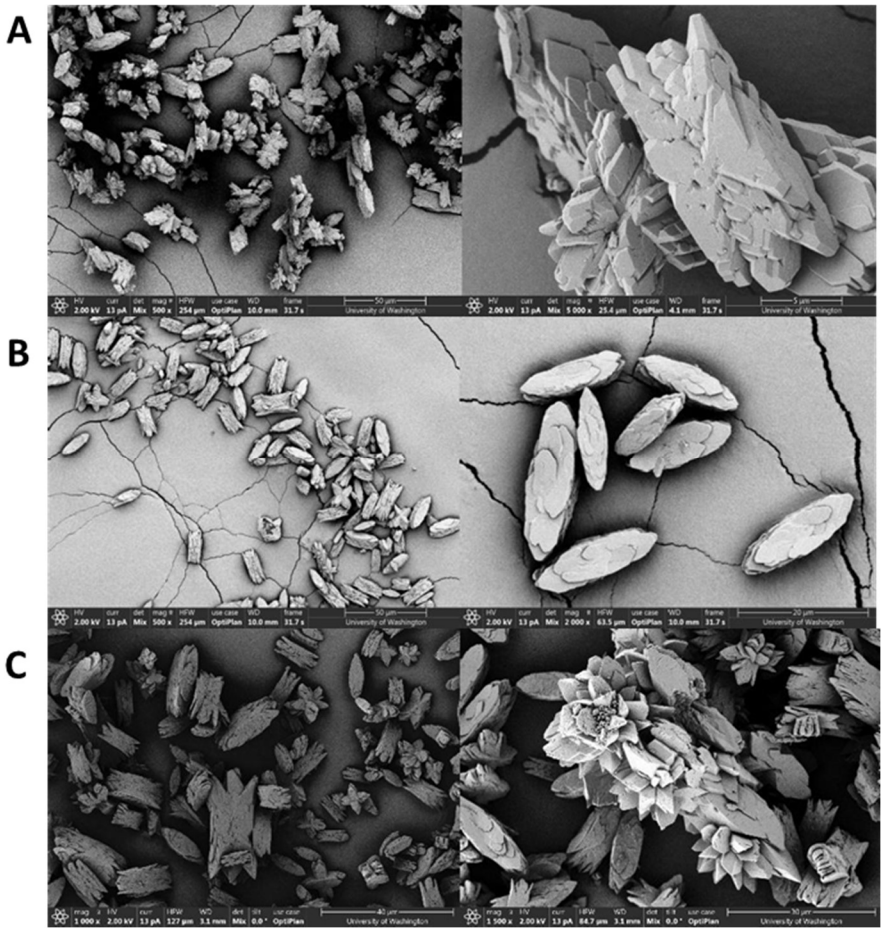

Figure 12. Scanning electron microscopy of COM crystals l: SEM images of COM populations generated under differing conditions. (a) Commercially sourced COM crystals, (b) crystals generated after 24-hour incubation at 27º C with a concentration ratio of 1:1 in a 1000 mL Erlenmeyer flask, (c) crystals generated after 1 hour incubation at 37º C with a concentration ratio of 2:3 in a 1000 mL Erlenmeyer flask, (d) crystals generated after 1-hour incubation at 37º C with a concentration ratio of 1:1 in a 2000 mL Erlenmeyer flask. Ratios are $Na_2C_2O_4$:$CaCl_2$.

We utilized EDS to confirm the chemical composition of these crystal preparations **(Figure 13a).** EDS spectra from these preparations showed the characteristic Ca:C:O ratio of 1:2:4 confirming that the preparations are CaOx. We then used FTIR to assess the hydration state of the COM preparations **(Figure 13b)**. Peaks at 950 cm^{-1} and 885 cm^{-1} confirmed the presence of COM in all preparation. Conversely, we did not observe any peaks at 912 cm^{-1} indicating that no COD

was present. Based on these results, we concluded that this protocol consistently produced preparations of COM crystals suitable for use in future experiments. The resolution of these biophysical techniques was unable to determine the presence of nano-scale COM crystals. While only micro-scale crystals can be confirmed by observations, if OS-related cytotoxic effects characteristic of nano presence observe are in the PTEC model of KSD, this will be strongly indicative of their presence.

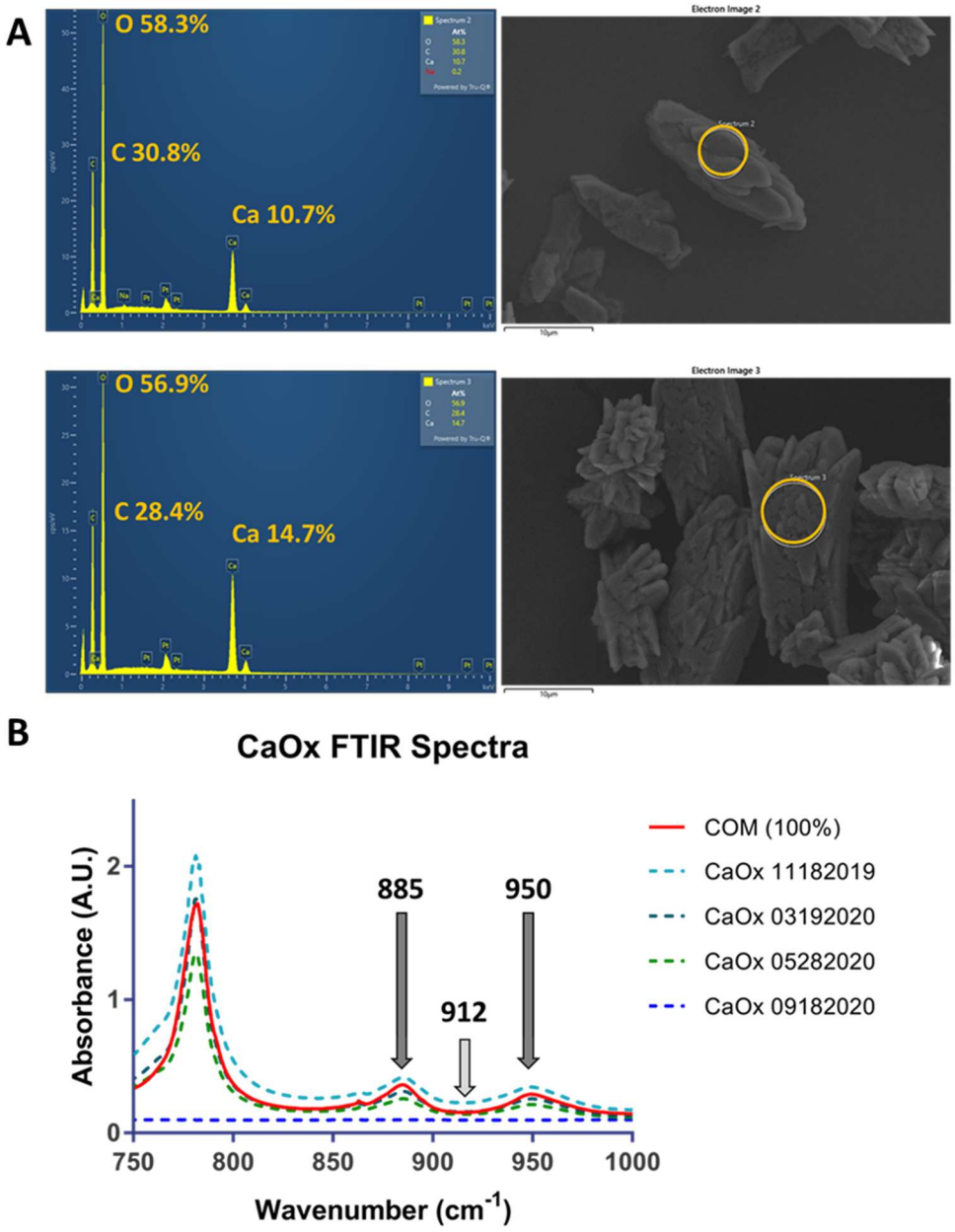

Figure 13. Spectrographic characterization lab generated COM crystals: (a) Energy-dispersive spectrographs (L) of COM crystals generated for use in KC-02 and corresponding SEM images (R) depicting the region sampled, and (b) Fourier-transform infrared spectrographs of COM crystal preparations.

Assessing COM crystal induced cytotoxicity in PTEC 2D culture

COM crystals have been demonstrated to cause cytotoxicity when in direct contact with epithelial cell membranes [74] [75] [76]. Concentrations as low as 200 µg/mL have been demonstrated to increase LDH release and cell death in 2D HK-2 cultures [77]. We exposed 2D cultures of human PTECs to 200 µg/mL COM crystals generated from combining stock solutions of 1 mM $CaCl_2$ and 1 mM Na_2Ox at ratios of [1 mM : 1 mM], [0.5 mM : 1mM], and [2 mM : 1 mM] for 24 hours **(Figure 14).** Despite previously reported studies, we observed no increase in cytotoxicity between crystal exposed cultures and control. Based upon these initial results, we chose to increase the concentration and duration of crystal exposure in all future experiments.

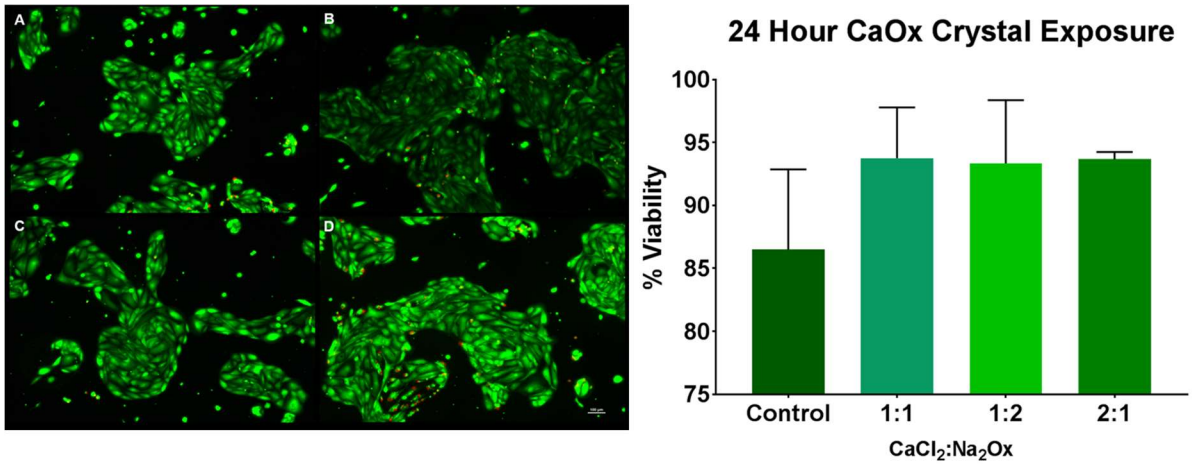

Figure 14. PTEC cytotoxicity after 24-hour exposure to CaOx crystals: (a) Control, (b-d) crystals generated from combining stock solutions of 1 mM $CaCl_2$ and 1 mM Na2Ox at molar ratios; (b) 1 mM : 1 mM, (c) 0.5 mM : 1mM, or (d) [1 mM : 0.5 mM]. Cell viability was measured using via LIVE/DEAD assay. (n =2-4).

To investigate the properties of lab prepared COM crystals as a physical stressor (sheer and rupture cell membranes) and to induce oxidative stress in PTECs, we treated 2D cultures for 12 and 32 hours with either 100 µg/mL COM crystals, 1000 µg/mL crystals, or 100 µM polymyxin B (PMB) as a pro-oxidant positive control (**Figure 15).** We observed no increase in either

CellROX or MitoSOX fluorescence signal between treatments and control at 12-hours. However, after 32 hours, both 100 µg/mL and 1000 µg/mL increased PTEC ROS and superoxide levels of over control, when assayed by CellROX fluorescence imaging, while PMB considerably increased both ROS and cell death in PTECs. This observation is consistent with previously reported COM time-dependent cytotoxicity [78]. When this experiment was repeated for 24 hours on separate RTEC cultures derived from either the cortical or medullary regions, we observed no significant regiospecific responses to COM crystal exposure between either culture source **(Figure 16).** Although it should be noted that we have not characterized molecular differences between proximal and medullary-derived RTECs. From this we conclude that the region the kidney RTECs are derived from did not represent a significant impact on COM induced ROS generation and that future COM exposure studies would run for a duration of 48 hours to account for the significant lag time between the exposure of COM to RTEC cultures.

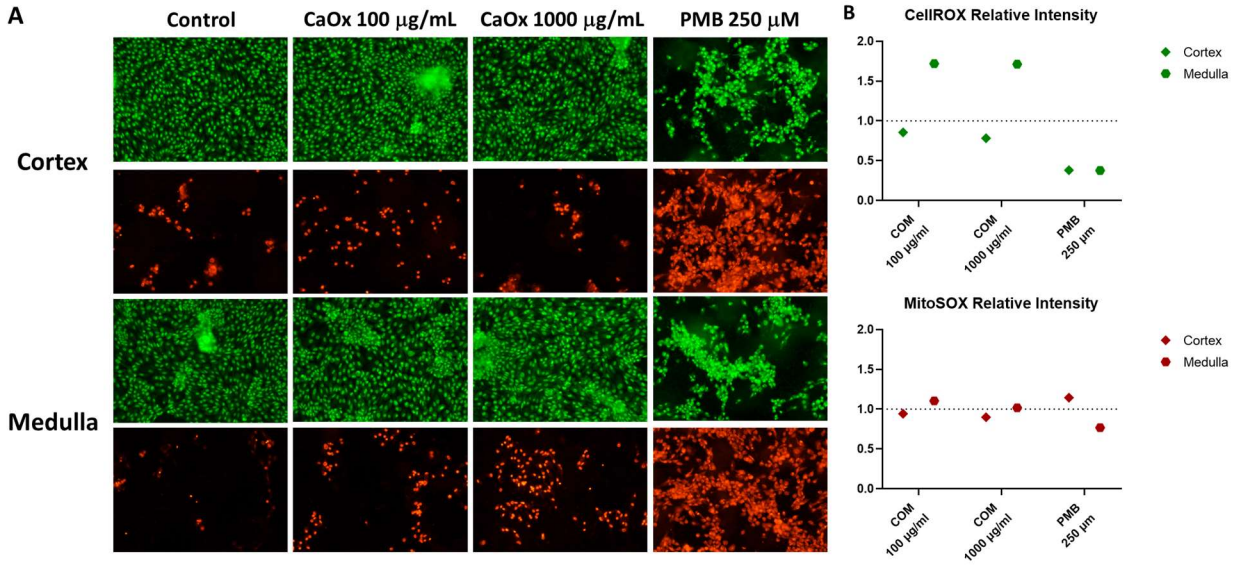

Figure 15. Evaluating COM crystal induced oxidative stress in RTECs cultured from cortex and medulla derived tissue: (a) ROS quantitation in cortex (Top) and medulla (Bottom) derived 2D PTEC cultures after 24-hour treatment with 100 µg/mL COM crystals, 1000 µg/mL COM crystals or 250 µM PMB, (b) fluorescence intensity quantified and normalized to control intensity

values. CellROX (**green**) is an indicator of overall intracellular ROS concentration. MitoSOX (**red**) is an indicator of mitochondrial-specific ROS.

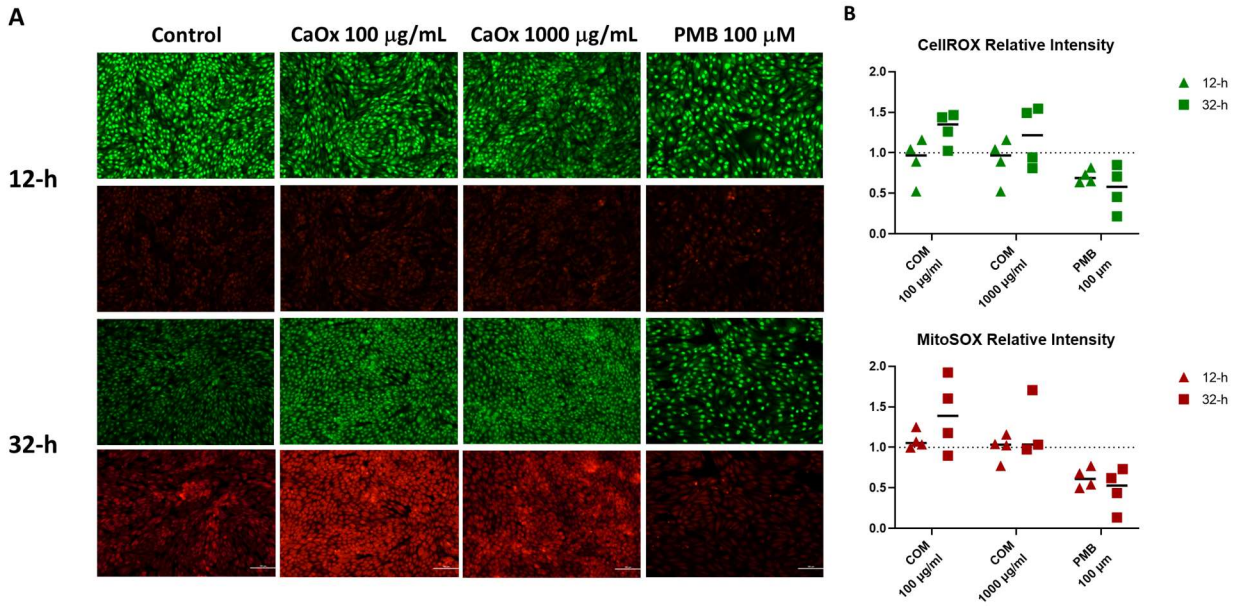

Figure 16. Evaluating the effect of COM crystal treatment duration on oxidative stress levels in 2D RTEC cultures at 12 and 32 hours: (a) ROS quantitation in 2D PTEC cultures after 12-hour (Top) and 32-hour (Bottom) treatment with 100 µg/mL COM crystals, 1000 µg/mL COM crystals or 250 µM PMB, (b) fluorescence intensity quantified and normalized to control intensity values. CellROX (**green**) is an indicator of overall intracellular ROS concentration. MitoSOX (**red**) is an indicator of mitochondrial-specific ROS.

To determine an appropriate pro-oxidative positive control for future experiments, we evaluated the pro-oxidant compounds antimycin A (10 µM), menadione (50 µM), and tert-butylhydroquinone (TBHQ) (50 µM) on PTECs in 2D culture **(Figure 17).** Of these compounds, only TBHQ generated fluorescence CellROX signal greater than control. When assayed by MitoSOX, antimycin A and menadione both increased mitochondrial superoxide release while TBHQ did not. We determined that the ability of menadione to reliably induce elevated superoxide levels in PTECs made it appropriate as a positive control in future experiments. However, current limitations prevent the use of both the CellROX and MitoSOX assays to evaluate cultures within MPS devices, so a different biomarker of PTEC ROS generation is needed.

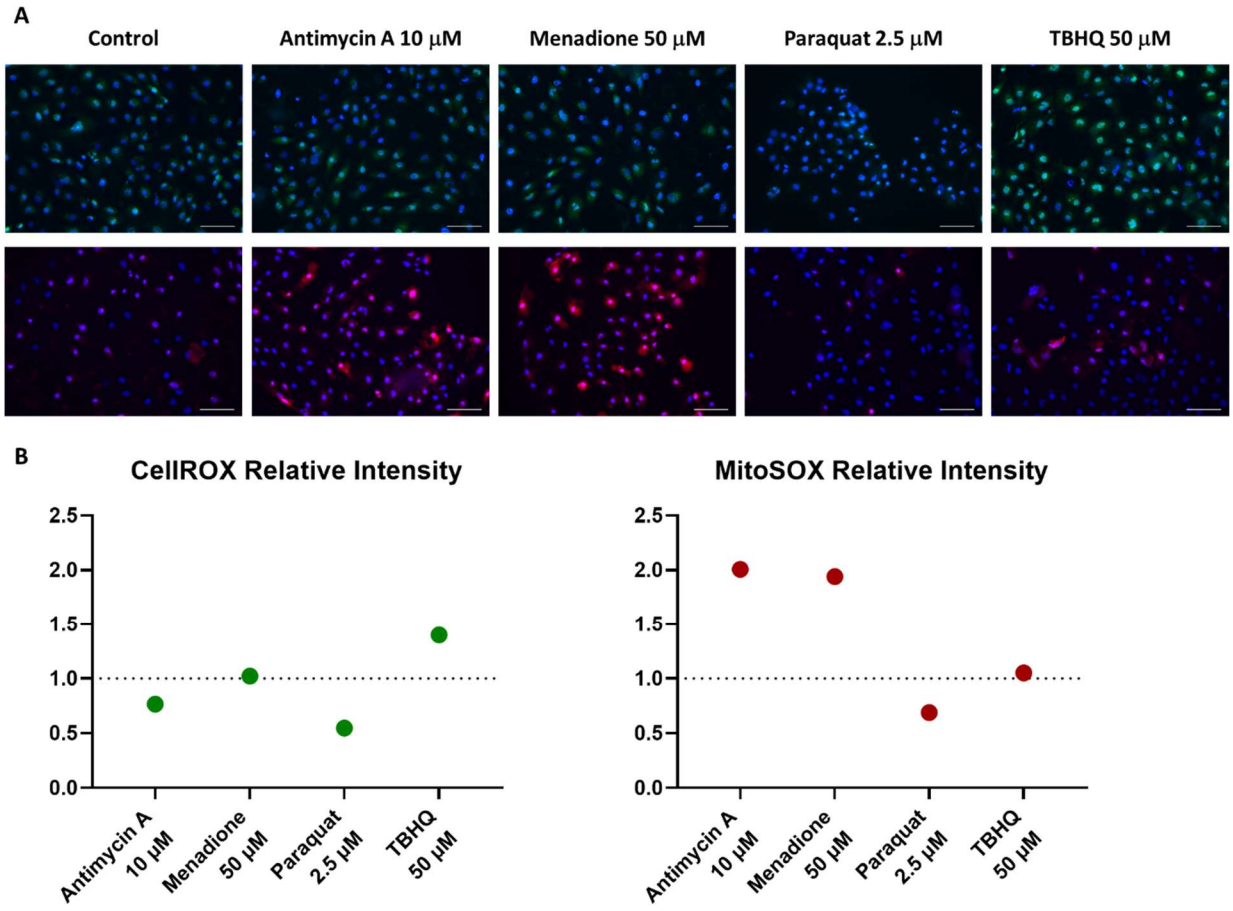

Figure 17. Evaluating oxidative stress inducing agents in 2D HK-2 cultures: ROS in 2D PTEC cultures evaluated by CellROX (**green**) and MitoSOX (**red**) after a 48-hour treatment with PTEC media control, 10 µM antimycin A, 50 µM Menadione, and 50 µM TBHQ. Data is shown normalized to control intensity.

2.5. Discussion

Oxidative stress may link metabolic disorders such as type 2 diabetes, metabolic syndrome, obesity, and hypertension with CKD and KSD. These metabolic disorders are risk factors for, and often co-morbid with both of these renal pathologies. It's been proposed that an environment of local or systemic inflammation associated with the development of one of these conditions may serve to exacerbate the progression of another [79]. In this chapter, the kidney MPS was proved to be an effective model capable of accurately evaluating PTEC nephrotoxicity induced by three pro-

oxidative compounds in 2D culture, and in the 3D continuous flow environment within the MPS device. Three primary prooxidative and nephrotoxic agents were assessed in these studies: the nephrotoxic antibiotic drug PMB, the plant-derived environmental toxin AA-1, and an endogenously generated physio-chemical stressor in the form of COM crystals. The utility of the PTEC MPS in toxicity screening has been discussed previously [51]. In a PME dose escalation study, treated PTEC MPS cultures showed does-depended toxicity characteristic of polymyxin antibiotic nephrotoxicity. The results of this study mirror those generated in a similar study assessing the toxicity of PMB in PTEC MPS [52].

We successfully developed a protocol in our lab to generate preparations of CaOx crystals composed entirely of COM and which were used in these and future experiments to model the early stages of KSD. These crystals mimic the early precursors within urine from which kidney stones ultimately develop. Our initial experiments involved direct exposure of PTEC monolayers to COM crystals for 24-hours and did not result in overt cell death. Further investigation revealed intracellular oxidative stress induction as a mechanism of COM induced cytotoxicity. An ideal positive control for future experiments investigating the role of OS in COM renal toxicity must also induce elevated mitochondrial superoxide release in renal epithelial cultures. Antimycin A and menadione exposure increased mitochondrial superoxide release in HK-2 cells while TBHQ did not, demonstrating that both are suitable options for a positive control in future COM exposure studies. Evidence indicates that menadione may induce intracellular ROS by triggering the release of cytochrome c from the mitochondria, or by impacting mitochondrial membrane integrity. We selected it over antimycin A based on menadione having been demonstrated to cause OS induced cytotoxicity in renal epithelial cells, with DTECs showing greater susceptibility to its effects than PTECs [70, 80, 81]. Experiments in which 2D PTEC cultures were exposed to COM crystals

provided the basis from which our PTEC MPS model of KSD was developed. To our knowledge, no one has investigated the impact of COM crystal exposure in a 3D MPS context. The development, characterization and evaluation of this model is described in detail in chapter 4.

The ability of the model to evaluate the nephrotoxicity of the plant toxin and agricultural contaminant, AA-1 was also tested. Both high dose acute and low dose chronic exposures to AA-1 are considerable health risks of interest globally. In our experiments, 48-hour exposure to AA-1 itself did not induce significant PTEC death. We were in the process of adopting the pneumatic system as these studies were being performed, so we ensured to establish that the MPS model performed as expected in this new context. Tripling the flow rate in a syringe pump setup did not increase cell death, nor did repeating the experiments in the Nortis pneumatic perfusion system. A faster flow rate improves PTEC health in MPS culture by increasing the flow of nutrients, more rapid clearance of cellular byproducts while helping maintain their proper phenotype.

To model long-term chronic AA-1 exposure, PTEC MPS had to be cultured and then treated over durations that significantly exceed those of previous studies performed by our group. Levels of secreted KIM-1 in effluents remained nominal over the duration of both 7- and 12-day treatment with AA-1 and was not significantly impacted by which perfusion platform was used. KIM-1 levels were also consistent between across all treatment groups and control This matches the observation that low exposure of AA-1 was not significantly toxic even after a week. However, the picture is different after roughly three weeks of continuous exposure to AA-1. In this context, even those MPS cultures tested with the low concentration of 1 μM AA-1 showed a significant increase in cell death over control. This duration of exposure lead to catastrophic cell death in devices dosed with 10 μM. This is in marked contrast to the effects of this concentration previously observed at timepoints between 1-12 days. The experiment had to be terminated at 23 days to

prevent further loss of MPS devices to attrition caused by mold and devices drying out due to variations in the humidity they experienced over that duration. However, the condition of the untreated control tubules in those devices that were still in culture after 23 days indicates that significantly longer culture durations are likely achievable. None of the concentrations of AA-1 tested led to an increase in AL-1 adduct formation which is consistent with the absence of a hepatocyte component in these experiments.

While the proximal tubule is the primary site for PMB and AA-1 toxicity, the events underlying the development of kidney stone disease occur across several sections of the nephron. Immunomagnetic cell separation is a valuable method for us to utilize while developing a DTEC MPS model. Our preliminary success with tubular cell separation based on the PNA and LTL suggest that it is the best method to pursue going forward. The yield of PNA+ cells obtained through IMS was significantly greater than from AQP2 based separation. Cells in the enriched for PNA stained strongly for PNA after separation, while the PNA depleted cultures retained moderate to high PNA fluorescent signal. It is not unexpected for PNA+ cells to remain in the depleted cultures, but it does indicate that additional modifications or refinements to the IMS protocol are required for optimal separation of DTECs and PTECs. The fact that PNA enriched DTEC cultures continued to demonstrate extensive PNA staining after cryopreservation suggests that it may be valuable perform IMS on all incoming donor kidneys, since a mixed DTEC/PTEC MPS cultures will reliably take on a more proximal phenotype. Culturing RTECs from whole kidneys without first performing IMS and preserving the DTEC fraction wastes a critical resource necessary to develop a DTEC MPS model.

ICC fluorescence imaging demonstrates that after the first passage, our RTEC cultures exclusively express AQP1, a proximal marker. A potential alternative approach would be to follow

a two-step protocol in which first AQP1+ cells were depleted through negative selection immediately followed by positive selection for AQP2+ cells may be a viable strategy for generating initial DTEC cultures. The PNA based separation method only requires a single antibody binding incubation rather than two as in the case of AQP2 based separation. This makes it the better option as it provides more flexibility when it comes to adapting this method to our cell isolation procedure. However, long-term maintenance of primary human DTECs remains challenging because they are predisposed to transdifferentiate over extended culture into a more proximal phenotype including downregulation of the distal marker THP [70]. We will need to determine specific DTEC culture conditions in both 2D and MPS culture in order to develop a DTEC MPS model. This will be a significant challenge, especially during the injection and seeding of DTEC MPS devices and in maintaining optimal conditions while regularly monitoring their phenotype to validate long-term DTEC characteristics.

3. Development of a Kidney Microphysiological System Hardware Platform for Microgravity Studies

Development of a Kidney Microphysiological System Hardware Platform for Microgravity Studies

Kendan A. Jones-Isaac[1], Kevin A. Lidberg[1*], Catherine K. Yeung[2,3], Jade Yang[1], Jacelyn Bain[1], Micaela Ruiz[1], Greta Koenig[4], Paul Koenig[4], Stefanie Countryman[4], Jonathan Himmelfarb[3] & Edward J. Kelly[1,3]

[1]Departments of Pharmaceutics and [2]Pharmacy, University of Washington, Seattle, WA; [3]Kidney Research Institute, Seattle, WA; [4]BioServe Space Technologies, Boulder, CO.

*Current Address: RayzeBio, San Diego, CA.

3.1. ABSTRACT

Study of the physiological effects of microgravity on humans is limited to non-invasive testing of astronauts. Microphysiological models of human organs recapitulate many functions and disease states. In this communication, we describe the development of an advanced, semi-autonomous hardware platform to support kidney microphysiological model experiments in microgravity.

3.2. INTRODUCTION

The microgravity environment induces many pathophysiological changes that resemble accelerated aging, including wasting of skeletal muscle,[19] bone demineralization,[20] and metabolic and cardiovascular dysregulation.[21], [22, 23] To maintain bone mineral homeostasis, kidneys control the excretion and retention of calcium, phosphate, and other essential ions.[24] They are also responsible for generation of the active form of vitamin D, $1\alpha,25\text{-}(OH)_2$ vitamin D_3, which plays a critical role in a multitude of biological functions including bone health.[25]

Directly evaluation of the impact of microgravity on kidney function at the molecular and cellular level is obviously not feasible in astronauts due to the invasiveness and inherent risks of performing renal biopsies;[31] while it is possible to conduct studies in rodents, the results may not truly reflect changes that occur in humans. To address concerns about the effects of microgravity on human physiology, the National Center for Advancing Translational Sciences (NCATS) at the National Institutes of Health created the "Tissue Chips in Space" program (Tissue Chips in Space | National Center for Advancing Translational Sciences (nih.gov)) that leveraged novel tissue engineering platforms to recapitulate human physiology in the environment of space. Selected research teams each sent two projects to the International Space Station National Lab (ISSNL) during the four-year funding period.

Microfluidic-based microphysiologic systems (MPS) represent an advancement in cell culture techniques aimed at better replicating the tissue-specific *in vivo* environment. We have previously reported our development of a MPS-based model of the kidney proximal tubule (PT-MPS) utilizing a commercially available platform developed by Nortis Inc.[38] The Nortis™ system is designed for use with a tubing-free pneumatic-driven pump system but requires a

substantial footprint, presents logistical challenges within the lab, and is not suitable in all research contexts. Therefore, the Kidney Chip Perfusion Platform (KCPP), a piston-driven device, was developed by BioServe Space Technologies, a University of Colorado (Boulder)-based implementation partner and payload developer, to support the MPS-based kidney proximal tubule model. The PT-MPS has been used to study a variety of disease states (e.g., aristolochic acid nephropathy and proteinuria[43, 44]) and the responses to drug/xenobiotic-induced kidney injury.[39, 45, 46] In addition, the robustness and reproducibility of this system was independently tested in collaboration with the NCATS-funded Tissue Chips Testing Centers.[47, 48]

To test the premise that microgravity can accelerate aging/disease progression, we evaluated proteinuria, kidney vitamin D metabolism, and nephrolithiasis (kidney stone disease) in a microgravity environment.[49] Adaptation of the system for installation into the infrastructure aboard the ISSNL, required the creation of a revolutionary hardware support system which required as 88% reduction in footprint, more than 2500 custom engineered and manufactured components, and independent control of temperature, humidity, and gas composition. Herein we report the development of the KCPP in support of two missions to the ISSNL.

3.3. KIDNEY CHIP PERFUSION PLATFORM SYSTEM OVERVIEW

For this project, we developed the KCPP hardware, addressed NASA safety and regulatory requirements, and facilitated the transition to a space flight certified and capable system. The KCPP is a precision, syringe pump-based platform designed to perfuse up to six Nortis™ Triplex (each unit has three independently perfused tubules) PT-MPS built to support NIH/NCATS Kidney Cell 1 and 2 experiments. The platform is composed of five components, the kidney MPS, the MPS housing and valve block, media cassettes, fixative cassettes, and the programable precision syringe pump **(Fig. 1)**. Each KCPP as shown in **Fig. 1** is comprised of over 2500 custom-designed and machined components. In the lab, preparing and assembling these components for experiments is a lengthy process and requires sustained, active engagement. The crewmembers aboard the ISS are allocated a limited and fixed number of hours to conduct scientific experiments and operate on a strict schedule. The major innovation of the KCPP compared with the in-lab process is a dramatic reduction in complexity and time required to perform experiments. For example, in the lab, switching between maintenance and experimental media can be a multi-hour effort. This process was simplified with a piston-driven pump interfacing the MPS housing and valve block that can accept pre-loaded media or fixative cassettes. The pump provides a continuous flow of media or fixative while maintaining temperature control at 37° C. The pump utilizes a stepper motor to provide translation of a carriage which simultaneously depresses 18 plungers. Preloading the media and fixative cassettes on the ground during the final pre-launch preparation phase streamlines the on-orbit protocol followed by the assigned astronaut on board the ISSNL. Additionally, the software for the pump only requires 5 operating modes for the experiment: the “Purge” command initiates the pump to engage the syringe pistons an prime the channels connecting the cassettes and the

MPS, the “Run” command initiates perfusion with media at 0.5 µL/min, the “Fix” command perfuses fixative at 10 µL/min, the “Retract” command resets the pump plunger positions for sample housing and valve block and media/fixative cassette removal, and “Halt” stops all piston movement. The perfusion rate for media and fixation can be reprogrammed as necessary. While the KCPP is a complex work of engineering, the interface for users on the ISSNL is intuitive and user-friendly.

Media is loaded into nine channels separated by effluent bag cavities within one media cassette. The media is contained in the channels between an O-ring piston and a septum. A cannula from the valve block pierces the septa when installed and allows the piston to push media into the PT-MPS. The media flows through the PT-MPS and is collected in the effluent bags that are sealed with septa that are also pierced by cannula. The effluent bag cavities have containment plugs with O-rings on a retention plate. The waste media fills the effluent bags and is contained for post-flight analysis.

Chip Housing & Valve Block

The MPS housing and valve block system is a protective sealed enclosure, designed with functions for purging bubbles during media or fixative cassette installation (**Fig. 2)**. Considerable effort is taken in the lab to mitigate the risk of bubbles entering the MPS since this will lead to disruption of media flow and compromise the integrity of the PTEC lumen. Since air bubbles in microgravity do not experience the same effects of buoyancy as on earth, they can readily bypass the bubble traps. The enclosure interfaces to the media cassette and fixative cassette via four alignment pins and 18 cannulae. The housing vents are sealed with two adhesive covers during launch operations to maintain a 5% CO_2 and 100% humidity within the MPS housing. The valve block is designed with a valve bar system to direct flow through the valve block. Purging is performed when the valve bar is in the upper position as shown in **Fig. 2**. When the valve bar is in purge mode, flow is diverted from the PT-MPS directly into the effluent bags; when the valve bar is in flow mode, flow is directed into the PT-MPS.

Media and Fixative Cassettes

The media cassette was designed to integrate directly with the chip housing and valve block and the KCPP to provide sufficient media to perfuse the PT-MPS for 10 days at a rate of 750 µL/day **(Fig. 3 A)**. The cassette consists of nine individual channels machined into an Ultem™ thermoplastic block. Each channel has a usable volume of 7.75 mL. The fluid is dispensed by mechanical plunger translation via the syringe pump. Once the fluid has passed out of the cassette and through the PT-MPS it returns to the housing and is stored in individually sealed bags in a chamber adjacent to the media channels. The fluid interfaces with the valve block via 18 cannulas piercing the corresponding septa in the bottom of the media cassette.

The sample effluent collection volume is sealed at the top of the cassette which provides an additional level of containment. When two levels of containment are required during cassette exchange operations, the KCPP system can be operated within the Microgravity Science

Glovebox or Life Science Glovebox which provides an additional level of containment (**Suppl. Fig. 1**).

The fixative cassette is a modified version of the media cassette **(Fig. 3 B)**. The cassette provides fixative for the final stage of the experiment to preserve the cells in the PT-MPS. The cassette has nine individual channels machined into a block of Ultem™. Each channel has a maximum volume of 3.8 ml. The fluid is dispensed via mechanical plunger translation via the syringe pump. Once the fluid has passed out of the cassette and through the PT-MPS it returns to the housing and is absorbed into layers of disposable absorbent material. The fluid interface to the valve block is via 18 cannulas piercing the corresponding septa in the bottom of the fixative cassette. The fixative cassette provides two levels of containment using O-rings on the pistons. Additional containment can be provided via outer bags when necessary.

KCPP Integration

The integration and assembly of the individual components of the KCPP are shown in **Fig. 4.** In brief, **Figs. 4A-C** depicts a valve block, PT-MPS and integrated assembly, respectively. A media cassette is shown in **Fig. 4D** and all the assembled components are seen in **Fig. 4E**.

KCPP Space Reduction Advancements

Although the overall footprint of an individual PT-MPS in the lab is small, the specialized equipment required to perfuse and maintain the devices is relatively large. As shown in **Fig. 5A/B**, the individual components required to run experiments in a conventional laboratory require an entire tissue culture incubator. The availability of space on ISSNL is extremely limited; the KCPP reduces the required footprint 8-fold (1100 L to 136 L) allowing 24 PT-MPS to be housed and perfused within the locker space allocated on board the ISSNL (**Figs. 5C-E**). We have previously used commercially available syringe pumps to run PT-MPS experiments, 24 PT-MPS require eight pumps to independently perfuse each of the 72 PT-MPS tubules. As seen in **Supplementary Fig. 2,** only two pumps can be used per tissue culture incubator, necessitating four separate incubators to maintain 24 PT-MPS. In addition to the significant space reductions from the KCPP, we have also eliminated the use of tubing, as the PT-MPS directly interface with the media blocks in the valve assembly. With syringe pumps, each individual PT-MPS tubule requires approximately 1 meter of tubing to connect media syringes outside of the incubators with PT-MPS within the incubator (**Suppl. Fig. 2**). Thus, in addition to creating a simplistic user-interface for operation on the ISSNL, the KCPP exponentially shrinks the footprint requirements compared to conventional terrestrial PT-MPS experiments.

3.4. TESTING & VALIDATION OF THE KCPP HARDWARE

An experiment validation test (EVT) was performed prior to launch to assess the ability of the perfusion platform to maintain kidney PT-MPS cultures over the duration of the proposed experiments (**Fig. 6**). Kidney PT-MPS were loaded into the MPS housing and then integrated with the valve block and then into the perfusion platform. The devices were then cultured for six days in maintenance media to simulate a period of acclimation to microgravity. At day six,

maintenance media cassettes were exchanged for treatment media cassettes and perfusion was continued for a 48-h treatment phase. At day eight, treatment media cassettes were removed and exchanged for fixative cassettes containing either RNAlater® or formalin. The effluent from both the maintenance and treatment media were stored at -80°C for later analysis. Once the fixative cassette was integrated with the system, fixative/preservative was perfused for 1 hour after which the platform components were deintegrated and the PT-MPS were stored at -80° C or 4° C for later analysis.

Kidney Injury Molecule-1 (KIM-1) is a protein secreted into the urinary filtrate by proximal tubule epithelial cells (PTECs) and is highly upregulated during acute kidney injury.[82] To assess the general health of our PT-MPS during the EVT, we measured the secretion of KIM-1 in effluents. We have previously shown that basal secretion of KIM-1 by PT-MPS is low but is markedly increased in response to nephrotoxic insults.[46-48] As shown in **Fig. 7**, we observed low levels of KIM-1 from multiple PT-MPS evaluated in the EVT. For reference, a sample of 2D PTEC culture supernatant was included, as KIM-1 is present at greater levels in proliferating 2D cultures.[47]

KCPP System Performance

To date, we have successfully completed two launches of the KCPP system to the ISSNL, on board SpaceX Commercial Resupply Services mission 17 (CRS-17) and SpaceX CRS-22. On the first launch we evaluated vitamin D metabolism and proteinuric responses, the second launch studied a calcium oxalate crystal model of nephrolithiasis. To assess overall performance of the KCPP hardware, we evaluated the ability to recover PT-MPS effluents for biomarker analyses as well as successful perfusion of RNAlater™ for gene expression studies. The basic study design and timelines for CRS-17 and CRS-22 are shown in **Fig. 8A/B**, respectively. Each launch consisted of 24 PT-MPS in-flight (microgravity) with a matched cohort of 24 ground-based PT-MPS. The CRS-17 launch consisted of 4 different PTEC donors (two males & two females) while CRS-22 included 6 different donors (three males & three females). The number of samples obtained for RNAseq analysis are shown in **Tables 1** and **2** for CRS-17 and -22, respectively while **Tables 3** and **4** show a similar breakdown for effluent retrievals for CRS-17 and -22, respectively. The criteria for determining a "usable" sample for RNAseq was based on the ability to retrieve RNA from the PT-MPS tubules with a detergent solution, and subsequent total RNA isolation, Bioanalyzer™ RNA integrity determination and RNAseq analysis. The criterium for "usable" sample for effluent analysis was based on retrieval of media in individual effluent bags after thawing of the KCPP media cassette blocks. It is worth noting the differences in the rates of "usable samples" between CRS-17 and CRS-22. In CRS-17, approximately 30% of the samples (RNAseq and effluents) were unusable for both flight and ground due to mold contamination of the PT-MPS. In contrast, nearly 100% of the samples were usable in CRS-22. The mold contamination observed in CRS-17 was not related to KCPP performance. Instead, it was driven by a combination of multiple launch delays that necessitated greater

handling/transport of the PT-MPS from standard cell culture incubators to launch lockers and small amounts of media which leaked from the cell injection port on the PT-MPS. To mitigate these issues for CRS-22, we employed PT-MPS cleaning protocols as well as applied a medical-grade silicone-based sealant (Silastic A®) over the PT-MPS cell injection ports. It is also worth noting that the issues with launch delays in CRS-17 did not occur with CRS-22.

3.5. CONCLUSIONS

KCPP is an integrated, automated, piston-based perfusion platform and self-contained cell culture environment designed to support MPS-based life sciences experimentation on board the ISSNL. Its compact design enables a significant reduction in the logistical challenges and spatial footprint required to implement these experiments aboard the confined space of the ISSNL. KCPP has been verified and space flight certified and is in compliance with current NASA safety and interface requirements for space flight and use aboard the ISSNL. The system has been successfully utilized to support two space-based experimental studies designed to test the impact of microgravity on the function and pathophysiology of PTECs cultured in MPS aboard the ISSNL. In each instance, KCPP performed nominally and facilitated the execution of experiments otherwise impossible to be conducted terrestrially in simulated microgravity. The improvement in the percentage of samples retrieved between missions emphasizes the importance of optimizing pre-flight preparation and handling of the MPS devices when adapting terrestrial lab-based protocols for use in microgravity. Looking to the future, extended studies using the KCPP system will facilitate the understanding of the long-term effects of microgravity on renal physiology as well as the effects of space radiation. We contend that autonomous MPS-based studies can be used to predict human health concerns caused by solar/cosmic radiation and microgravity that may occur during long- term human space exploration.

3.6. ACKNOWLEDGEMENTS

This work was supported by the National Center for Advancing Translational Sciences (UH3TR000504, UG3TR002158 and UH3TR002178), jointly by the National Center for Advancing Translational Sciences and the Center for the Advancement of Science in Space (UG3TR002178), the National Institute of Environmental Health Sciences (P30ES00703 & T32ES00732) and an unrestricted gift from Northwest Kidney Centers to the Kidney Research Institute. BioServe's work was supported in part by NASA contracts 80JSC020F0019 and 80JSC017F0129. We would like to thank the Life Science and Research Support Staff at Kennedy Space Center, most notably John Catechis and Anne Currin. In addition, we would like to express our gratitude to SpaceX and NASA for supporting our studies on CRS-17 and -22, in particular the astronauts Christina Koch & Anne McClain (CRS-17) and Megan McArthur & Mark Vande Hei (CRS-22). Finally, we would like to acknowledge the members of the BioServe Space Technologies team who enabled the successful design, development and launch of the KCPP.

3.7 MATERIALS & METHODS

Tissue Acquisition & Cell Culture

Whole human kidneys that were not suitable for human transplantation were obtained from Novabiosis, Inc. (Research Triangle Park, NC) with all patient identifiers removed in accordance with a University of Washington-approved IRB protocol. Primary human proximal tubule epithelial cells (PTECs) were isolated by mechanical and enzymatic dissociation and cultured as previously reported.[83] PTEC cultures were maintained serum-free in DMEM/F12 (Gibco, Grand Island, NY, Cat. #11330-032) supplemented with 1x insulin-transferrin-selenium-sodium pyruvate (ITS-A, Gibco, Cat. # 51300044), 50 nM hydrocortisone (Sigma, St. Louis, MO, Cat. # H6909), and 1x Antibiotic-Antimycotic (Gibco, Cat. #15240062). Upon reaching 75-80% confluence, PTECs were passaged by enzymatic digestion with 0.05% trypsin EDTA (Gibco, Cat. #25200056) and manual cell scraping to obtain a single-cell suspension which was subsequently neutralized with defined trypsin inhibitor/DTI (Gibco, Cat. #R007100) at a volume:volume ratio of 2:1 DTI:trypsin, cells were then pelleted by centrifugation at 200 x g for 7 minutes, resuspended in maintenance media, and plated in cell culture treated flasks at >25% confluency (referred to as passage 1 or P1).

Preparation of Nortis Kidney MPS

Kidney MPS devices were purchased from Nortis, Inc (Woodinville, WA) and prepared as previously reported.[38] In brief, for all experiments run for EVT, CRS-17 &CRS-22, PTECs of passage 2 or lower were used from each individual donor kidney. In the cases of experiments run for CRS-17 & CRS-22, PTECs were shipped on dry ice to a lab at Kennedy Space Center. Following recovery from cryopreservation and expansion in 2D culture, MPS were seeded and allowed to culture as described in **Figs. 6 & 8**.

Quantification of organ-specific injury biomarker KIM-1

DuoSet© ELISA kits were used to quantify human KIM-1 (R&D Systems, Minneapolis, MN, Cat. #DY1780B) in PT-MPS effluents following the manufacturer's protocol. In brief 50-100 µL of effluent were tested in duplicates and concentrations determined based on the standard curves generated from manufacturer-supplied controls.

4. Evaluating the Impact of Microgravity on a PTEC MPS Model of Kidney Stone Disease

4.1. Introduction

The kidney is a primary organ of excretion responsible for efficient elimination of both endogenous and exogenous water-soluble waste compounds through the formation of urine. It is estimated that 15% of the US adult population have developed some degree of chronic kidney disease [1]. Kidney dysfunction can precipitate serious medical conditions including proteinuria, osteoporosis, and the development of nephrolithiasis kidney stone disease (KSD). Nearly 12% of the global population will develop KSD in their lifetime with the experience being reported as exceedingly painful and debilitating for the patient. Furthermore, estimated recurrence rates for KSD have been reported between 6.1% and 66.9% further compounding the considerable disease burden on the individual patient and economic strain on healthcare systems globally [2]. The development of KSD results from nano and micron-sized crystalline aggregations within the tubule lumen. These deposits subsequently aggregate, forming larger stones, as they pass through the urinary system causing tissue damage and blocking urinary filtrate flow. Roughly 80% of kidney stones contain calcium in the form of crystalized calcium phosphate (CaP) or calcium oxalate (CaOx) either individually or in combination.

While the mechanisms that lead to the formation of kidney stones are not yet fully understood, evidence indicates that the nidus of stone formation occurs in the basement membrane of the LoH [4]. Elevated calcium levels in the urinary filtrate resulting from increased bone resorption in microgravity is a risk factor for developing kidney stone disease (KSD) and several epidemiological studies have reported a history of KSD as a potential risk factor in the development and progression of CKD [6]. Several theories describing the pathophysiology of stone formation in the nephron have been proposed, but an overarching similarity involves

particle retention and an initial nidus for stone formation, such as a crystal or an interstitial plaque. Stationary nidi have been found in renal papillae below Loops of Henle and near the distal collecting duct [8]. Over time, ions use such nidi to form microscopic crystalline structures and eventually, calculi.

Exposure to microgravity increases the risk of kidney stone disease in humans [32]. The conditions experienced by in crewmembers stationed on the International Space Station result in a dehydration-like state caused by altered body fluid distribution, accelerated bone and muscle atrophy, and oxidative stress responses to elevated ROS generation during spaceflight [32]. Renal dysfunction and progression of disease states is frequently accelerated and exacerbated in microgravity. Extended exposure to the environment present during spaceflight increases inflammation and oxidative stress response [33]. Altered physiology and urine chemistry resulting from exposure to microgravity increases the risk for astronauts of developing kidney stones [34]. In addition to the physiological impacts, dietary factors such as increased dietary protein and sodium can of promote kidney stone formation elevating the risk to crewmember health and mission success [11, 32]. A recent study characterized the incidence rates for CaOx kidney stones in astronauts to quantify the impact of microgravity on the relative risk of developing KSD. The authors reported that a 28% increase of prescribed fluid intake during spaceflight would be required to reduce the relative risk to a pre-flight level and noted that countermeasures against microgravity induced bone reabsorption could reduce this recommendation. This situation in which spaceflight induces alterations in kidney stone disease risk relative to terrestrial 1G highlights the ever-growing confluence of traditional terrestrial

biomedical research and space-based endeavors is continuously revealing new paths of investigation.

Reactive oxygen species (ROS) induced oxidative stress is a feature of many pathologies, both as a cause and an outcome. Cardiovascular disease, arthritis, diabetes, Alzheimer's disease and various metabolic syndromes have all been linked to elevated levels of oxidative stress [17]. Oxalate, a primary component in ~64% of all kidney stones, and has been shown to induce oxidative stress, mitochondrial damage, and immune response signaling [12]. Oxalate exposure to the proximal tubule epithelial cell line HK-2 led to increased IL-6 secretion [18]. Calcium oxalate monohydrate (COM) and dihydrate (COD) crystals are commonly observed constituents in the urinary filtrate with COD crystals being more abundant in normal urine and COM more abundant in stone formers. These crystals are present in sizes ranging from <50nm to >10μm with larger sizes being more associated with developing KSD [5]. Micron-sized crystals physically interact extensively with the tubule epithelium and resulting in extracellular matrix disruption, phospholipid degradation and outer membrane rupture caused by physical contact with CaOx crystals. In these cases, cell death is most frequently necrotic in nature. Conversely, nano-sized crystals readily transit the apical and lysosomal membranes precipitating lysosome dissolution, release of free Ca^{2+} and Ox^{2+} and disruption of mitochondrial membrane potential resulting in increased ROS generation and oxidative stress responses [12]. In this scenario, resulting cell death will be apoptotic in nature (Fig. 1) [5].

Cellular oxidative stress response to ROS is a key feature in the pathogenesis and progression of KSD. Once generated, ROS readily react and modify several classes of endogenous biomolecules creating covalent adducts or lesions which disrupt normal cellular functions.

Oxidative modification of polyunsaturated lipids can disrupt membrane function, adducted amino acids can lead to malformed proteins and oxidation of specific co-factors leads to inactivated enzymes. Oxidation of the nucleic acid base components of DNA and RNA are readily oxidized by superoxide ($O_2^{\bullet -}$) radicals resulting in mutagenic lesions in the dsDNA template and the production of abnormal proteins from modified mRNAs [26, 27]. Guanine has the lowest oxidation potential of the nucleic acid bases resulting in a high susceptibility to oxidation by ROS forming the oxidized DNA product 8-oxo-7,8-dihydro-2'-deoxyguanosine (8-oxo-dGsn) and oxidized RNA product 8-oxo-7,8-dihydroguanosine (8-oxo-Gsn). Both of these oxidatively generated nucleic acid damage products have been studied as urinary biomarkers for chronic kidney disease (CKD) and their levels are elevated in the urine of patients with kidney stone disease [28-30]. 8-oxo-dGsn is by far the most studied and abundant modified product and progressive accumulation of 8-oxo-dGsn DNA lesions have long been considered as a marker of progressing physiologic age [26]. However, the correlated RNA product, 8-oxo-Gsn, has been less studied. Relative to DNA, mRNA is more abundant, differentially localized, less stable and lacks repair machinery. Due to these differences, 8-oxo-Gsn potentially represents a biomarker more responsive to in-vitro experimentation and provides a more representative snapshot of cellular response to oxidative stress conditions.

In Chapter 2, a microphysiologic model of the proximal tubule (PT-MPS) was used to assess the impact of nephrotoxic impact of a selection of pro-oxidative agents, including COM crystals prepared in the lab representing the principal early constituents of oxalate containing kidney stones. We describe here a test of the impact of spaceflight at the International Space Station National Laboratory (ISS-NL) on our PT-MPS model of KSD and compare these results to

a replicate ground study conducted concurrently at Kennedy Space Center (KSC). To evaluate the response of the proximal tubule epithelial cells (PTECs) to conditions replicating the early stages of kidney stone disease, we challenged the PT-MPS with micron-scaled calcium oxalate crystals with the aim of identifying biomarkers reflective of renal tubule response to micro-crystal exposure on earth and in orbit. Citrate supplementation in the form of potassium citrate (KCit) is an established pharmacologic countermeasure which has been demonstrated to decrease the risk of kidney stone formation in spaceflight crew members by reducing hypercalciuria [11]. Citrate inhibits stone formation by preferentially complexing with Ca^{2+}, preventing crystal nucleation and aggregation [9]. We also evaluated the effects of citrate in our MPS model of nephrolithiasis.

4.2. Materials & Methods

Tissue Acquisition & Cell Culture

Donor tissue acquisition and all cell culture methods were as previously described in Chapters 2.3 and 3.3.

Test Compounds & COM Microcrystals

Stocks of AA-1, menadione, TBHQ, KCit, and COM crystals were obtained previously as described in Chapter 2.

KCPP Hardware

Use of the KCPP for the maintenance of PT-MPS devices and exposure of pro-oxidative compounds, COM crystals, and KCit on the ground at KSC, or at the ISS-NL was performed as previously described in Chapter 3.

Introduction of COM Microcrystals into PT-MPS Devices

During the EVT phase, COM crystals were introduced into the PT-MPS devices by use of a 5 μL Hamilton Syringe to puncture the injection port upstream of the PTEC tubule. A volume of 5 μL of 1000 μg/mL COM crystals suspended in PTEC maintenance media were perfused through the lumen towards the downstream injection port by gently depressing the plunger on the syringe. For both the flight and ground KC-02 experiments, COM crystals were only present in the treatment media itself ensuring that any crystals observed with the devices themselves or the device effluents would have to originate from the treatment cassettes.

Handling of Post-Experiment Cryopreserved PT-MPS Devices and Effluents

After the completion of the fixation (via perfusion with RNAlater®) step, both in flight and on the ground, the fixed PT-MPS devices and media cassettes containing device effluents were stored at -80^{o} C and shipped on dry ice back to laboratory facilities at the University of Washington in Seattle, WA. Upon receiving the devices and cassettes, they were slowly thawed in a 4^{0} C refrigerator where they were stored during analysis. Media cassettes were weighed, and that value compared against the preflight measurement. Device effluents were then recovered as previously described in Chapter 3 and stored as 0.5 mL aliquots in 2 mL screw-top cryopreservation tubes at -80^{o} C for downstream analysis.

RNA Collection from PT-MPS Devices

Collection of RNA samples from PT-MPS tubules, RNA extraction and RNAseq analysis were performed as previously described in Chapter 3. Gene ontology analysis was performed using the Comparative Toxicogenomics Database (http://ctdbase.org/basicQuery.go?bqCat=go&bq=GpRIN3).

Quantification of KIM-1 & IL-6 in PT-MPS effluents

Quantification of both KIM-1 and IL-6 levels in PT-MPS effluents was performed as previously described in Chapters 2 and 3.

Statistical analysis

Data are reported as individual measurements with means ± standard errors. For comparison of biomarker mean levels, multiple unpaired t-tests were applied using GraphPad software (La Jolla, CA).

KC-02 Project and Experimental Designs and Timelines

Demographic and health information on the six donors from which the cells in these experiments have been sourced, and the overall timeline of the KC-02 project can be found in Fig. 1. The EVT experimental design and SABL layout and experimental timeline are depicted in Fig 2. The experimental timeline followed both in flight at the ISS-NL, and on the ground at KSC, are depicted and described in Fig. 5.

4.3. Results

KC-02 Overview

Cryopreserved PTECs from three female and three male donors were selected for the final KC-02 flight and launch experiments. Demographic and health information for each donor is summarized in Fig. 1a. The KC-02 project progressed in three phases which are designated

relative to the Engineering Validation Testing (EVT) (Fig. 1b). Model development and donor screening were performed during the period preceding EVT (Pre-EVT) with selection and assessment of the final candidates occurring throughout all three phases. All experiments were performed as described in Chapters 2 and 3. All of the female donor cells used in this experiment were sourced from frozen cell culture stocks depleted of cells of distal tubule origin by peanut agglutinin (PNA) based immunomagnetic separation (IMS) resulting in PNA-depleted (PNA-) and PNA-enriched (PNA+) populations as described in Chapter 2. The use of only donors from these PNA+ stocks for the female donors and the lack of inclusion of any male PNA+ cultures in these studies was unintentional on the part of the authors. As we do not know the impact of this difference in donor cell processing, sex-based comparisons were not possible.

A

Donor ID	Isolated	Assessed	LTL/PNA	Sex	Age	Ethnicity	Cause of death	Pre-existing conditions
PT5-F	2/25/2020	Pre-EVT	PNA-depleted	F	47	Hispanic	Cerebrovascular stroke	ESRD, diabetes, hypertension, high cholesterol
PT6-F	3/6/2020	EVT	PNA-depleted	F	45	White	Cerebrovascular stroke	HTN, GERD, early diabetes
PT7-M	6/29/2020	Post-EVT	N/A	M	49	Hispanic	Cerebrovascular stroke	High cholesterol
PT8-F	8/3/2020	Post-EVT	PNA-depleted	F	51	Black	N/D	Recent alcohol detox
PT9-M	9/7/2020	EVT	N/A	M	38	White	Head trauma	N/D
PT10-M	10/17/2020	Pre-EVT	N/A	M	49	White	Anoxia, cardiovascular	Osteomyelitus, HTN, PMH T1DM, CVA, chronic anemia

B

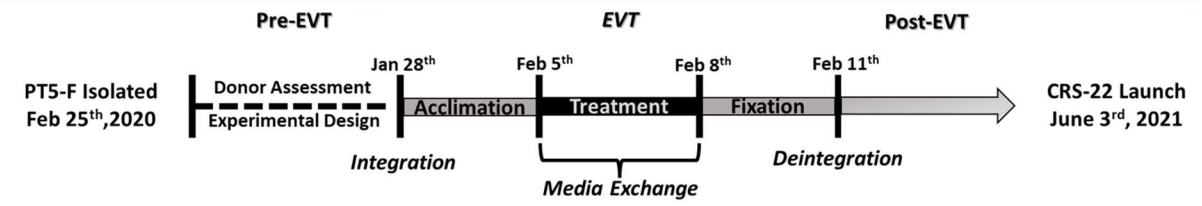

Figure 1: Donor Kidney Details & KC-02 Project Timeline

Study Overview & Hardware Performance

The experimental SABL design and timeline for EVT are described in Fig. 2. Two donors, one male and one female, and three treatment groups were tested to validate the PT-MPS model of KSD. The KSD treatment groups consisted of 1000 μg/mL COM crystals and 1000 μg/mL COM crystals with 250 μM KCit in addition to a control group. COM crystals were used to simulate micro-sized precursors to fully developed kidney stones while KCit is available as a pharmacologic treatment for calcium containing kidney stones in the form of Urocit-K. The pro-oxidative agents menadione and aristolochic acid-I (AA-1), also discussed in Chapter 2, were included in EVT as established treatment articles to compare against the KSD related treatment groups. COM crystals were injected into the PT-MPS devices during EVT and preferentially settled in the injection ports immediately upstream and downstream of the PTEC tubules (Fig. 3 A). This is due to the characteristics of the internal pressure environment of the MPS devices themselves. While individual crystals were found within the PTEC tubules, they were scattered and infrequently observed. Multiple crystals in close proximity were observed in a few instances of tubules with non-obstructive deformations with the crystals settling in regions where local fluid flow was altered from that in standard PT-MPS tubules (Fig. 3 A). This suggests that the ability to consistently introduce regions of abnormal flow will promote crystal settling and membrane interactions.

The performance of the KCPP hardware throughout EVT was nominal with no significant issues or aberrations to report. The nominal effluent volume recovery rates for all KC-02 experiments are summarized in Table 1. Nominal effluent volume was defined as calculated expected volume ± 20%, or 6 ± 1.2 mL for maintenance media effluents and 1.5 ± 0.3 for

treatment effluents. The overall total rate for device effluents in EVT was 100% with the nominal volume recovery rate being 82%. This confirmed that the platform hardware was ready for use in the post-EVT phase. However, the abnormally low KIM-1 levels detected in device effluents generated during EVT was indicative of our difficulties quantifying KIM-1 levels in effluents generated during post EVT launch and ground experiments.

SABL	PUMP	HOUSING	DONOR	CHIP #	Treatment
1	1	A	PT6-F	1	CONTROL
			PT6-F	2	
			PT6-F	3	COM 1000 µg/mL
		B	PT6-F	4	
			PT6-F	5	COM 1000 µg/mL 250 µM KCit
			PT6-F	6	
	2	C	PT6-F	7	Control
			PT6-F	8	Menadione 100 µM
			PT6-F	9	PTEC + DMSO
		D	PT6-F	10	Aristolochic acid I 10 µM
			PT6-F	11	TBHQ 100 µM
			PT6-F	12	Colistimethate 500 µM
2	3	E	PT9-M	13	CONTROL
			PT9-M	14	
			PT9-M	15	COM 1000 µg/mL
		F	PT9-M	16	
			PT9-M	17	COM 1000 µg/mL 250 µM KCit
			PT9-M	18	
	4	G	PT9-M	19	Control
			PT9-M	20	Menadione 100 µM
			PT9-M	21	PTEC + DMSO
		H	PT9-M	22	Aristolochic acid I 10 µM
			PT9-M	23	TBHQ 100 µM
			PT9-M	24	Colistimethate 500 µM

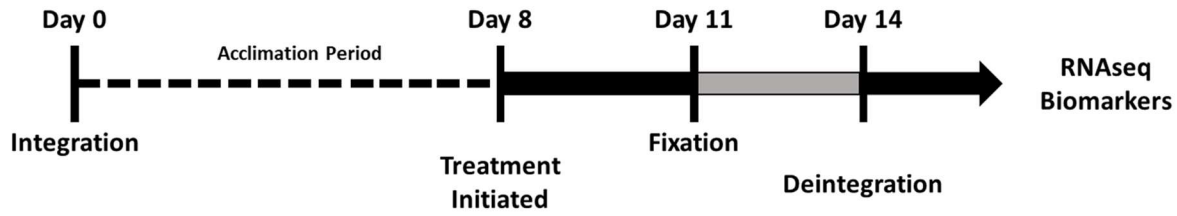

Figure 2. SABL Configuration & Experimental Timeline for KC-02 Engineering Validation

Table 1: Summary of nominal effluents recovery for EVT & KC-02.

		Chip Housing							
		A	B	C	D	E	F	G	H
EVT									
	82%	6/9	9/9	7/9	8/9	9/9	7/9	7/9	7/9
Flight									
M	76%	4/9	8/9	8/9	6/9	9/9	8/9	4/9	8/9
T	82%	7/9	8/9	9/9	7/9	9/9	8/9	4/8	7/9
Ground									
M	58%	6/9	4/9	3/9	4/9	5/9	9/9	6/9	5/9
T	72%	9/9	5/9	6/9	4/9	6/9	9/9	7/9	6/9

*** Reported as post-flight recovered tubules over initial tubule count.**

Quantification of the Kidney Specific Injury Marker KIM-1

During EVT, no significant increase in KIM-1 was observed. The levels were considerably lower than normal (Fig. 3 B&C). KIM-I levels measured from devices perfused via the KCPP are considerably lower compared to pre-EVT MPS experiments. Pre-EVT KIM-I levels were typically greater than 10-fold higher than their corresponding EVT treatments. Even considering the difference in donor cells used (PT5F and PT10M for pre-EVT, PT6F and PT9M for EVT), this considerable discrepancy in KIM-I levels indicates that the KCPP hardware itself has an impact on detectable KIM-I in sample effluents. This observation is further supported by the absence of detectable KIM-1 levels in all flight and ground effluents recovered from launch and ground devices during the post-EVT phase.

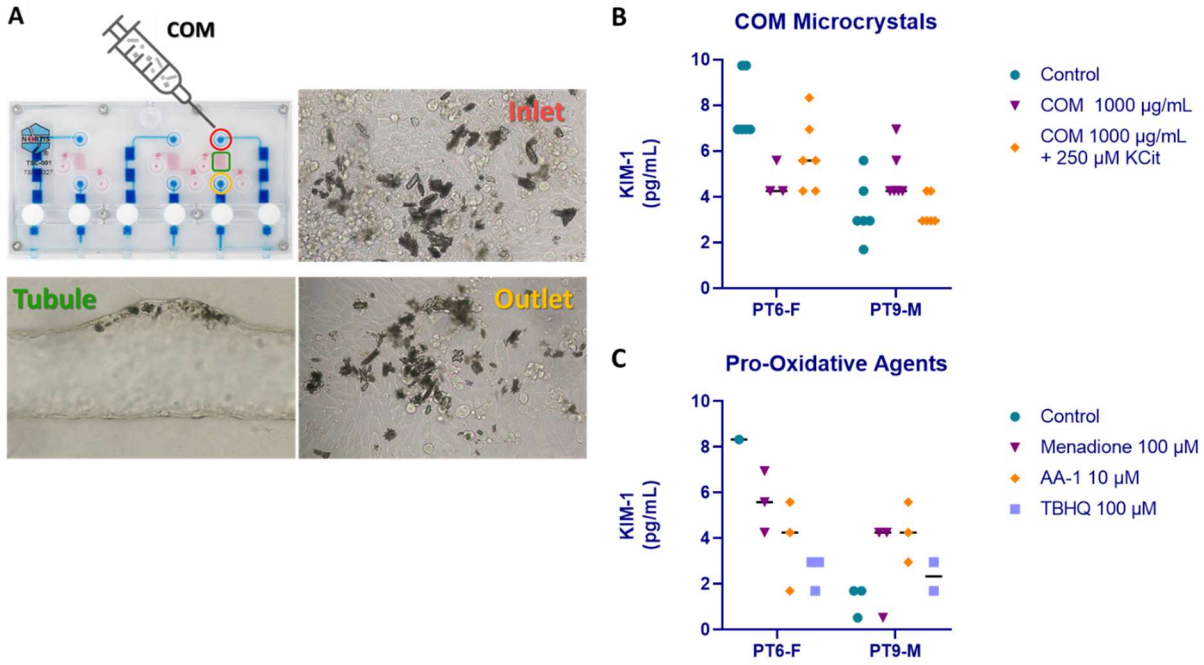

Figure 3. Experimental approach for KC-02 Engineering Validation Testing: (a) COM crystals were into PTEC MPS devices (donor PT6F) via direct injection into the input injection port, (b-d) 10X magnification brightfield images of COM crystals in the PTEC tubule and injection ports, (B & C) KIM-I release from MPS cultures after exposure to COM crystals, COM + KCit, menadione, AA-1 or TBHQ for 48 hours. (n= 2 donors)

Differential Gene Expression Analysis

Transcriptomic profiling was conducted by RNAseq analysis for EVT test groups and presented in Fig. 4. The greatest number of differentially expressed genes (DEGs) was observed for AA-1 Treatment (11,634 DEGs), followed by menadione (3997 DEGs), COM (114 DEGs) and COM + KCit (3 DEGs). Treatment with COM + KCit resulted in the fewest number of DEGs. Both BCL3 and PPP1R10 were each downregulated with logFC values of 0.33 and 0.22 respectively, while BCL3 was upregulated by a logFC of 0.47. Gene ontology (GO) search for PSG4 reveals limited results with the only two associated being pathways identified as being female pregnancy and extracellular region.

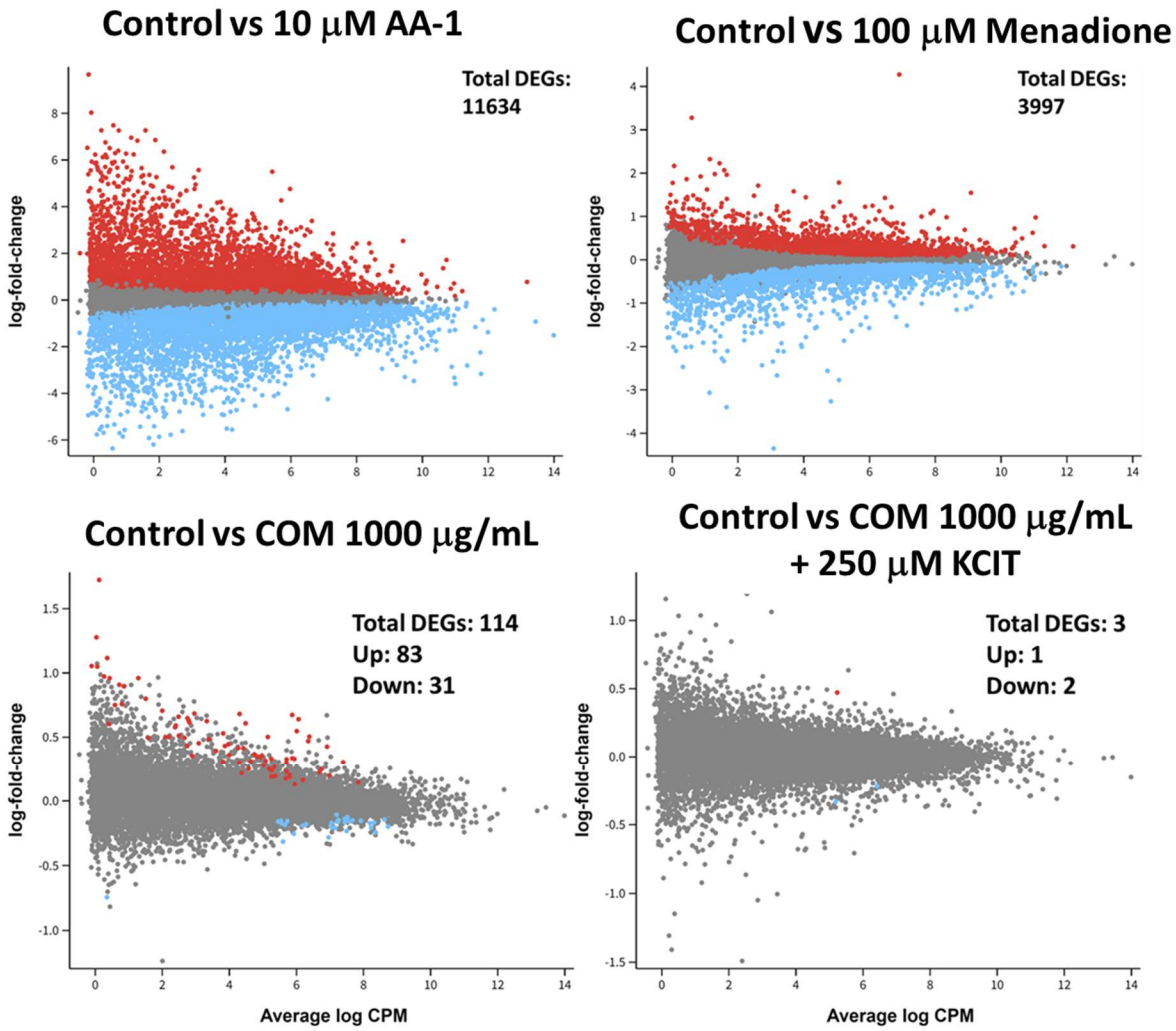

Figure 4. KC-02 EVT impact on PTEC differential gene expression: Volcano plots summarizing DEGs across; (a) impact of flight status, (b) treatment impact in flight, and (c) treatment impact on the ground. (n= 2 donors)

KC-02 Modeling of PT-MPS model of KSD at the ISS-NL and KSC

The final selection of six donors for use in the KC-02 launch experiments occurred during the pre-EVT and EVT phases (Figs. 1 & 5). The SABL configuration depicted in Fig. 5 was designed to distribute donor assignments in such a way to minimize the potential loss of experimental data in the case of hardware failure. As such, a matched pair of PT-MPS devices were included in the study design, one for each SABL. Based on their pre-EVT growth characteristics, PTEC cultures from donors PT6F and PT10M were selected. This arrangement of

donors was intended to ensure that, in the event of the loss of a single SABL, a balanced study design with triplicate samples from two male and two female donors was still preserved. The donor PTEC cultures were all assessed to be excellent choices based on growth characteristics in 2D culture, consistency in generating confluent tubules, and total availability in stock required to seed the minimum requirement of 12-15 fully seeded MPS devices per donor. This quantity of devices far in excess of routine lab use. Flasks from each donor reached >80% confluency by seven days after initial culture from vials cryopreserved at P1 with the exception of cultures from PT7M (Fig. 6). In this case, additional cryopreserved vials were thawed and cultured to reach the number of cells required for device seeding. Donor cultures did not grow at a uniform rate during the pre-injection phase. Cultures initiated from donor PT6F displayed the most rapid growth and was passaged three days after plating. The remaining donors were passaged four days after initial seeding.

SABL	PUMP	HOUSING	DONOR	CHIP #	Treatment
1	1	A	PT10M	1	CONTROL
			PT10M	2	COM 1000 µg/mL
			PT10M	3	COM 1000 µg/mL + 250 µm KCit
		B	PT5F	4	Control
			PT6F	5	
			PT7M	6	
	2	C	PT5F	7	COM 1000 µg/mL
			PT6F	8	
			PT7M	9	
		D	PT5F	10	COM 1000 µg/mL + 250 µm KCit
			PT6F	11	
			PT7M	12	
2	3	E	PT6F	13	CONTROL
			PT6F	14	COM 1000 µg/mL
			PT6F	15	COM 1000 µg/mL + 250 µm KCit
		F	PT8F	16	Control
			PT9M	17	
			PT10M	18	
	4	G	PT8F	19	COM 1000 µg/mL
			PT9M	20	
			PT10M	21	
		H	PT8F	22	COM 1000 µg/mL + 250 µm KCit
			PT9M	23	
			PT10M	24	

Figure 5. SABL Configuration & Project Timeline for KC-02 CRS-22 Launch

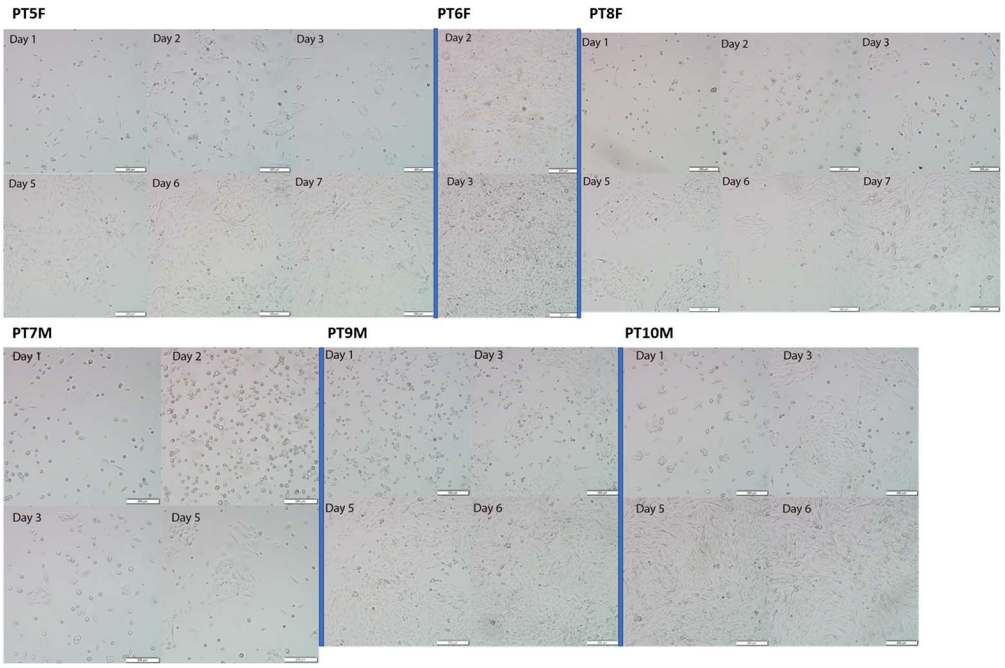

Figure 6. Time course of KC-02 donors in pre-injection culture at KSC.

The purpose of performing the flight arm of the KC-02 experiments at the ISS-NL was to test the hypothesis that the combination of microgravity and other factors associated with human health impacts during spaceflight (e.g., cosmic and solar radiation) would enhance our MPS model of KSD by increasing the frequency and dynamic nature of interactions between the COM crystals in solution and the PTEC luminal surface (Fig. 7 A). At 1 G, the density of the crystals prevents them from transiting through the devices. This is the case with both pneumatic and piston-based perfusion platforms. At the ISS-NL, the experimental system will experience a state of freefall in which net vectors of force are zero and the crystals can move freely in any direction unrestricted by the influence of gravity. In this situation, the force provided by KCPP hardware should transit the crystals along with the flow of the treatment media and crystals would not need to be introduced via injection port. Indeed, there is evidence that this was the case. COM

crystals were observed inside of the injection ports of several flight chips treated with COM or COM + KCit. While observing crystals within the tubules themselves remained rare, one specific device contained >200 individual crystals within a single malformed tubule (Fig. 7 B). Malformed tubules are a frequent occurrence when preparing kidney MPS devices. Typically, they do not block or otherwise prevent normal operation of the devices or their use in experiments. However, they do possess altered pressure and fluid dynamics that may account for the ready accumulation of crystals crystals in this tubule. Similar scenarios occurred throughout the KC-02 development process including one documented in Chapter 1. This indicates that deliberately altering the internal pressure characteristics of the MPS devices themselves may be required to progress the relevancy and predictive ability of the KC-02 model of KSD. Our hypothesis that in a microgravity environment, COM crystals would freely perfuse throughout the flowpath of the PT-MPS devices is supported by the presence of COM crystals in the injection ports, lumens and recovered MPS effluents (Fig. 7 B & C). Consistent with previous observations during EVT, settled crystals were only observed in tubules containing deformations that would impact media flow and shear stress forces.

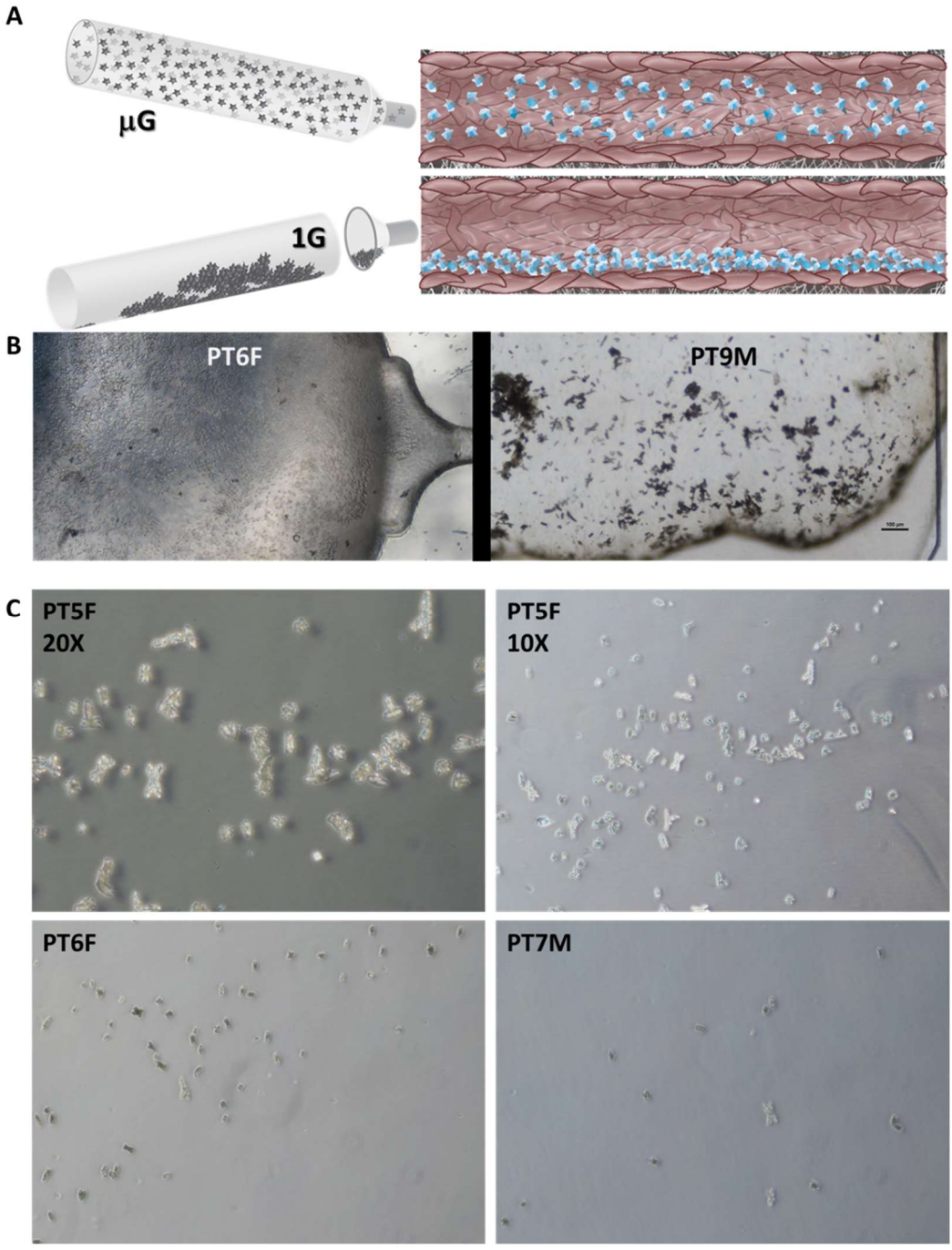

Figure 7. CRS-22 Premise and execution of KC-02 project in flight at the ISS-NL and on ground at KSC: (a) In microgravity (top) will allow full distribution of COM crystals within the treatment media volume facilitating free distribution throughout the culture device in contrast to crystals introduced using a Hamilton Syringe at 1G (bottom). (B & C) Brightfield images of flight chips treated with COM 1000 µg/mL depicting COM crystals within an injection port (PT6F), a deformed PTEC tubule (PT9M) magnification and device effluents from donors PT5F, PT6F & PT7M.

Information on the recovery rate of MPS effluents for EVT and KC-02 are summarized in Table 1. For EVT, the recovery rate for nominal volume of treatment effluents was 82 with nominal volume defined as ±20% of expected volume of 6 mL (4.8-7.2 mL) of maintenance media and 1.5 mL (1.2-1.8 mL) of treatment media (Table 1). Total sample recovery during EVT was 100%. Nominal effluent recovery from CRS-22 flight devices was 76% for maintenance media and 82% for treatment media with, the recovery rates for ground devices were 58% and 72% respectively. As reported in Chapter 3, 88% of flight and 93% of ground effluents recovered were available for use in biomarker analysis. Recovery of isolated RNA for RNAseq analysis was 97% for both flight and ground as also reported in Chapter 3. Only four samples were non-recoverable, two ground and two flight, out of a total of 144 devices tested. The only instance where just a single sample from a device was recovered for RNAseq analysis was from a PT7M device treated with COM + KCit in flight. Similarly, only a single sample usable for biomarker analysis was obtained for PT8M devices treated with COM in flight. In all other cases, at least two replicate samples were available for use for each donor and treatment combination. These results represent a considerable improvement over the recovery rates obtained during CRS-17 as discussed in Chapter 3.

Effluent Biomarker Analysis

The KC-02 project consisted of MPS devices seeded with cells sourced from six different demographically diverse donors. These devices were seeded, and flow initiated in 1 G at KSC. The experimental treatment arms included an untreated media control, media containing 1000 μg/mL COM crystals, or 1000 μg/mL COM crystals + 250 μM KCit. A total of 24 kidney MPS devices totaling 72 individuals independent PTEC tubules were sent to orbit at the ISS-NL. A matched set

of 24 MPS devices remained on the ground at KSC to serve as a 1 G control comparison. A full sample set for KC-02 KSC includes 144 individual effluent and RNA extraction samples each. The highest possible standards of quality and accuracy are required to effectively handle such a large sample set. Upon return to the laboratory facilities at the University of Washington in Seattle, collected effluents were thawed, measured for volume, and then aliquoted into three separate cryopreservation vials for a total of 432 effluent and 144 RNA samples stored for downstream analysis.

Quantification IL-6 and KIM-1

Biomarker analysis of KIM-I by ELISA assay was attempted three times with appropriate positive controls. However, despite detecting nominal levels of KIM-I in positive controls, no quantifiable KIM-I was observed in flight or ground KC-02 samples (data not shown). Performing repeated KIM-I assays depleted the stock of stored effluents faster than anticipated impacting the amount of post-flight analysis we could perform. When all flight and ground data is compared, IL-6 levels in flight PT-MPS were elevated by 40%. Flight status differentially impact each treatment group (Fig. 8 A). While IL-6 levels in effluents collected from control media treated and COM + KCit treated showed a significant increase during spaceflight of 71% and 41% respectively (Fig. 8 B & D). There was no significant difference in IL-6 levels in effluents from COM treated devices based on flight status (Fig. 8 C), although this is likely attributable to the comparably higher baseline IL-6 in this group in comparison to control and COM + KCit treated devices. These findings support the assertion that spaceflight would induce a differential response in PTEC cultured in the PT-MPS, which in this case is in the form of a secreted biomarker.

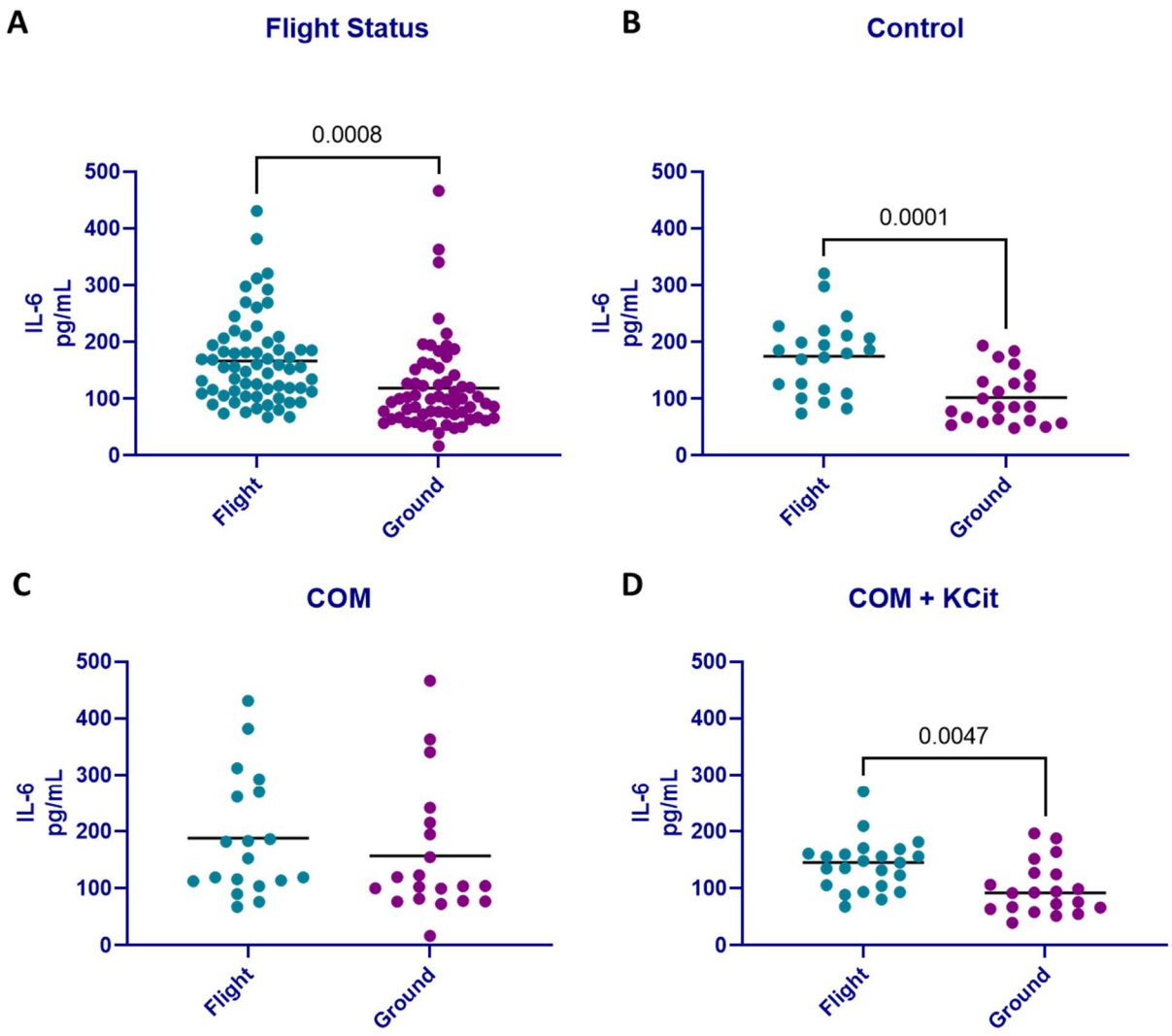

Figure 8. Impact of flight status and treatment on PT-MPS IL-6 release. Flight vs Ground comparison of IL-6 levels in device effluents depicting; (a) flight status, (b) control group (c) COM treatment group, (d) COM + KCit treatment group measured by ELISA (n= 6 donors)

Each tubule within a single PT-MPS device represents a technical replicate and not biological one. Therefore, biomarker analysis of individual donor responses cannot be assessed with confidence. With that consideration, we observed levels of IL-6 in both flight and ground effluents from PT5F and PT6F changed in response to treatment. In flight, PT5F showed an 81% increase in IL-6 levels between COM and control treatments and a corresponding 57% decrease

with the addition of KCit to the treatment. The only other treatment impact observed in flight was a 44% reduction in IL-6 levels in PT6F effluents was a 41% decrease with the addition of KCit to the treatment (Fig. 9 A). The pattern was similar for PT5F and PT6F devices on the ground, COM + KCit treatment reduced IL-6 levels by 58% and 42% respectively, in comparison to COM treatment alone while COM treatment increased IL-6 levels by 72% in comparison to control (Fig. 9 B). These results indicate that PTECs respond to the stress of spaceflight in a pro-inflammatory manner with citrate playing a role in regulating PTEC immune signaling by inhibition of IL-6 secretion.

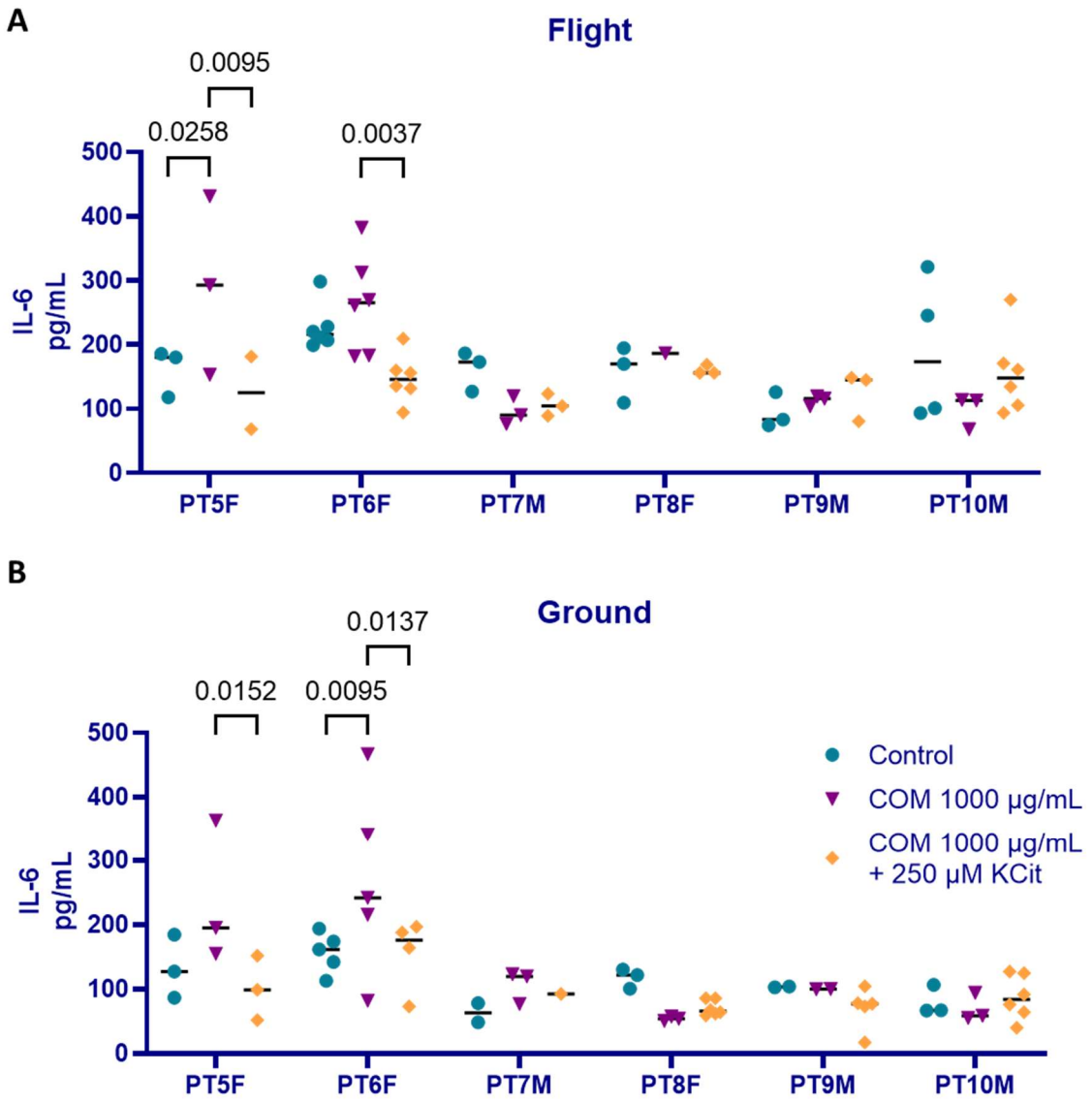

Figure 9. Impact of treatment on PT-MPS IL-6 release by individual donor. Individual flight (a) and ground (b) IL-6 levels measured by ELISA.

Flight status interacted with donor sex when comparing IL-6 levels in treatment effluents in flight and ground. On the ground, all three treatments generated greater IL-6 release from female donor seeded devices than from male. When comparing female to male ground effluents,

Il-6 levels were increased by 115% in control effluents, 161% in COM effluents, and 141% in COM + KCit effluents. Only COM treatment demonstrated a sex-associated differential impact on IL-6 secretion in flight with the levels in female flight effluents elevated by 160% over male donor effluents. Both donors PT6F and PT10M received replicate experiments present in each SABL in flight and on the ground. In order to check for inter-SABL variability, we compared IL-6 levels across SABLs for both donors. No cross-SABL differences were observed supporting the merit of distributing the devices in this manner (Fig. 10 C & D).

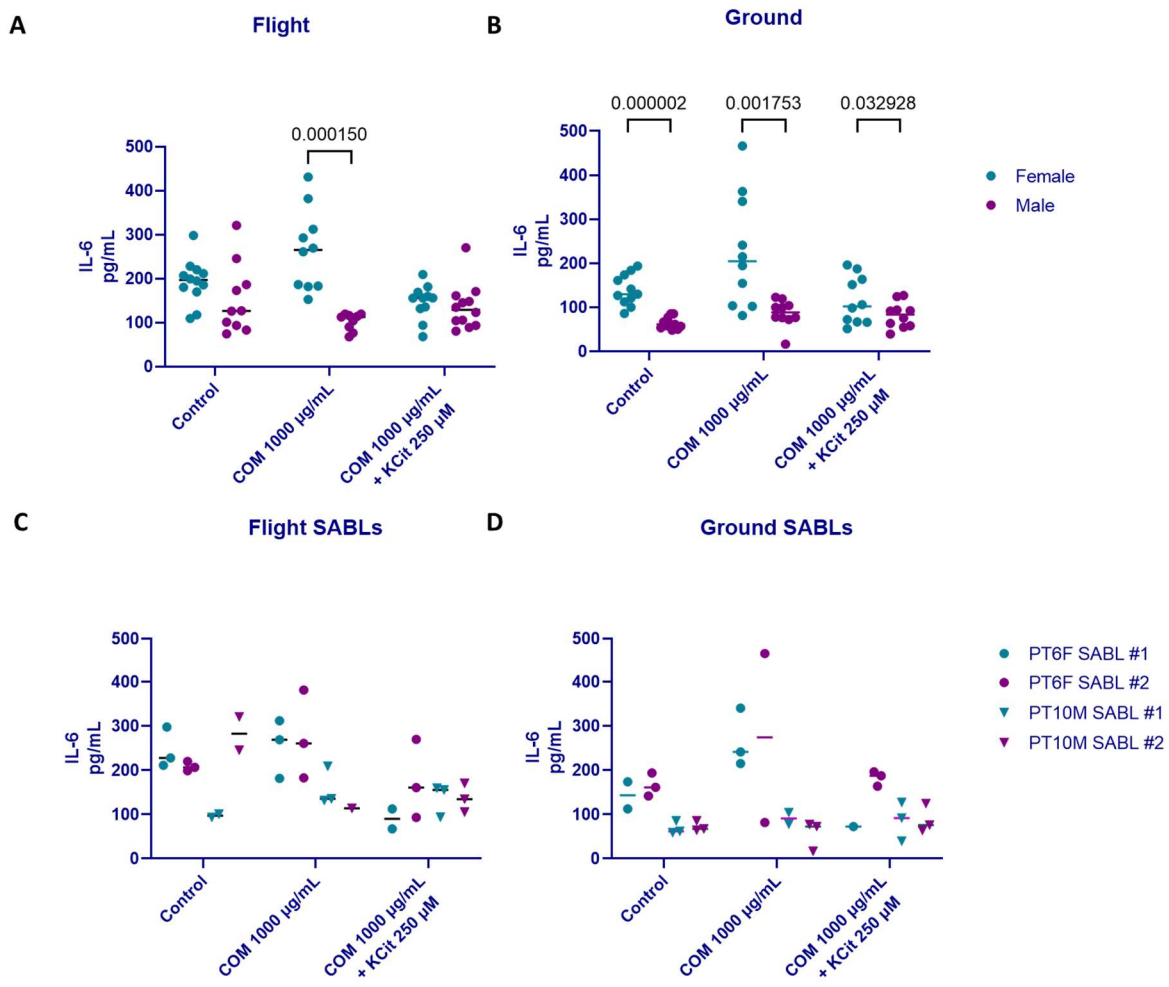

Figure 10. Impact of donor sex and SABL assignment on PT-MPS IL-6 release. Flight and ground IL-6 levels in device effluents based on (a & b) sex (n= 3 per sex), and (c & d) SABL assignment measured by ELISA.

Quantification of Secreted Kidney Injury Biomarkers

To identify additional potential biomarkers sensitive to COM treatment we performed a kidney injury biomarker assay measuring levels of clusterin, cystatin C, lipocalin-2/NGAL and osteopontin in device effluents. Across both ground and flight, the only significant change in these kidney injury biomarkers occurred in flight effluents between COM treated devices and controls. A GO analysis implicates clusterin in multiple mitochondrial membrane related pathways.

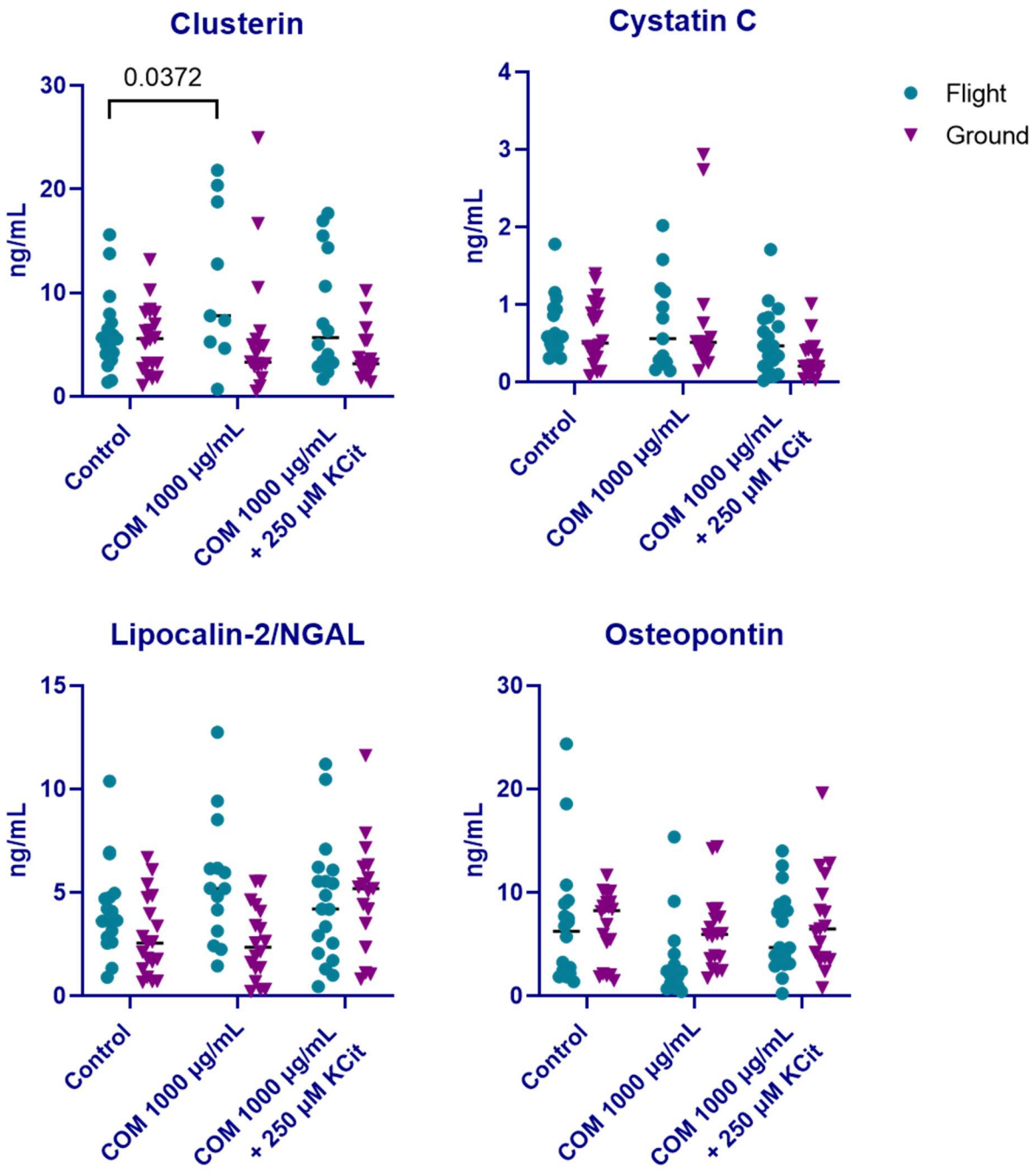

Figure 11. Impact of flight status and treatment on kidney injury markers: Flight only (top) and Flight/Ground comparisons of kidney injury biomarkers in two responsive donors; a) Clusterin, (b) Cystatin C, (c) Lipocalin-2/NGAL, (d) Osteopontin (n= 6 donors)

Differential Gene Expression Analysis

We performed RNAseq based global transcriptomics to assess the impact of microgravity and treatment on gene expression in PTEC MPS devices. Volcano plots depicting the total number of DEGs associated with each treatment and flight croup comparison are depicted in Fig. 12. Flight status had by far the greatest impact on differential gene expression. Comparing flight to ground control, COM and COM + KCit treatment groups results in 4982, 4404 and 3239 DEGs respectively. The greatest difference between flight and ground treatment effects occurred between the control and COM treated groups. COM crystal treatment on the ground resulted in 593 differentially expressed genes in contrast to only 9 DEGs attributable to COM treatment in flight. When comparing flight vs ground, KCit treatment resulted in 153 and 271 DEGs respectively. The comparison of COM treatment to COM + KCit treatment results in 475 DEGs in flight and 372 on the ground. The top 20 genes upregulated and downregulated for all comparisons are summarized in Supplemental Tables 1-9.

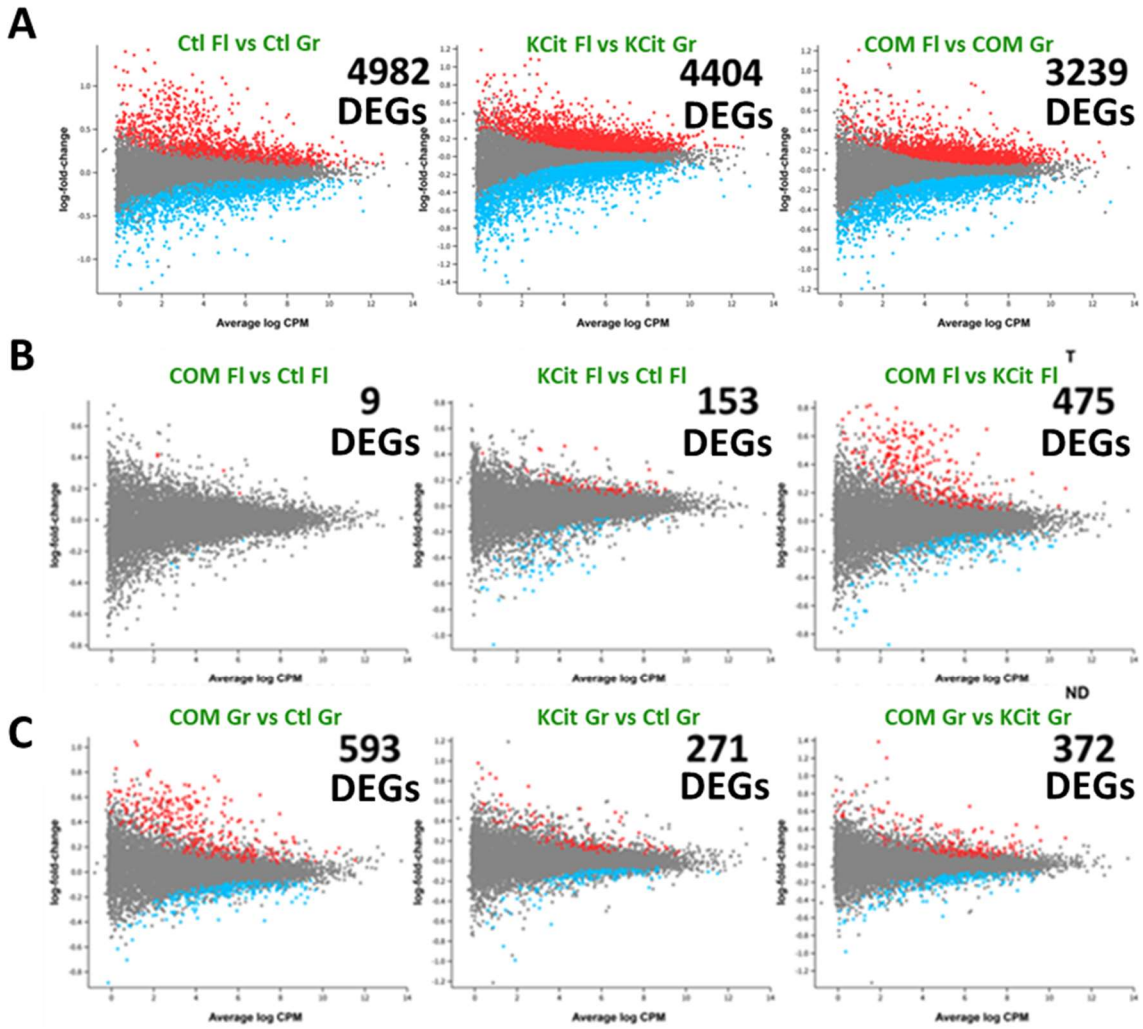

Figure 12. KC-02 CRS-22 experimental impact on PTEC differential gene expression: Volcano plots summarizing DEGs across; (a) impact of flight status, (b) treatment impact in flight, and (c) treatment impact on the ground. (n= 6 donors)

The comparison of COM treatment in flight to control directly tests the underlying premise of the KC-02 experiment that microgravity allows COM crystals to perfuse through the MPS system and interact with the PTEC tubules. Those genes differentially expressed in response to COM crystal treatment in spaceflight can be attributed to the impact of free-floating COM crystals having continuous, dynamic interactions with the luminal membrane of the PTEC tubules. Only nine genes were significantly differentially expressed in response to COM crystals in flight,

four were upregulated and five downregulated (Table 2). These DEGs represent potential early molecular markers associated with the pathophysiology of kidney stone development.

Table 2 Differentially Expressed Genes Fold Change.

	COM_F - Ctrl_F	COM_G - Ctrl_G	KCit_F - Ctrl_F	KCit_G - Ctrl_G	COM_F - KCit_F	COM_G - KCit_G	Ctrl_F - Ctrl_G	COM_F - COM_G	KCit_F - KCit_G
ADRB2	1.34	NS	NS	NS	NS	NS	NS	NS	NS
GPRIN3	1.33	NS	NS	NS	NS	NS	1.26	NS	1.24
LTBP2	1.24	NS	NS	NS	NS	NS	NS	1.35	1.17
STK17A	1.13	NS	NS	NS	1.12	NS	1.16	NS	NS
COL4A3BP	0.91	NS	NS	NS	NS	NS	0.91	0.87	0.91
HSPA14.2	0.88	NS	NS	NS	NS	NS	NS	NS	NS
LINC01123	0.82	NS	0.83	NS	NS	NS	NS	0.77	0.87
ZNF439	0.81	NS	0.82	0.88	NS	0.84	NS	NS	0.82
ZNF470	0.86	NS	NS	NS	NS	NS	NS	0.87	0.89

The four genes upregulated in response to COM treatment in flight were ADRB2, GPRIN3, LTBP2 and STK17A which were upregulated by 1.34-fold, 1.33-fold, 1.24-fold, and 1.13-fold respectively. The gene **ADRB2** encodes a beta-2-andrenergic G protein-coupled receptor and is found in direct association with its effector class C L-type calcium channel CaV1.2. Therefore, the signal transduction pathway associated with ADRB2 is calcium dependent and likely sensitive to elevated free CA^{2+} ion concentration in the treatment media or hypercalcinuric renal filtrate. This gene is linked by gene ontology to biomineralization (GO:0110148), response to stress (GO:0006950), response to oxygen-containing compound (GO:1901700), regulation of blood pressure (GO:0008217) and was not differentially expressed in any other treatment comparison. This gene has also been linked to Alzheimer's and Parkinson's diseases, genetic obesity, type 2 diabetes, asthma and cardiovascular disease.

G protein-regulated inducer of neurite outgrowth 3 (GPRIN3 or GRIN3) encodes for the NR3 a subunit of a calcium sensitive *N*-Methyl-d-aspartate (NMDA) receptor that plays a role in

neuronal cell development (GO:0048468), cell differentiation (GO:0030154) and has also been linked to Parkinson's disease [84]. Despite their typical associate with neuronal development and function, all NMDA receptor transcripts have been detected in the kidney and their activity may be involved in some renal pathologies. The NR3 subunit located in the proximal tubule and medullary collecting duct [85]. Incorporation of a NR3 subunit where it regulates the concentration of urine in place of a NR2 subunit reduces Ca2+ permeability into and was upregulated by COM treatment in flight and by spaceflight itself in the case of control and KCit treated devices [86] [87]. NMDA receptor activation may assist in the maintenance of epithelial phenotype in PTECs acting in opposition to inflammatory mediators like TGFβ. There is evidence to support that excessive NMDA receptor activation is toxic (excitotoxicity) to renal cells both in vivo and in vitro. Exposure of podocytes to extended NMDA signaling resulted in cytoskeleton rearrangement, marked increase of ROS generation and accumulation, NFAT activation, and the initiation of cell death featuring a combination of necrotic and apoptotic characteristics [88] [89].

LTBP2 is an extracellular matrix protein and member of the latent transforming growth factor (TGF)-beta binding proteins (LTBP) family. LTBP2 is suggested to have multiple functions including establishment of protein localization to extracellular region (GO:0035592), which suggests a role a role in cell adhesion that may be disrupted by interactions with COM crystal edges. STK17A, is a DAP kinase-related apoptosis-inducing protein kinase, involved in positive regulation of apoptotic process (GO:0043065), regulation of reactive oxygen species metabolic process (GO:2000377).

Treatment with COM in flight led to the downregulation of COL4A3BP (0.91-fold), HSPA14 (0.88-fold), ZNF439 (0.81-fold) and ZNF 470 (0.86-fold) and one non-protein encoding RNA, LINC01123 (0.82-fold). The long intergenic non-protein coding RNA, LINC01123 does not have any GO entries, but literature suggests that it promotes cell proliferation, migration and invasion in colorectal cancer and immune escape in head and neck squamous-cell carcinoma [90] [91]. COL4A3BP (CERT1) encodes a kinase that specifically phosphorylates the N-terminal region of the non-collagenous domain of the alpha 3 chain of type IV collagen. This region being known as the Goodpasture antigen with Goodpasture disease resulting from autoimmune reactions against antigen. Gene ontology links CERT1 to mitochondrion morphogenesis (GO:0070584), mitochondrion organization (GO:0007005) and response to stress (GO:0006950). CERT1 was downregulated by flight in all three treatment groups and further downregulated by COM in flight.

The heat shock protein family A (Hsp70) member 14 (HSPA14) gene encodes a chaperone protein which plays a role in cellular response to stress (GO:0033554), to organic substances (GO:0071310) to topologically incorrect protein (GO:0035967), to unfolded protein (GO:0034620), protein folding (GO:0006457), protein refolding (GO:0042026). The zinc finger proteins ZNF439 and ZNF470 are primarily involve with the regulation of RNA biosynthetic processes (GO:2001141), regulation of RNA metabolic processes (GO:0051252), and regulation of transcription by RNA polymerase II (GO:0006357). The expression of two genes, ADRB2 and HSPA14, were altered exclusively in response to COM treatment in flight. In the case of ADRB2 upregulation, increased levels of free Ca^{2+} in the treatment media may replicate the effects of hypercalcinuria in initiating the events leading to kidney stone development. The upregulation

of HSPA14 may be in response to proteins damaged during membrane interactions with COM crystal surfaces. The direction of differential effect attributable to COM flight treatment was always the same direction as the impact of flight itself, suggesting a basis for an increased susceptibility to kidney stone formation in or after spaceflight.

The addition of KCit reversed the impact of COM treatment on seven of the nine genes. Only LINC01123 and ZNF439 remained insensitive to the effects of KCit. In both cases, the genes remained downregulated to the same extent as with COM treatment alone. Citrate acts as an inhibitor of COM crystallization and precipitation crystal growth in a by preferentially complexing with Ca^{2+} on the surface of COM crystals to form the highly insoluble calcium citrate (CaCit). This has the effects of reducing Ca^{2+} supersaturation, reducing crystal size, and blunting the sharp crystal edges responsible for the disruptive adhesion of the crystal to the PTEC membrane [92]. Irreversible binding of COM crystal surfaces to microvilli on the surface of renal epithelial cells leads to their internalization and aggravates cell damage [93]. Therefore, citrate plays a protective role by reducing the frequency of crystal-membrane interactions and attenuating the damage caused by these interactions.

4.4. Conclusions

We successfully developed a PT-MPS model of early COM kidney stone development and tested the impact of spaceflight on COM crystal treated PTEC tubules. PT-MPS devices seeded with cells sourced from 6 demographically diverse donors were exposed to COM crystals during spaceflight at the ISS-NL and on the ground at KSC. Treatment with KCit was also tested to assess its impact on PTEC response to COM treatment. A modified version of the PT-MPS KSD model in which COM crystals were injected directly into the devices was assessed during EVT along with

AA-1 and menadione for comparison. COM crystals seem to preferentially settle in deformed regions within PTEC tubules regardless of how they are introduced into the MPS devices. This is most likely the result of altered pressure characteristics impacting the local flow rate and shear stress. When injected into the MPS devices, the great majority of crystals settled on the cells growing in the injection ports on either side of the PTEC tubules. In contrast, those PT-MPS treated with COM during spaceflight are predicted to experience a more even distribution of crystal interactions across all regions of the system. The lack of these dynamic crystal interactions is likely the reason for the reduced impact of COM and KCit treatment on gene expression during EVT. The cause of the unusually low levels of KIM-1 detected in treatment effluents during EVT remains unknown and, to date, we have been unable to detect KIM-1 in both flight and ground effluents.

The premise of the KC-02 MPS model of KSD was confirmed by the results of this study. The presence of COM crystals in post-flight PT-MPS devices and treatment effluents can only be attributed to crystals freely flowing from the media cassettes through the system. No crystals were found in the treatment effluents during EVT or from those devices treated on the ground. Spaceflight was associated with a significant increase in IL-6 secretion overall and in control and KCit treated devices with KCit treatment reducing this effect. Treatment with COM did not cause a significant increase, however, baseline IL-6 levels in COM treated devices on the ground was elevated compared to control and KCit treated ground devices. Of the individual donors tested, donors PT5F and PT6F appeared to respond to COM treatment by increasing IL-6 release with KCit reversing the effect both in flight and on the ground. Additional biological replicates are required to confirm this result, it does emphasize the importance of diverse donor selection for

any study of this kind. This point is underscored by baseline differences in female and male donor IL-6 levels across all treatment on the ground and with COM treatment in flight.

Taken together, these findings indicate that the primary pathogenic effects of COM crystals on PTECs include disruptive adhesion to the renal epithelial surface, damaged and misfolded protein response, disruption of mitochondrial organization, oxidative stress response and pro-apoptotic signaling. This conclusion is supported by the upregulation of genes involved in extracellular matrix maintenance and cell adhesion, ROS metabolism, pro-apoptotic regulation, and cellular stress responses. A corresponding downregulation in genes involved in repairing damaged and misfolded proteins, RNA biosynthesis and metabolism, and mitochondrial membrane organization would account for an increase in cellular ROS and points to likely accumulation of oxidatively damaged RNA and proteins. This is consistent with the currently proposed models of kidney stone development such as those developed by Sun and colleagues [73, 77, 78, 94].

4.5 Supplemental Tables

Supplemental Table 1

Flight COM vs Flight Control					
Upregulated			**Downregulated**		
Gene	**Log2FC**	**p-value**	**Gene**	**Log2FC**	**p-value**
ADRB2	0.42	4.60E-02	COL4A3BP	-0.13	4.60E-02
GPRIN3	0.41	2.90E-02	HSPA14	-0.18	2.90E-02
LTBP2	0.32	7.00E-03	LINC01123	-0.28	4.60E-02

STK17A	0.17	7.00E-03	ZNF439	-0.30	1.90E-02
			ZNF470	-0.22	3.50E-02

Supplemental Table 2

Ground COM vs Ground Control					
Upregulated			**Downregulated**		
Gene	**Log2FC**	**p-value**	**Gene**	**Log2FC**	**p-value**
CYGB	1.04	4.00E-03	IGKV1OR2-1	-0.70	8.00E-03
SPC25	1.02	2.47E-04	LGI2	-0.62	4.30E-02
MIR155HG	0.83	5.00E-03	MFAP2	-0.54	1.60E-02
CDCA3	0.81	9.23E-04	LINC02331	-0.44	3.70E-02
PBK	0.79	6.00E-03	ZNF711	-0.43	7.00E-03
KIF18B	0.77	3.00E-03	RPS10P7	-0.43	4.20E-02
HIST1H1B	0.77	3.00E-03	HHIPL1	-0.43	3.80E-02
CENPM	0.74	2.00E-03	YPEL1	-0.41	9.00E-03
HIST1H3B	0.73	2.00E-03	LCAL1	-0.40	3.90E-02
HIST1H2BM	0.72	5.00E-03	UST	-0.40	5.00E-03
HIST1H3G	0.70	6.00E-03	MAP2	-0.39	5.00E-03
HIST2H3A	0.70	3.00E-03	MDK	-0.38	1.20E-02
DEPDC1	0.69	3.00E-03	PCDH9	-0.38	1.40E-02

HIST2H3C	0.69	3.00E-03	SEMA6D	-0.37	7.46E-04
KIF14	0.68	7.46E-04	EPHA10	-0.35	2.80E-02
MYBL2	0.67	3.00E-03	ATP10B	-0.34	4.60E-02
NUF2	0.67	4.00E-03	NACAD	-0.34	6.00E-03
SLC10A2	0.67	3.90E-02	ZMYND15	-0.33	4.30E-02
FAM72C	0.65	1.20E-02	KIF7	-0.33	3.70E-02
HAPLN3	0.65	9.00E-03	FGF12	-0.33	9.00E-03

Supplemental Table 3

Flight KCit vs Flight Control					
Upregulated			**Downregulated**		
Gene	**Log2FC**	**p-value**	**Gene**	**Log2FC**	**p-value**
CXCL2	0.46	2.80E-02	SALL3	-1.07	4.00E-02
CCN2	0.45	6.24E-05	TROAP	-0.73	2.80E-02
DNM1P47	0.44	3.80E-02	HIST1H2BO	-0.66	9.00E-03
CXCL3	0.43	4.80E-02	MVK	-0.65	2.30E-02

CYP51A1P2	0.41	3.80E-02	CEACAM6	-0.64	4.10E-02
PPAN	0.31	4.80E-02	CAPN10-DT	-0.63	1.00E-02
ORAI3	0.29	1.30E-02	DLGAP5	-0.57	2.20E-02
CXCL1	0.28	6.24E-05	ESCO2	-0.55	1.50E-02
DTNB	0.27	6.24E-05	HIST1H2BB	-0.54	4.90E-02
TMEM170B	0.27	4.80E-02	ERCC6L	-0.54	2.80E-02
PAIP2B	0.24	4.90E-02	KIF20A	-0.53	2.90E-02
SMIM29	0.24	4.60E-02	SHCBP1	-0.52	3.80E-02
CDK18	0.22	4.00E-02	TOP2A	-0.52	1.90E-02
BAD	0.21	9.00E-03	FAM111B	-0.50	4.10E-02

TRIB1	0.21	6.24E-05	UBE2C	-0.50	4.00E-02
ID2	0.20	8.00E-03	CCNE2	-0.50	4.80E-02
BEX4	0.20	1.00E-02	NCAPG	-0.50	2.80E-02
DANCR	0.20	4.80E-02	POLE2	-0.49	2.60E-02
BDH1	0.20	2.70E-02	SPC24	-0.48	4.80E-02
AGTRAP	0.19	1.80E-02	E2F8	-0.48	1.30E-02

Supplemental Table 4

Ground KCit vs Ground Control					
Upregulated			**Downregulated**		
Gene	**Log2FC**	**p-value**	**Gene**	**Log2FC**	**p-value**
HLA-DRB1	0.98	3.00E-02	TNS4	-0.99	4.20E-02

GGTLC5P	0.87	5.00E-03	ITPKA	-0.85	3.20E-02
POU2F2	0.83	1.20E-02	MMP2	-0.66	2.40E-02
FAM3B	0.82	4.50E-02	KRT16	-0.63	1.20E-02
SLC38A4	0.75	1.38E-04	OSBPL6	-0.62	4.20E-02
IL13RA2	0.66	3.00E-02	MEX3B	-0.54	2.00E-02
SPC25	0.66	4.20E-02	KCNJ6	-0.52	2.70E-02
ZNF492	0.58	2.50E-02	ADAMTS7	-0.49	1.70E-02
HLA-DPB1	0.57	2.20E-02	SMIM2-AS1	-0.49	2.00E-02
ADAM7	0.57	4.80E-02	TRIM29	-0.47	4.00E-03
DEPDC1	0.56	4.00E-02	CHAC1	-0.44	1.70E-02

RN7SL471P	0.56	3.50E-02	SLC6A9	-0.39	2.20E-02
MIR210HG	0.53	2.40E-02	FBXL8	-0.39	3.10E-02
SAA2	0.52	2.40E-02	ZNF333	-0.38	4.00E-03
ZNF98	0.52	4.70E-02	SMIM32	-0.38	4.80E-02
BCYRN1	0.51	1.70E-02	UST	-0.37	3.00E-02
SAA1	0.49	1.90E-02	ADM2	-0.33	4.90E-02
HIST1H2AH	0.48	4.00E-02	KCNMA1	-0.31	4.50E-02
PTTG1	0.45	3.50E-02	C1orf226	-0.31	1.20E-02
AK4P1	0.45	1.20E-02	NR1D1	-0.28	4.70E-02

Supplemental Table 5

Flight COM vs Flight KCit					
Upregulated			**Downregulated**		
Gene	**Log2FC**	**p-value**	**Gene**	**Log2FC**	**p-value**
ERCC6L	0.82	1.09E-04	HHIPL1	-0.65	6.00E-03
HIST1H3J	0.81	2.00E-03	MGAT5B	-0.64	1.90E-02
HIST1H2BO	0.80	2.70E-04	PLPP4	-0.63	4.70E-02
GAL	0.77	1.50E-02	ARHGAP27P1-BPTFP1-KPNA2P3	-0.57	4.70E-02
CDCA3	0.75	7.77E-04	PTP4A1	-0.45	4.10E-02
SPC24	0.72	3.35E-04	C4orf47	-0.45	2.50E-02
MIR155HG	0.72	3.10E-02	HCN4	-0.44	1.90E-02

TROAP	0.72	1.50E-02	RENBP	-0.43	5.00E-03
DLGAP5	0.70	1.00E-03	ANKDD1B	-0.38	1.60E-02
HIST1H3G	0.69	2.00E-03	RSAD2	-0.38	2.00E-03
CKAP2L	0.68	6.09E-04	PSG4	-0.37	2.00E-03
MYBL2	0.68	1.00E-03	GPNMB	-0.35	2.00E-03
TOP2A	0.67	4.66E-04	LRP3	-0.34	4.70E-02
HIST1H2BL	0.66	7.00E-03	CASP8	-0.33	3.50E-02
SHCBP1	0.65	2.00E-03	ZNF222	-0.32	2.10E-02
MKI67	0.65	2.00E-03	SEMA6C	-0.31	4.50E-02
DEPDC1	0.65	2.00E-03	SULT1C2	-0.31	2.00E-03

ASPM	0.64	1.00E-03	SHROOM1	-0.30	1.30E-02
HIST1H2BB	0.64	6.00E-03	EID2	-0.30	1.00E-03
RRM2	0.64	1.00E-03	FAXC	-0.30	4.10E-02

Supplemental Table 6

Ground COM vs Ground KCit					
Upregulated			**Downregulated**		
Gene	**Log2FC**	**p-value**	**Gene**	**Log2FC**	**p-value**
TNS4	1.39	2.00E-03	FAM3B	-0.98	1.50E-02
IL1RL1	1.20	1.00E-03	LGI2	-0.66	4.60E-02
ITPKA	0.89	1.80E-02	ZNF98	-0.63	1.40E-02
KCNN4	0.79	2.30E-02	AEBP1	-0.63	5.00E-02
ANKRD18B	0.71	2.40E-02	GGTLC5P	-0.62	2.80E-02
CEACAM6	0.70	3.80E-02	APOE	-0.59	6.00E-03
SLC13A4	0.66	5.00E-02	ADAM7	-0.58	4.30E-02
MUC16	0.66	3.10E-02	HLA-DPB1	-0.51	3.70E-02
EREG	0.63	1.50E-02	TUBBP5	-0.50	3.30E-02

KCNJ6	0.62	5.00E-03	MAP6	-0.50	1.00E-02
CENPM	0.62	2.10E-02	SLC19A3	-0.47	2.30E-02
TM4SF18	0.60	8.00E-03	VTRNA1-3	-0.47	2.40E-02
CSKMT	0.60	4.10E-02	PTGER3	-0.47	1.40E-02
LINC01322	0.59	9.00E-03	GABRB3	-0.46	2.50E-02
LHFPL3-AS2	0.58	4.10E-02	ZNF730	-0.44	3.40E-02
PTGS1	0.57	5.00E-03	BAAT	-0.44	1.30E-02
ISM1	0.56	1.80E-02	PSG4	-0.42	1.00E-03
PDE1C	0.55	1.20E-02	PSG9	-0.42	3.50E-02
FABP5P7	0.55	1.20E-02	MME	-0.42	1.10E-02
RRAD	0.54	1.00E-03	GRM8	-0.42	1.00E-02

Supplemental Table 7

Flight Control vs Ground Control					
Upregulated			**Downregulated**		
Gene	**Log2FC**	**p-value**	**Gene**	**Log2FC**	**p-value**
KRT81	1.42	1.92E-05	KRT20	-1.34	4.40E-06
SLC38A5	1.40	1.00E-06	ADCY1	-1.27	1.00E-06
PLA2G2F	1.36	1.01E-06	BAAT	-1.18	1.00E-06
SNCG	1.27	1.00E-06	HRK	-1.09	1.00E-06

APCDD1L-DT	1.22	4.61E-06	FAT3	-1.07	4.13E-05
CYGB	1.20	1.06E-05	CNTN4	-1.06	1.82E-06
SPC25	1.17	1.00E-06	PHYHIPL	-1.03	1.00E-06
CDH13	1.16	6.74E-04	LRP2	-1.02	3.90E-02
HIST1H3G	1.13	1.00E-06	TAC1	-1.02	1.00E-06
HIST1H1B	1.10	1.00E-06	ACHE	-0.96	6.71E-06
OLFM4	1.07	1.00E-06	CCND2	-0.95	1.00E-06
ALDOC	1.05	1.00E-06	ADAMTS14	-0.95	1.00E-06
CDC20	1.04	1.00E-06	CXCL12	-0.93	7.82E-05
PBK	1.03	2.55E-06	RGS4	-0.93	2.40E-04
HIST1H3B	1.03	1.00E-06	NYAP2	-0.91	9.86E-06
EDN2	1.01	1.00E-06	MMP2	-0.90	6.38E-06
KCNQ2	1.01	5.00E-03	SYT14	-0.89	1.00E-06
HIST1H4L	1.01	2.86E-04	TMEM255B	-0.88	1.00E-06
GAL	1.00	3.49E-05	IGFBPL1	-0.87	2.77E-04
HIST1H1D	0.98	1.00E-06	UST	-0.86	1.00E-06

Supplemental Table 8

Flight COM vs Ground COM					
Upregulated			**Downregulated**		
Gene	**Log2FC**	**p-value**	**Gene**	**Log2FC**	**p-value**

STAC2	1.19	4.00E-03	MGAT5B	-1.33	1.00E-06
ALDOC	1.09	1.00E-06	NYAP2	-1.27	1.00E-06
CLDN19	1.08	1.00E-06	DEFB103B	-1.18	4.16E-05
EDN2	1.02	1.00E-06	BAAT	-1.16	1.00E-06
WNK4	0.92	1.00E-06	CEP295NL	-1.16	9.62E-05
APCDD1L	0.92	5.00E-03	HS3ST2	-1.12	3.00E-03
CDH13	0.91	7.00E-03	RDM1P2	-1.06	4.70E-04
PLA2G2F	0.91	1.00E-03	DEFB103A	-1.05	2.81E-04
SNCG	0.90	1.07E-05	LHX4	-1.03	1.67E-04
GAL	0.88	3.83E-04	RPS14P4	-1.02	3.00E-03
SERPINA5	0.84	2.00E-03	HRK	-1.01	4.17E-06
BSND	0.83	2.21E-04	ALOXE3	-0.96	2.00E-03
AEBP1	0.83	2.65E-04	AC058791.1	-0.95	2.00E-03
COL11A1	0.81	1.01E-04	ARHGAP27P1-BPTFP1-KPNA2P3	-0.94	5.53E-06
SLC38A5	0.80	6.90E-04	ZSCAN12P1	-0.94	1.39E-06
PLTP	0.76	1.00E-06	PCA3	-0.92	2.00E-03
NPR3	0.74	9.04E-04	RPS3AP49	-0.92	2.00E-03
AQP4	0.74	1.87E-06	DPYSL4	-0.91	2.22E-04

DRC7	0.73	3.39E-04	CXCL12	-0.91	2.00E-03
HIST1H2BL	0.73	2.18E-04	SBF1P1	-0.88	1.00E-03

Supplemental Table 9

Flight KCit vs Ground KCit					
Upregulated			**Downregulated**		
Gene	**Log2FC**	**p-value**	**Gene**	**Log2FC**	**p-value**
RPL26P30	1.21	1.40E-02	KRT20	-1.20	6.24E-04
CDH13	1.10	6.00E-03	BAAT	-1.17	1.00E-06
IL1RL1	1.06	1.58E-04	HRK	-1.13	1.00E-06
PITX3	0.91	3.97E-04	RGMA	-1.05	3.92E-05
MUC16	0.87	1.52E-04	PHYHIPL	-1.04	1.72E-06
GALNT9	0.86	4.00E-02	LURAP1L-AS1	-0.90	7.09E-04
EGR1	0.85	1.00E-06	ABCB4	-0.88	5.31E-05
ANKS1B	0.85	3.45E-04	SNORD3C	-0.88	2.00E-03
MIR205HG	0.83	1.40E-02	LINC01291	-0.88	1.10E-02
SNCG	0.81	9.11E-04	ADCY1	-0.87	7.44E-06
FOS	0.79	7.32E-04	SCARNA5	-0.84	5.00E-03
SERPINA1	0.78	1.00E-06	MTUS2	-0.83	6.00E-03
CD70	0.78	3.30E-02	POLE	-0.80	5.00E-03

ACE	0.78	1.11E-04	IGFBPL1	-0.77	2.00E-03
TNS4	0.78	3.50E-02	SLC9C1	-0.76	7.57E-04
MFAP5	0.77	4.70E-02	ZNF208	-0.76	2.00E-02
KIAA1324	0.70	8.00E-03	RDM1P2	-0.74	1.20E-02
NLGN4X	0.69	2.30E-02	LINC00113	-0.73	1.00E-03
COL11A1	0.69	4.00E-03	PPP1R1C	-0.73	3.00E-03
CYGB	0.68	2.90E-02	MAPK6P3	-0.72	3.00E-03

5. Conclusions and Future Directions

As both public sector and commercial spaceflight endeavors continue to expand at an accelerated rate, health concerns specific to individuals who have experienced spaceflight will become increasingly relevant to the general public. Our project looks specifically at the factors and pathways that underlie the development and progression of kidney disease. The over-arching goal is to gain a better understanding of early pathophysiological changes which may uncover novel therapeutic targets that can be used in the development of pharmacologic agents to maintain the health of space explorers as well as the health of the general public. Particular areas of focus in these studies are proteinuria, osteoporosis, and kidney stone disease (KSD).

The KC-02 project launched on 17:29 UTC June 5, 2021, as part of the payload aboard the SpaceX Commercial Resupply Service mission 22 (CRS-22). KC-02 was preceded two years earlier by KC-01. In these studies, we aimed to demonstrate the ability of our proximal tubule epithelial cell (PTEC) microphysiologic system (PT-MPS) to accurately assess the cytotoxic capabilities of several pro-oxidative and cytotoxic agents. In the case of kidney stone disease, the

density of calcium oxalate crystals prevents them from freely perfusing into our PT-MPS at terrestrial 1G, presenting a practical challenge for this approach. Therefore, we required a microgravity environment to conduct the testing of our PT-MPS model of KSD.

We tested two hypotheses in the KC-02 project related to the development and testing of our PT-MPS model of KSD in the microgravity environment aboard the International Space Station National Laboratory (ISSNL). Our first hypothesis was that calcium oxalate monohydrate (COM) crystals induce acute kidney injury via direct crystal interactions with the outer membrane of the epithelial surface and increase oxidative stress. Our second hypothesis was that the microgravity environment aboard the ISS is a superior environment in which to test our PT-MPS model of KSD. The results generated from the PT-MPS devices that experienced spaceflight support both hypotheses.

Specifically, we found that MPSs and the microgravity environment available during spaceflight are both effective research tools. Evaluating our PT-MPS model of KSD in this environment allowed us to observe specific pathophysiological events with limited variables. Due to the nature of the PT-MPS as a monoculture of PTECs, the environment within our PT-MPS model of KSD during spaceflight simulated the specific interaction of COM crystals with the outer membrane of the epithelial surface.

Our protocol for the KC-02 project started with generating and characterizing COM crystals using microscopy and spectrographic techniques. We then assessed acute-phase responses to COM crystal exposure in 2D PTEC culture and in 3D PT-MPS during ground-based testing. In so doing, we developed a protocol for reproducible preparation of primarily COM crystal populations. We found that treatment of PTECs with COM in 2D culture resulted in time-dependent elevation in mitochondrial superoxide release (Figure 1).

The experimental design for both the spaceflight and ground SABLs included a (1) control, (2) COM treatment, and (3) COM + potassium citrate (KCit) treatment. We included the COM + KCit treatment to assess the mechanisms underlying its efficacy as a protective pharmacologic countermeasure against KSD. PTECs cultured in the PT-MPS can remain stable and healthy for months when properly maintained. Considering this, it follows that those PT-MPS devices which demonstrated spaceflight-induced stress responses can be thought of as experiencing a chronic, underlying pathologic condition that may mimic chronic human diseases characteristic of accelerated aging. Therefore, the COM and COM + KCit treatment groups in spaceflight represent the addition of only a single or pair of variables exacerbating an already pre-existing pathology.

Spaceflight itself was by far the most significant stressor experienced by PT-MPS devices during both KC-01 and KC-02. The release of the cytokine IL-6 was responsive to spaceflight and, our data suggests, to COM treatment in the presence and absence of KCit. Supporting this observation is the increase in clusterin levels also attributable to COM treatment in spaceflight.

A number of stress response pathways were activated in spaceflight; impacting the expression of 4,982 genes between spaceflight and ground untreated controls. While a great deal fewer genes were differentially expressed in response to COM treatment in spaceflight, nine in total, this likely confirms the premise of hypothesis one by highlighting a specific selection of genes that are impacted by a narrowly defined set of interactions, namely, large crystal-induced scrape injury of the luminal epithelial surface affecting the ECM, and intracellular dysregulation of Ca^{2+} ion homeostasis, proper folding of naïve peptides, of ceramide lipid homeostasis, and mitochondrial function resulting in a cellular response to ROS. Thus, even if we could perform a true terrestrial control group that mimicked the capability of COM crystals to freely transit through the PT-MPS, the most critical genes activated in response to COM in specific may be masked by

the upregulation of more general stress responses. In this way, in vitro studies performed in spaceflight may reveal novel pharmacotherapeutic targets for a wide variety of human diseases. Those genes which are differentially expressed in response to a stimulus while a cell population is in a generalized stress state are likely to be most integral to the processes underlying disease progression. This means that efforts to expand orbital R&D capacity and reduce costs will be of great value to pharmaceutical research into potential drug targets to treat aging related diseases. Of the eight protein-coding genes, each has predicted cellular localizations and cellular functions consistent with current literature models of calcium oxalate renal tubule toxicity **(Figure 1)** [5, 14, 73, 77, 78, 94-96].

The treatment of PT-MPS devices with COM crystals during spaceflight induced the differential expression of eight protein expressing genes and downregulated expression of the long non-coding RNA LINC01123 (Table 1). Of the eight, four genes were upregulated ADRB2, GPRIN3, LTBP2, STK17A, while CERT1, HSPA14.2, ZNF439, and ZNF470 were each downregulated in response to COM treatment in flight. Co-treatment of COM with KCit reversed this effect in seven of the nine genes. The two genes left unaffected were LINC01123 and ZNF439. Consistent with KCit's role in regulating free Ca^{2+} ion concentrations, each of the seven genes responsive to KCit treatment are directly connected to Ca^{2+} ion levels at the cellular level. Taken together these genes highlight a connection between calcium KSD and a number of associated comorbidities, several of which are also implicated in aging pathologies. It is important to note that none of the genes differentially expressed in response to COM treatment are predicted to take a part in oxalate disposition. The data generated from our PT-MPS model of KSD indicates that calcium alone is likely sufficient to induce disruptions in numerous homeostatic processes and that oxalate primarily acts to facilitate the Ca^{2+} toxicity by creating a highly insoluble, local source of

excess Ca^{2+} ions in the form of COM crystals. These excess ions will then diffuse into regions located in proximity to the developing kidney stone causing localized toxicity and likely further contributing to disease progression.

The inclusion of KCit in this study allowed us to better define the therapeutic mechanisms underlying its inhibitory effects against the progression of KSD. Of the nine genes that were impacted by COM treatment in flight, only LINC01123 and ZNF439 remained uneffected by the addition of KCit to COM treatment. Literature and GO searches have failed to identify a connection between ZNF439 expression and any function relating to calcium regulation, oxalate regulation, ROS genration and OS, or extracellular adhesion. However, several reports identify LINC01123 as a promotor of tumor growth that promotes a switch in ATP generation from oxidative physporylation to glycolysis [90, 91, 97-104]. Thus, downregulation of LINC01123 is likely to suppress cellular have an antiproliferative effect consistant with cells experiencing stress and undergoing apoptotic processes. The characteristics of the seven genes remaining genes that were responsive to KCit can serve to illuminate the specifics of KCit's activity as an inhibitor of KSD progression and may point to promising potential targets for pharmacotherapies. Therefore, it is necessary to assess the role that each gene plays in the dynamics of KSD and their wider connection to human diseases, particularly aging related ones.

Those genes that were upregulated in response to COM treatment in flight are likely responding either directly or indirectly to Ca^{2+} ligand binding. The G protein-regulated inducer of neurite outgrowth complex 3 (GPRIN3 or GRIN3) gene encodes the varient NR3 subunit of the calcium sensitive N-Methyl-d-aspartate (NMDA) receptor. The NMDA receptor is an important subtype glutamate receptor that acts as a nonselective cation channel highly permeable to both calcium (Ca^{2+}) and sodium (Na^{+}). The structure of a functional NMDA receptor is

heterotetrameric, typically consisting of two NR1 subunits and two NR2 subunits in association and this receptor complex plays a key role in the development of extracellular neurite outgrowths during neruonal development. Activation of the NMDA receptor by results in prologned increases in intracellular Ca^{2+} concentration [105]. Alternative splice varients of the NMDA receptor that incorporate NR3 subunitits in place of NR2 subunits result in reduced Mg^{2+} sensitivity, altered requirements for glutamate and glycine ligand binding, and reduced Ca^{2+} permeability [106]. Given that an increase in the relative abundance of NR3 containg NMDA receptors over those containing only NR1 and NR2 subunits results in decreased permeablity to Ca^{2+} ions, a similar protective effect may be achievable by a pharmacotherapeutic that can modify this balance specifically in the kidney.

The ADRB2 gene codes for the beta-2-adrenergic receptor which localizes to the apical plasma membrane and ECM where its activated by voltage-gated L-type calcium channels. ADRB2 plays a role in a wide variety of cellular functions including negative regulation of urine volume, Ca^{2+} ion transport across plasma membranes, ossification and bone resorption, hypoxia response, aging, and cellular senesence. Alterations in this gene's activity due to polymorphysims, point mutations or ideopathic downregulation are associated with an increased risk of Parkinsons' Disease, obesity, type 2 diabetes and cardiovascular disease. Upregulation of ADRB2 during COM KSD actually exacerbate disease progression if it results in alterations to urine volume and composition that increase supersaturation of Ca^{2+} ions in the urinary filtrate.

The DAP kinase-related apoptosis-inducing protein kinase 1 (DAPK1 or STK17A) gene product is a voltage gated Ca^{2+} ion-dependent kinase and positive regulator of apoptosis activated in response to various stimuli. DAPK activity stabilizes actin stress fibers through the phosphorylation of cytoskeltal-associated substrates and facilitates mechanosensitive signal

transduction via stress fibers and focal adhesion structures [107]. Interestingly, DAPK2 has been identified as a marker of cortical fibroblasts indicating that mechanosensitive responses in closely associated cells likely contributes to the pathogenic response [108]. In addition to these functions, DAPK1 is also a tumor suppressor and has been demonstrated to modulate cisplatin toxicity and ROS generation in testicular cancer cells [109].

LTBP2 is a member of latent TGF-beta binding proteins that engages in Ca^{2+} ion binding in the extracellular matrix to carry out functions related collagen biosynthesis and secretion of TGFβ into the extracellular space. As a member of the TGFβ-complex, once localized into the ECM, LTBP2 also acts as a structural component of microfibrilses engaged in cell adheasion processes. Its strucutral role in the assembly, architecture and orgnaization of elastic fibers may facilitate PTEC detection and response to COM-induced mechanophysisical stress. Acting through the p62-Keap1-Nrf2 pathway, LTBP2 is a negative regulator of ferroptosis in gastric cancer cells and is associated with poorer prognosis in gastric cancers [110, 111].

Elevated Ca^{2+} ion concentrations in the microenvironment created at the interface between COM crystal surfaces and the tubule epithelial surface increases NMDA ligand binding stimulating the upregulation of GPRIN3. This is a scenario consistant with the proposed mechanism of KCit KSD inhibition. An increase in the relative abundance of NR3 over NR2 subunits in the heterotetrameric structure of the NMDA receptor would result in a decrease in its Ca^{2+} permeablility and serves the likely purpose of attenuating a sudden increase in cellular Ca^{2+} ion levels. Since the increase in ADRB2 and DAPK1 expression is likely linked to the activity of NMDA, their response to KCit treatment is most likely attributable to a reduction of Ca^{2+} ions available to bind that receptor. In turn, the activity of either or both of these gene products in the nucleous is the likely factor impacting the expression of CERT1, HSPZNF470 In a similar fashion,

the Ca^{2+} ion binding-dependent nature of LTBP2 activity is the most probable cause of its upregulation in response to COM treatment. However, the effect of KCit has the potential to be counterproductive in this case if crystal scrape injury occurs necessitating ECM remodeling and cell adhesion repair in the absense accompanying surge in Ca^{2+} ion concentration to signal the need.

Those genes that were both downregulated in response to COM treatment in flight and responsive to KCit treatment share the common feature of being involved in the synthesis and regulation of major classes of intracellular biomolecules. The gene products of CERT1, HSPA14 and ZNF470 play important roles in lipid homeostasis, naïve peptide handling and transcriptional regulation in the nucleous respectively. CERT1 is a calcium-stimulated ceramide lipid kinase with three transcript varients resulting in differing isoforms expressed in the kidney. One isoform is a ceramide intracellular transport protein responsible for lipid bilayer homeostasis throughout the cell including, critically, both the mitochondrial and outer cell membanes. A different isoform posesses kinase activity that specifically phosphorylates the N-terminal region of the non-collagenous domain of the alpha 3 chain of type IV collagen. The activity of this latter isoform demonstrated an increase in its apparent V_{max} when stimulated with Ca^{2+} at micromolar concentrations with little observable impact on its K_m [112]. Thus, a precipitous elevation in Ca^{2+} levels would have the like impact of disrupting the CERT1-mediated lipid bilayer maintenance. CERT1 was the only gene that was not only responsive to COM treatment in flight, but also differentially expressed in response to flight across all three treatment groups. Spaceflight itself resulted in downregulation in CERT1 expression similar to that observed in PT-MPS devices treated with COM in flight. Recently, human ceramide mixtures have been investigated as anti-aging pharmactotherapies via collagen and fibrillin expression in dermal fibroblasts [113]. This

connection represents an additional link between aging related conditions and esposure to spaceflight. A member of heat shock protein family A, **HSPA14** is the only member of within its phylogenetic group and exibits limited sensitivity to temperature stimuli. However, the closely related human HSPA13, which is also insensitive to heat treatment, has high motif similarity and is induced by elevated intracellular calcium while its downstream response element HSPA5 is sensitive to elevated platelet Ca^{2+} concentrations [114]. ZNF470 is plays a role in cartilage physiology and is expressed at comparable levels in primary chondrocytes, chondrocyte cell lines and osteoarthritic chondrocytes with no observed impacted due to age [115]. It also serves a function during intermediate stage chondrocyte differentiation where it is transiently expressed immediately before the maximal expression of COL2A1, so its its downregulation in response to COM treatment may indicate that expression of important renally expressed collagen fibrils may be compromised in KSD [116].

During KC-02, KCit treatment was included in combination with COM to identify the mechanisms of its pharmacologic effect. When our data is considered in its entirety, we see indications of the protective mechanisms of KCit. Reduction of the overall concentration of free Ca^{2+} ions in the urinary filtrate, and at the crystal surface on the nano scale, are the most probable mechanisms underlying the observed therapeutic impact of KCit on COM induced PTEC toxicity. At the nano scale, citrate ions bind free calcium by competitively forming highly soluble CaCit with Ca^{2+} ions at the surface of COM crystals resulting in a blunting effect on the crystal edges reducing their damaging potential by making them essentially more COD in morphology [96]. The seven genes that responded to the addition of KCit each have functions intrinsically linked to local Ca^{2+} ion concentrations. Calcium signaling is also important in epigenetic regulation, a common

feature of aging related diseases [117]. Therefore, these genes may represent the therapeutic targets against the development of KSD and other, aging related ailments.

In vivo, the pathophysiologic events occur in differing renal tubule cell types across the length of the nephron. Therefore, efforts should be made to establish MPS models of renal tubule epithelial cell (RTEC) populations from the Loop-of-Henle (OH) and distal tubule (DTEC) regions so that the impact of COM on these cultures can be assessed and compared against these current results to identify regiospecific events with the potential for pharmacotherapeutic intervention. Our PT-MPS model of KSD is agnostic to the type of kidney stone precursors are tested. Future studies can assess calcium phosphate, uric acid, cystine, and struvite precursor components in a method similar to that used here to assess COM toxicity. One useful tool for continuing to improve and iterate off of this model would be a soluble biomarker indicative of the reactive oxygen species (ROS) state within MPS cultured renal epithelial cells. The nature of the PT-MPS makes other ROS detection assays impractical, so an analyte either secreted into the device effluents, or one accessible by whole cell lysate would be ideal. The oxidatively damaged nucleic acid products 8-oxo-Gsn and 8-oxo-dGsn are both elevated intracellularly during periods of oxidative stress and have been investigated as a biomarkers predictive of the onset of frailty associated with aging [17, 29, 30]. While the relatively slow rate of DNA replication makes 8-oxo-dGsn a suitable measure of chronologic aging, that being the duration an individual has been alive, 8-oxo-gsn has been more recently proposed as a biomarker of physiological aging [27]. However, the ELISA based methods of detecting the two are not capable of differentiating between the two. A novel UPLC-MS/MS assay was reported that has the capability of quantifying both 8-oxo-Gsn and 8-oxo-dGsn independently, allowing 8-oxo-gsn to serve as a biomarker of physiologic aging, which refers to those accumulated physiologic dysfunctions which contribute to frailty and other deleterious

conditions associated with aging. Levels of both 8-oxo-dGsn and 8-oxo-Gsn are elevated in patients with KSD further linking a pro-stone forming intraluminal microenvironment to increased generation of ROS [28].

Given that treatment with COM is likely to elevate the levels of oxidatively damaged nucleic acids in both cell lysates and in device effluents in a transient manner, 8-oxo-Gsn may prove an appropriate candidate biomarker for assessment in future experiments, and even in future clinical settings. The half-life of DNA in urine is too short to detect and the half-lives of mRNAs and lncRNAs in whole blood have been reported as 16.4 and 17.6 hours respectively [118]. This makes DNA, lncRNA and mRNAs unsuitable as biomarkers in long term exposure studies in MPS cultures. However, the half-lives of the major intracellular RNA classes differ considerably and can be impacted by the cells' growth phase. One study estimated half-lives of nine hours for cytoplasmic RNAs in 3T3 and 3T6 fibroblast cell line cultures. In comparison, the half-life of cellular tRNA increased from 36 hours in resting cells to 60 hours in growing cells Interestingly, rRNAs are more stable in growing than resting cells and each subunit displayed a different half-life in resting cells at about 50 hours for the 28S RNA and about 72 hours for the 18S RNA. This means that a cell at rest must synthesize the larger unit at a higher rate while a growing cell should synthesize them in equal quantities [119]. In vivo kidney stones induce superoxide induced OS responses in renal cells and release of the DNA biomarker 8-oxo-dGsn [120].

KSD risk increases with age, therefore, we assessed our PT-MPS model KSD in a context similar to underlying chronic pathophysiology of aging. Our research supports the proposition that experiencing spaceflight induces physiological changes in the human body that mirror pathologies related to aging. Taken together, we can paint a picture of PTEC response to dynamic COM crystal

interactions that is only available to us due to the environmental context in which these experiments conducted.

Our data indicates that experiencing spaceflight induces an aging-like stress state in PTECs cultured in MPS devices. This highlights a major advantage to be gained from performing in vitro toxicology and drug screening in orbit. In our study, the specific mechano-physiologic dynamics involved in COM crystal induced scrape injury could not be adequately assessed terrestrially. We adopted our PT-MPS model of KSD to be assessed in microgravity to better recapitulate the crystal-cell interactions critical to in vivo disease progression. In vitro modeling of diseases with a mechanosensitive component may benefit from an environment in which all gravitational forces are net zero resulting in a freefall effect. Research efforts in bone, muscle and other tissue remodeling may benefit from this effect allowing researchers to control the direction, orientation and rate of tissue growth using defined stimuli. Our PT-MPS model of KSD is also readily capable of assessing the cytotoxic effects of crystals composed of uric acid, struvite cystine and calcium phosphate (CaP), the latter of which is frequently an integral component in the development of both COM and COD kidney stones. We predict that PT-MPS devices treated with crystals composed of these alternatives to COM will activate a constellation of genes in response that are directly responsible for regulating local cellular homeostasis of the constituent ions. In this way, each variation of KSD can be identified by a replicable activation of genes characteristic to each type during the stone-developing stage and prior to symptomatic disease. Identifying secreted or gene expression level biomarkers unique to each variety of kidney stones should be pursued as a subsequent research objective.

Two mechanisms underlying COM induced PTEC toxicity function as two independent, but synergistic processes. The first is disruption of homeostasis pathways due to elevated

intracellular Ca^{2+} and oxalate ion concentrations. However, a simultaneous process of COM-induced mechanophysical scrap injury damages the tubule epithelial surface, compromising its integrity and necessitating extensive repair efforts on the part of the injured cell. Depending on the initial condition of the renal epithelium and the relative impact of these two mechanisms, the resulting cell death may more closely resemble apoptotic, or necrotic processes in character. Terrestrial studies can investigate disruptions intracellular homeostasis, but cannot accurately model the dynamic mechanophysical interactions characteristic of KSD with currently available models. To our knowledge, there are no other studies that have investigated the pathophysiology of KSD using a model comparable to our own. A better understanding of the factors and pathways that underlie proper cellular structure and the development and progression of kidney diseases may uncover novel therapeutic targets that can be used in the development of pharmacologic agents that can maintain the health of ISS crewmembers as well as the health of the general public by preventing or reversing renal damage caused by proteinuria, osteoporosis, or kidney stones.

Our PT-MPS model is based upon devices designed to create straight tubules lined with ECM and RTECs with single pass flow and no crosstalk between different RTEC types. In their native context, nephrons form highly convoluted tubules which descend to various depths of the inner cortex and medullary regions of the kidney. Extensive regulatory cross signaling occurs between PTECs and distal epithelial cells when they meet in close association after the loop of Henle. A linked series of kidney MPS devices seeded with RTECs representing multiple nephron regions with independent local osmolalities with respect to COM crystal promotors and inhibitors would be a powerful tool for continued investigation of KSD pathophysiology and for investigating other renal pathologies. The natural progression from such a development will ultimately be to link MPS devices cultured with primary human cells representing various organs,

tissues and functions in an integrated system capable of evaluating the pathophysiology of complex, multi organ diseases. It will be critically important to consider possible applications and enhancements provided by spaceflight and microgravity and to implement features that will best take advantage of this environment.

Applied physics and advanced materials sciences are clear cases of fields in which research can be enhanced by access to microgravity and orbital conditions. However, it is becoming increasingly clear that biopharmaceutical research can benefit greatly from access to orbital facilities. Factors specific to orbitally based R&D efforts will need to be constantly identified and addressed to best optimize the use of this resource. For example, cytochrome P450 enzymes (CYPs) are a dominant topic within pharmaceutical research. Within our dataset, certain renally expressed CYPs genes exhibited a change in expression in response to flight, COM treatment, and treatment with COM and KCit (Table 2). If the same holds true for hepatic and intestinally expressed CYPs, a great deal of consideration will be required to ensure that results obtained in orbit possess relevance for use in the terrestrial context.

The primary objective for commercial spaceflight entities must be to provide facilities that provide benefits unavailable terrestrially. This applies across a range of areas including sports, entertainment, tourism and the same principles will apply to biopharmaceutical research performed in orbit. Buildup of orbital research infrastructure requires a tipping point at which the monetary benefits of conducting commercial R&D in orbit exceed the associated costs and risks. This highlights the critical importance of studies such as ours that aim to identify the unique benefits offered by performing in vitro studies in spaceflight. Each new discovery attributable to research in orbit lowers the risk profile for future investments leading to a virtuous cycle resulting in ever accelerated adoption of orbital R&D. Academic research will play a critical role here in conducting

exploratory research designed to better understand pathophysiologies and potential therapeutic targets that can be successfully translated into marketable pharmacotherapeutics. Cooperation between private industry and academia to ensure robust access for academic labs carries the added benefit of providing adequate opportunities for scientists in training at all levels to become integrated into a burgeoning orbital research community which will further accelerate the pace at which adoption of orbital research facilities takes place.

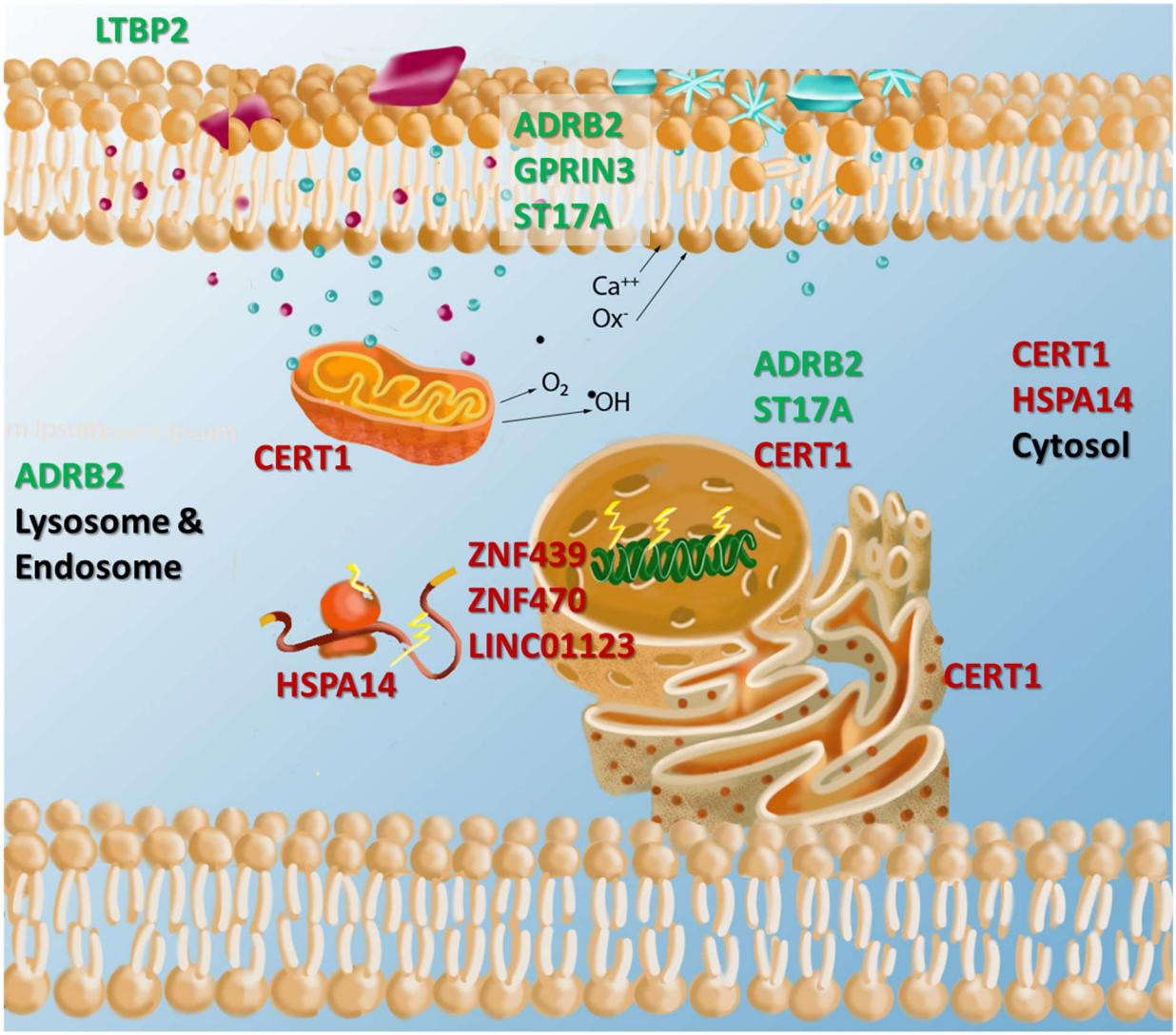

Figure 1. Schematic illustration depicting subcellular localization of nine genes differentially expressed by MPS cultured PTECs in response to COM crystal treatment during spaceflight.

Table 1. Select Genes Differentially Expressed in KC-02 EVT & Flight vs Ground

	COM vs Control	COM + KCit vs Control			Flight vs Ground		
	Flight	EVT	Flight	Ground	Control	COM	KCit
BCL3	-	0.79	-	-	1.17	1.23	1.23
PPP1R10	-	0.86	-	-	1.10	-	-
PSG4	-	1.43	0.77		-	-	-
ADRB2	1.34	-	-	-	-	-	-
GPRIN3	1.33	-	-	-	1.26	-	1.24
LTBP2	1.24	-	-	-	-	1.35	1.17
STK17A	1.13	-	-	-	1.16	-	-
CERT1	0.91	-	-	-	0.91	0.87	0.91
ZNF439	0.81	-	0.82	0.88	-	-	0.82
HSPA14.2	0.88	-	-	-	-	-	-
ZNF470	0.86	-	-	-	-	0.87	0.89
LINC01123	0.82	-	0.83	-	-	0.77	0.87

∗ Criteria for selection: Adj. P Value ≤0.05

Table 2. Cytochrome P450 Genes Differentially Expressed in Response Spaceflight

	Flight vs Ground		
	Control	COM	KCit
CYP1B1	1.21	-	-
CYP2E1	1.48	1.21	-
CYP2J2	-	0.84	0.85
CYP2U1	0.89	-	-
CYP4F11	1.14	1.15	-
CYP4V2	0.88	0.91	-
CYP7B1	0.74	0.78	0.78
CYP27C1	1.37	-	-
CYP39A1	-	1.35	-
POR	0.88	0.87	-

∗ Criteria for selection: Adj. P Value ≤0.05

6. References

1. Prevention, C.f.D.C.a., *Chronic Kidney Disease in the United States* 2021.
2. Wang, K., et al., *Risk factors for kidney stone disease recurrence: a comprehensive meta-analysis.* BMC Urology, 2022. **22**(1): p. 62.
3. Clinics, U.o.I.H. *Frequently Asked Questions about Kidney Stones*. 2020; Available from: https://uihc.org/health-topics/frequently-asked-questions-about-kidney-stones#:~:text=How%20long%20does%20it%20take,in%20a%20matter%20of%20weeks.
4. Chung, H.-J., *The role of Randall plaques on kidney stone formation.* Translational Andrology and Urology, 2014. **3**(3): p. 251-254.

5. Sun, X.Y., Q.Z. Gan, and J.M. Ouyang, *Calcium oxalate toxicity in renal epithelial cells: the mediation of crystal size on cell death mode.* Cell Death Discovery, 2015. **1**(1): p. 15055.
6. Uribarri, J., *Chronic kidney disease and kidney stones.* Curr Opin Nephrol Hypertens, 2020. **29**(2): p. 237-242.
7. Niu, X., et al., *Calcium concentration dependent collagen mineralization.* Materials Science and Engineering: C, 2017. **73**: p. 137-143.
8. Matlaga, B.R., et al., *The Role of Randall's Plaques in the Pathogenesis of Calcium Stones.* Urology, 2007. **177**(1): p. 31-38.
9. Ratkalkar, V.N. and J.G. Kleinman, *Mechanisms of Stone Formation.* Clinical reviews in bone and mineral metabolism, 2011. **9**(3-4): p. 187-197.
10. Lieske, J.C., S. Deganello, and F.G. Toback, *Cell-crystal interactions and kidney stone formation.* Nephron, 1999. **81 Suppl 1**: p. 8-17.
11. Whitson Peggy, A., et al., *Effect of Potassium Citrate Therapy on the Risk of Renal Stone Formation During Spaceflight.* Journal of Urology, 2009. **182**(5): p. 2490-2496.
12. Marengo, S.R. and A.M.P. Romani, *Oxalate in renal stone disease: the terminal metabolite that just won't go away.* Nature Clinical Practice Nephrology, 2008. **4**(7): p. 368-377.
13. Schepers, M.S., et al., *Oxalate is toxic to renal tubular cells only at supraphysiologic concentrations.* Kidney international, 2005. **68**(4): p. 1660-9.
14. Sun, X.Y. and J.M. Ouyang, *New view in cell death mode: effect of crystal size in renal epithelial cells.* Cell Death & Disease, 2015. **6**(12): p. e2013-e2013.
15. Wigner, P., et al., *The Molecular Aspect of Nephrolithiasis Development.* Cells, 2021. **10**(8): p. 1926.
16. Patel, M., et al., *Oxalate induces mitochondrial dysfunction and disrupts redox homeostasis in a human monocyte derived cell line.* Redox biology, 2018. **15**: p. 207-215.
17. Tan, B.L., et al., *Antioxidant and Oxidative Stress: A Mutual Interplay in Age-Related Diseases.* Frontiers in pharmacology, 2018. **9**: p. 1162-1162.
18. Huang, M.Y., et al., *Oxalate stimulates IL-6 production in HK-2 cells, a line of human renal proximal tubular epithelial cells.* Kidney Int, 2005. **68**(2): p. 497-503.
19. Lee, P.H.U., et al., *Factors mediating spaceflight-induced skeletal muscle atrophy.* Am J Physiol Cell Physiol, 2022. **322**(3): p. C567-C580.
20. Man, J., et al., *The effects of microgravity on bone structure and function.* NPJ Microgravity, 2022. **8**(1): p. 9.
21. Vernikos, J. and V.S. Schneider, *Space, gravity and the physiology of aging: parallel or convergent disciplines? A mini-review.* Gerontology, 2010. **56**(2): p. 157-66.
22. Overbey, E.G., et al., *Spaceflight influences gene expression, photoreceptor integrity, and oxidative stress-related damage in the murine retina.* Sci Rep, 2019. **9**(1): p. 13304.
23. Mao, X.W., et al., *Impact of Spaceflight and Artificial Gravity on the Mouse Retina: Biochemical and Proteomic Analysis.* Int J Mol Sci, 2018. **19**(9).
24. Blaine, J., M. Chonchol, and M. Levi, *Renal control of calcium, phosphate, and magnesium homeostasis.* Clin J Am Soc Nephrol, 2015. **10**(7): p. 1257-72.
25. Young, K., et al., *Regulation of 1 and 24 hydroxylation of vitamin D metabolites in the proximal tubule.* Exp Biol Med (Maywood), 2022: p. 15353702221091982.

26. Radak, Z. and I. Boldogh, *8-Oxo-7,8-dihydroguanine: links to gene expression, aging, and defense against oxidative stress.* Free radical biology & medicine, 2010. **49**(4): p. 587-596.
27. Gan, W., et al., *Urinary 8-oxo-7,8-dihydroguanosine as a Potential Biomarker of Aging.* Frontiers in aging neuroscience, 2018. **10**: p. 34-34.
28. Boonla, C., et al., *Urinary 8-hydroxydeoxyguanosine is elevated in patients with nephrolithiasis.* Urological Research, 2007. **35**(4): p. 185-191.
29. Mao, Y.-H., et al., *Levels of 8-oxo-dGsn and 8-oxo-Gsn in random urine are consistent with 24 h urine in healthy subjects and patients with renal disease.* Free Radical Research, 2017. **51**(6): p. 616-621.
30. Mao, Y.-H., et al., *The Ratio of Plasma and Urinary 8-oxo-Gsn Could Be a Novel Evaluation Index for Patients with Chronic Kidney Disease.* Oxidative Medicine and Cellular Longevity, 2018. **2018**: p. 8.
31. Koirala, A. and J.A. Jefferson, *How Safe Is a Native Kidney Biopsy?* Clin J Am Soc Nephrol, 2020. **15**(11): p. 1541-1542.
32. Whitson, P., et al. *Renal stone risk during spaceflight: assessment and countermeasure validation*. in *2004 IEEE Aerospace Conference Proceedings (IEEE Cat. No.04TH8720)*. 2004.
33. Stein, T.P., *Space flight and oxidative stress.* Nutrition, 2002. **18**(10): p. 867-871.
34. Goodenow-Messman, D.A., et al., *Numerical characterization of astronaut CaOx renal stone incidence rates to quantify in-flight and post-flight relative risk.* npj Microgravity, 2022. **8**(1): p. 2.
35. Tourovskaia, A., et al., *Tissue-engineered microenvironment systems for modeling human vasculature.* Experimental biology and medicine, 2014. **239**(9): p. 1264-71.
36. Van der Hauwaert, C., et al., *Isolation and Characterization of a Primary Proximal Tubular Epithelial Cell Model from Human Kidney by CD10/CD13 Double Labeling.* PLOS ONE, 2013. **8**(6): p. e66750.
37. Mount, D.B., *Thick Ascending Limb of the Loop of Henle.* Clinical Journal of the American Society of Nephrology : CJASN, 2014. **9**(11): p. 1974-1986.
38. Weber, E.J., et al., *Development of a microphysiological model of human kidney proximal tubule function.* Kidney Int, 2016. **90**(3): p. 627-37.
39. Adler, M., et al., *A Quantitative Approach to Screen for Nephrotoxic Compounds In Vitro.* J Am Soc Nephrol, 2016. **27**(4): p. 1015-28.
40. Chang, S.-Y., et al., *Human liver-kidney model elucidates the mechanisms of aristolochic acid nephrotoxicity.* JCI Insight, 2017. **2**(22): p. e95978.
41. Weber, E.J., et al., *Development of a microphysiological model of human kidney proximal tubule function.* Kidney international, 2016. **90**(3): p. 627-37.
42. Chapron, B.D., et al., *Reevaluating the role of megalin in renal vitamin D homeostasis using a human cell-derived microphysiological system.* ALTEX, 2018.
43. Chang, S.Y., et al., *Human liver-kidney model elucidates the mechanisms of aristolochic acid nephrotoxicity.* JCI Insight, 2017. **2**(22).
44. Lidberg, K.A., et al., *Serum Protein Exposure Activates a Core Regulatory Program Driving Human Proximal Tubule Injury.* J Am Soc Nephrol, 2022. **33**(5): p. 949-965.

45. Lidberg, K.A., et al., *Antisense oligonucleotide development for the selective modulation of CYP3A5 in renal disease.* Sci Rep, 2021. **11**(1): p. 4722.
46. Weber, E.J., et al., *Human kidney on a chip assessment of polymyxin antibiotic nephrotoxicity.* JCI Insight, 2018. **3**(24).
47. Maass, C., et al., *Translational Assessment of Drug-Induced Proximal Tubule Injury Using a Kidney Microphysiological System.* CPT Pharmacometrics Syst Pharmacol, 2019. **8**(5): p. 316-325.
48. Sakolish, C., et al., *Technology Transfer of the Microphysiological Systems: A Case Study of the Human Proximal Tubule Tissue Chip.* Sci Rep, 2018. **8**(1): p. 14882.
49. Chapron, B.D., et al., *Reevaluating the role of megalin in renal vitamin D homeostasis using a human cell-derived microphysiological system.* Altex, 2018. **35**(4): p. 504-515.
50. Khan, S.R., et al., *Kidney stones.* Nature Reviews Disease Primers, 2016. **2**: p. 16008.
51. Van Ness, K.P., et al., *Microphysiological Systems to Assess Nonclinical Toxicity.* Curr Protoc Toxicol, 2017. **73**: p. 14.18.1-14.18.28.
52. Weber, E.J., et al., *Human kidney on a chip assessment of polymyxin antibiotic nephrotoxicity.* JCI insight, 2018. **3**(24): p. e123673.
53. Perazella, M.A. and M.H. Rosner, *Drug-Induced Acute Kidney Injury.* Clinical Journal of the American Society of Nephrology, 2022: p. CJN.11290821.
54. Yu, F.-Y., et al., *Aristolochic acid I induced oxidative DNA damage associated with glutathione depletion and ERK1/2 activation in human cells.* Toxicology in Vitro, 2011. **25**(4): p. 810-816.
55. Zhao, Y.-Y., et al., *Metabolomics analysis reveals the association between lipid abnormalities and oxidative stress, inflammation, fibrosis and Nrf2 dysfunction in aristolochic acid-induced nephropathy.* Scientific Reports, 2015. **5**(1): p. 12936.
56. Wang, Y., et al., *Aristolochic acid induces mitochondrial apoptosis through oxidative stress in rats, leading to liver damage.* Toxicology Mechanisms and Methods, 2021. **31**(8): p. 609-618.
57. Van Ness, K.P., et al., *Microphysiological systems in absorption, distribution, metabolism, and elimination sciences.* Clin Transl Sci, 2022. **15**(1): p. 9-42.
58. Chen, L., et al., *Renal-Tubule Epithelial Cell Nomenclature for Single-Cell RNA-Sequencing Studies.* Journal of the American Society of Nephrology, 2019. **30**(8): p. 1358-1364.
59. Pizzonia, J.H., et al., *Immunomagnetic separation, primary culture, and characterization of cortical thick ascending limb plus distal convoluted tubule cells from mouse kidney.* In Vitro Cellular & Developmental Biology - Animal, 1991. **27**(5): p. 409-416.
60. Cain, K. and J.E. Gurney, *Immunomagnetic purification of rat proximal kidney cells.* Toxicol In Vitro, 1994. **8**(1): p. 13-9.
61. Baer, P.C., et al., *Isolation of proximal and distal tubule cells from human kidney by immunomagnetic separation: Technical Note.* Kidney International, 1997. **52**(5): p. 1321-1331.
62. Osman, O., et al., *Microfluidic immunomagnetic cell separation using integrated permanent micromagnets.* Biomicrofluidics, 2013. **7**(5): p. 54115.
63. Chen, J., et al., *Isolation and identification of senescent renal tubular epithelial cells using immunomagnetic beads based on DcR2.* Exp Gerontol, 2017. **95**: p. 116-127.

64. Sutermaster, B.A. and E.M. Darling, *Considerations for high-yield, high-throughput cell enrichment: fluorescence versus magnetic sorting.* Sci Rep, 2019. **9**(1): p. 227.
65. Vasilopoulou, E., *Isolating and Culturing Mouse Podocyte Cells to Study Diabetic Nephropathy.* Methods Mol Biol, 2020. **2067**: p. 53-59.
66. LeHir, M., et al., *Binding of peanut lectin to specific epithelial cell types in kidney.* American Journal of Physiology-Cell Physiology, 1982. **242**(1): p. C117-C120.
67. Forbes, M.S., B.A. Thornhill, and R.L. Chevalier, *Proximal tubular injury and rapid formation of atubular glomeruli in mice with unilateral ureteral obstruction: a new look at an old model.* American journal of physiology. Renal physiology, 2011. **301**(1): p. F110-F117.
68. Biotec, M. *MS Columns Specifications*. [cited 2022 12/23/2022]; Available from: https://www.miltenyibiotec.com/US-en/products/ms-columns.html#gref.
69. Biotec, M. *Germinal Center B Cell (PNA) MicroBead Kit Data Sheet*.
70. Baer, P.C., et al., *Transdifferentiation of Distal but Not Proximal Tubular Epithelial Cells from Human Kidney in Culture.* Nephron Experimental Nephrology, 1999. **7**(4): p. 306-313.
71. Ho, S.P., et al., *Architecture-Guided Fluid Flow Directs Renal Biomineralization.* Scientific reports, 2018. **8**(1): p. 14157-14157.
72. Thongboonkerd, V., T. Semangoen, and S. Chutipongtanate, *Factors determining types and morphologies of calcium oxalate crystals: Molar concentrations, buffering, pH, stirring and temperature.* Clinica Chimica Acta, 2006. **367**(1): p. 120-131.
73. Sun, X.Y., Q.Z. Gan, and J.M. Ouyang, *Size-dependent cellular uptake mechanism and cytotoxicity toward calcium oxalate on Vero cells.* Sci Rep, 2017. **7**: p. 41949.
74. Peerapen, P. and V. Thongboonkerd, *p38 MAPK mediates calcium oxalate crystal-induced tight junction disruption in distal renal tubular epithelial cells.* Scientific Reports, 2013. **3**: p. 1041.
75. Rabinovich, Y.I., et al., *Adhesion force between calcium oxalate monohydrate crystal and kidney epithelial cells and possible relevance for kidney stone formation.* Journal of Colloid and Interface Science, 2006. **300**(1): p. 131-140.
76. Thongboonkerd, V., et al., *Proteomic Analysis of Calcium Oxalate Monohydrate Crystal-Induced Cytotoxicity in Distal Renal Tubular Cells.* Journal of Proteome Research, 2008. **7**(11): p. 4689-4700.
77. Sun, X.-Y., M. Xu, and J.-M. Ouyang, *Effect of Crystal Shape and Aggregation of Calcium Oxalate Monohydrate on Cellular Toxicity in Renal Epithelial Cells.* ACS omega, 2017. **2**(9): p. 6039-6052.
78. Sun, X.Y., K. Yu, and J.M. Ouyang, *Time-dependent subcellular structure injuries induced by nano-/micron-sized calcium oxalate monohydrate and dihydrate crystals.* Mater Sci Eng C Mater Biol Appl, 2017. **79**: p. 445-456.
79. Khan, S.R., *Is oxidative stress, a link between nephrolithiasis and obesity, hypertension, diabetes, chronic kidney disease, metabolic syndrome?* Urological research, 2012. **40**(2): p. 95-112.
80. Lash, L.H. and J.J. Tokarz, *Oxidative stress in isolated rat renal proximal and distal tubular cells.* Am J Physiol, 1990. **259**(2 Pt 2): p. F338-47.

81. Loor, G., et al., *Menadione triggers cell death through ROS-dependent mechanisms involving PARP activation without requiring apoptosis.* Free radical biology & medicine, 2010. **49**(12): p. 1925-1936.
82. Han, W.K., et al., *Kidney Injury Molecule-1 (KIM-1): a novel biomarker for human renal proximal tubule injury.* Kidney Int, 2002. **62**(1): p. 237-44.
83. Van Ness, K.P., et al., *Microphysiological Systems to Assess Nonclinical Toxicity.* Curr Protoc Toxicol, 2017. **73**: p. 14 18 1-14 18 28.
84. Karadurmus, D., et al., *GPRIN3 Controls Neuronal Excitability, Morphology, and Striatal-Dependent Behaviors in the Indirect Pathway of the Striatum.* J Neurosci, 2019. **39**(38): p. 7513-7528.
85. Rastaldi, M.P., et al., *Glomerular podocytes contain neuron-like functional synaptic vesicles.* Faseb j, 2006. **20**(7): p. 976-8.
86. Sproul, A., et al., *N-methyl-D-aspartate receptor subunit NR3a expression and function in principal cells of the collecting duct.* Am J Physiol Renal Physiol, 2011. **301**(1): p. F44-54.
87. Frøkiær, J., *Collecting duct expression of N-methyl-D-aspartate receptor subtype NR3a regulates urinary concentrating capacity.* Am J Physiol Renal Physiol, 2011. **301**(1): p. F42-3.
88. Kim, E.Y., M. Anderson, and S.E. Dryer, *Sustained activation of N-methyl-D-aspartate receptors in podoctyes leads to oxidative stress, mobilization of transient receptor potential canonical 6 channels, nuclear factor of activated T cells activation, and apoptotic cell death.* Mol Pharmacol, 2012. **82**(4): p. 728-37.
89. Han, H., et al., *Novel role of NOD2 in mediating Ca2+ signaling: evidence from NOD2-regulated podocyte TRPC6 channels in hyperhomocysteinemia.* Hypertension, 2013. **62**(3): p. 506-11.
90. Li, H., et al., *LINC01123 promotes immune escape by sponging miR-214-3p to regulate B7-H3 in head and neck squamous-cell carcinoma.* Cell Death Dis, 2022. **13**(2): p. 109.
91. Liu, Z., et al., *Long non-coding RNA LINC01123 promotes cell proliferation, migration and invasion via interacting with SRSF7 in colorectal cancer.* Pathol Res Pract, 2022. **232**: p. 153843.
92. De Bellis, R., et al., *In vitro effects on calcium oxalate crystallization kinetics and crystal morphology of an aqueous extract from Ceterach officinarum: Analysis of a potential antilithiatic mechanism.* PLoS One, 2019. **14**(6): p. e0218734.
93. Tombolini, P., et al., *Lithotripsy in the treatment of urinary lithiasis.* J Nephrol, 2000. **13 Suppl 3**: p. S71-82.
94. Sun, X.-Y., J.-M. Ouyang, and K. Yu, *Shape-dependent cellular toxicity on renal epithelial cells and stone risk of calcium oxalate dihydrate crystals.* Scientific Reports, 2017. **7**(1): p. 7250.
95. Sun, X.-Y., et al., *Preparation, characterization, and in vitro cytotoxicity of COM and COD crystals with various sizes.* Materials Science and Engineering: C, 2015. **57**: p. 147-156.
96. Sun, X.-Y., et al., *Preparation, properties, formation mechanisms, and cytotoxicity of calcium oxalate monohydrate with various morphologies.* CrystEngComm, 2018. **20**(1): p. 75-87.

97. Hua, Q., et al., *LINC01123, a c-Myc-activated long non-coding RNA, promotes proliferation and aerobic glycolysis of non-small cell lung cancer through miR-199a-5p/c-Myc axis.* Journal of Hematology & Oncology, 2019. **12**(1): p. 91.
98. Li, C., et al., *Knockdown of LINC01123 inhibits cell viability, migration and invasion via miR-361-3p/TSPAN1 targeting in cervical cancer.* Exp Ther Med, 2021. **22**(4): p. 1184.
99. Pan, X., et al., *LINC01123 enhances osteosarcoma cell growth by activating the Hedgehog pathway via the miR-516b-5p/Gli1 axis.* Cancer Sci, 2021. **112**(6): p. 2260-2271.
100. Qin, H., C. Wang, and Y. Hua, *LINC01123 is associated with prognosis of oral squamous cell carcinoma and involved in tumor progression by sponging miR-34a-5p.* Oral Surg Oral Med Oral Pathol Oral Radiol, 2022. **133**(1): p. 50-59.
101. Tian, W., et al., *LINC01123 potentially correlates with radioresistance in glioma through the miR-151a/CENPB axis.* Neuropathology, 2022. **42**(1): p. 3-15.
102. Weng, G., et al., *LINC01123 promotes cell proliferation and migration via regulating miR-1277-5p/KLF5 axis in ox-LDL-induced vascular smooth muscle cells.* J Mol Histol, 2021. **52**(5): p. 943-953.
103. Ye, S., et al., *LINC01123 facilitates proliferation, invasion and chemoresistance of colon cancer cells.* Biosci Rep, 2020. **40**(8).
104. Zhang, M., et al., *ZEB1-activated LINC01123 accelerates the malignancy in lung adenocarcinoma through NOTCH signaling pathway.* Cell Death Dis, 2020. **11**(11): p. 981.
105. Xin, W.-K., et al., *A Functional Interaction of Sodium and Calcium in the Regulation of NMDA Receptor Activity by Remote NMDA Receptors.* The Journal of Neuroscience, 2005. **25**(1): p. 139-148.
106. Low, C.-M. and K.S.-L. Wee, *New Insights into the Not-So-New NR3 Subunits of N-Methyl-d-aspartate Receptor: Localization, Structure, and Function.* Molecular Pharmacology, 2010. **78**(1): p. 1.
107. Burridge, K. and C. Guilluy, *Focal adhesions, stress fibers and mechanical tension.* Exp Cell Res, 2016. **343**(1): p. 14-20.
108. Balzer, M.S., T. Rohacs, and K. Susztak, *How Many Cell Types Are in the Kidney and What Do They Do?* Annual review of physiology, 2022. **84**: p. 507-531.
109. Mao, P., et al., *Serine/threonine kinase 17A is a novel p53 target gene and modulator of cisplatin toxicity and reactive oxygen species in testicular cancer cells.* J Biol Chem, 2011. **286**(22): p. 19381-91.
110. Wang, T., et al., *LTBP2 Knockdown Promotes Ferroptosis in Gastric Cancer Cells through p62-Keap1-Nrf2 Pathway.* Biomed Res Int, 2022. **2022**: p. 6532253.
111. Zhang, X., et al., *A novel metabolism-related prognostic gene development and validation in gastric cancer.* Clin Transl Oncol, 2023. **25**(2): p. 447-459.
112. Bajjalieh, S., T. Martin, and E. Floor, *Synaptic vesicle ceramide kinase: a calcium-stimulated lipid kinase that co-purifies with brain synaptic vesicles.* Journal of Biological Chemistry, 1989. **264**(24): p. 14354-14360.

113. Sugahara, Y., et al., *Anti-skin-aging effects of human ceramides via collagen and fibrillin expression in dermal fibroblasts.* Bioscience, Biotechnology, and Biochemistry, 2022. **86**(9): p. 1240-1246.
114. Xu, K., H. Xu, and Z. Han, *Genome-Wide Identification of Hsp70 Genes in the Large Yellow Croaker (Larimichthys crocea) and Their Regulated Expression Under Cold and Heat Stress.* Genes, 2018. **9**(12): p. 590.
115. He, Y., et al., *The role of SIRT3-mediated mitochondrial homeostasis in osteoarthritis.* Cellular and Molecular Life Sciences, 2020. **77**: p. 1-15.
116. Hering, T.M., et al., *Characterization and chondrocyte differentiation stage-specific expression of KRAB zinc-finger protein gene ZNF470.* Exp Cell Res, 2004. **299**(1): p. 137-47.
117. Puri, B.K., *Calcium Signaling and Gene Expression.* Adv Exp Med Biol, 2020. **1131**: p. 537-545.
118. Wang, C. and H. Liu, *Factors influencing degradation kinetics of mRNAs and half-lives of microRNAs, circRNAs, lncRNAs in blood in vitro using quantitative PCR.* Scientific Reports, 2022. **12**(1): p. 7259.
119. Abelson, H.T., et al., *Changes in RNA in relation to growth of the fibroblast: II. The lifetime of mRNA, rRNA, and tRNA in resting and growing cells.* Cell, 1974. **1**(4): p. 161-165.
120. Pavlakou, P., et al., *Oxidative Stress and the Kidney in the Space Environment.* International journal of molecular sciences, 2018. **19**(10): p. 3176.